# Zwischenbericht zum Helmholtz-Forschungszentrum "Nanostrukturforschung an funktionalen Materialien mit kurzen Kohärenzlängen am TTF-VUV-FEL"

## Januar 2003 – Februar 2005

Projektverantwortliche:

**Prof. Dr. Michael Rübhausen und Prof. Dr. Ulrich Merkt**
Institut für Angewandte Physik und Zentrum für Mikrostrukturforschung, Universität Hamburg

**Dr. Josef Feldhaus und Prof. Dr. Jochen Schneider**
HASYLAB/DESY

Das Helmholtz-Forschungszentrum ist Teil eines größeren Vorhabens, dessen Ziel der Aufbau eines neuartigen VUV-Raman-Spektrometers am HASYLAB/DESY ist. Das Spektrometer wird einzigartige Forschungsmöglichkeiten auf den Gebieten der Physik, Chemie, Biologie und Medizin ermöglichen. Die Leistungsfähigkeit des Spektrometers soll durch Pilotexperimente zu den Themen Korrelationseffekte in Festkörpern, atomare und molekulare Systeme sowie Biophysik demonstriert werden. Das Spektrometer selbst wird vom BMBF finanziert. Das Helmholtz-Forschungszentrum stellt notwendiges Personal für den Aufbau und den Betrieb des Spektrometers zur Verfügung. Darüber hinaus unterstützt es die wissenschaftlichen Arbeiten innerhalb eines internationalen Wissenschaftsnetzwerks, an dem Gruppen aus Deutschland (Institut für Angewandte Physik und Zentrum für Mikrostrukturforschung der Universität Hamburg, HASYLAB/DESY, Hahn-Meitner-Institut, Max-Planck-Institut für Festkörperforschung), Schweden (Chalmers University of Technology, Uppsala University) und den USA (Cornell University, University of Illinois at Urbana Champaign) beteiligt sind. Zum Ausbau der Kooperationen dienen verschiedene Veranstaltungen, die vom Helmholtz-Forschungszentrum mitorganisiert werden (siehe Übersicht).

### Startphase

Die im Februar 2003 bewilligte Anschubfinanzierung von 20.000 € (Universität Hamburg)/15.000 € (HASYLAB/DESY) wurde überwiegend für die dreimonatige BAT IIa-Stelle von Frau Dr. Katrin Buth verwendet, die wesentlich an der Koordination und Redaktion der Anträge sowie an der Kommunikation mit den Wissenschaftlern beteiligt war. Die restlichen Mittel wurden für die Ausarbeitung des Spektrometer-Konzepts, einen Workshop zum technischen Design des Spektrometers und für Gäste verwendet. Der Hauptantrag für das Helmholtz-Forschungszentrum wurde im April 2003 eingereicht und im September 2003 sehr positiv bewertet. Der offizielle Zuwendungsbescheid ist aber erst im Januar 2004 eingegangen. Die ursprünglich für 2003 vorgesehenen Mittel wurden daher im Jahr 2004 vertragsgemäß verwendet.

Nach Fertigstellung des Technical Design Reports hat das BMBF im Juni 2004 die Mittel für das VUV-Raman-Spektrometer bewilligt. Im Technical Design Report (siehe Anlage) werden die besonderen Eigenschaften des neuen VUV-Raman-Spektrometers ausführlich beschrieben. Die dargestellten ray-tracing-Simulationen belegen die Durchführbarkeit des Projekts. Das Konzept des VUV-Raman-Spektrometers wurde innerhalb einer internationalen Wissenschaftlerkollaboration entwickelt, an der im Umgang mit Synchrotronstrahlung erfahrene Wissenschaftler beteiligt sind. Im April 2004 wurde hierzu ein Technical Design

Review Workshop "High-Resolution Double Monochromator at the VUV-FEL of the TESLA Test Facility 2" am HASYLAB/DESY veranstaltet. Dieser Workshop diente gleichzeitig als sogenanntes Kick-Off Meeting, wie es im HGF-Antrag genannt wird. Dabei wurden insbesondere die Kontakte mit der Gruppe von Prof. Dr. Wilfried Wurth, die unter anderem im Rahmen des Helmholtz-Forschungszentrums "Physik mit kohärenten Strahlungsquellen" den für das VUV-Raman-Spektrometer wichtigen hochauflösenden Primärmonochromator aufbaut, und den für die Experimentierhalle am HASYLAB/DESY verantwortlichen Personen intensiviert.

**Beschaffung und Aufbau des VUV-Raman-Spektrometers**

Im September 2004 wurde in Kooperation mit der Finanzbehörde Hamburg die internationale Ausschreibung des VUV-Raman-Spektrometers begonnen. Das Ausschreibungsverfahren ist ein Verhandlungsverfahren mit vorgeschaltetem öffentlichen Teilnahmewettbewerb. Der Aufruf zur Interessensbekundung wurde im Supplement to the Official Journal of the European Union, im Physik Journal, in Physics Today, im Hamburger Abendblatt und im Internet veröffentlicht. Die eingegangenen Interessensbekundungen von Firmen aus Europa und den USA werden zur Zeit von einer Kommission evaluiert. Dazu wurden von einigen Kommissionsmitgliedern auch Besuche bei den Firmen durchgeführt, um die Herstellungsverfahren vor Ort zu begutachten. In der folgenden Tabelle sind alle Kommissionsmitglieder aufgeführt.

| Mitglied | Vertreter |
|---|---|
| Prof. Dr. Michael Rübhausen<br>Institut für Angewandte Physik, Universität Hamburg | |
| Prof. Dr. Ulrich Merkt<br>Institut für Angewandte Physik, Universität Hamburg | |
| Dr. Katrin Buth<br>Institut für Angewandte Physik, Universität Hamburg | |
| Dr. Benjamin Schulz<br>Institut für Angewandte Physik, Universität Hamburg | Michael Wellhöfer<br>Institut für Experimentalphysik, Universität Hamburg |
| Dr. Ruben Reininger<br>SAS – Scientific Answers & Solutions, USA | |
| Dr. Michael Martins<br>Institut für Experimentalphysik, Universität Hamburg | Prof. Dr. Wilfried Wurth<br>Institut für Experimentalphysik, Universität Hamburg |
| Dr. Josef Feldhaus<br>HASYLAB/DESY | Dr. Elke Plönjes<br>HASYLAB/DESY |
| Dr. Ulrich Hahn<br>HASYLAB/DESY | Dr. Kai Tiedtke<br>HASYLAB/DESY |

Die Evaluation der Interessensbekundungen wird bis spätestens Mitte April 2005 abgeschlossen sein. Die geeigneten Firmen werden dann zur Angebotsabgabe aufgefordert. Ziel ist es, das Verhandlungsverfahren bis Herbst 2005 abzuschließen. Die Arbeiten zur Optik, Elektronik und Mechanik liegen im Zeitplan

Die Spezifikationen der Gitter und Spiegel sollen von der Arbeitsgruppe von Dr. Fred Senf und Dr. Heiner Lammert am BESSY mit der Nano Optic Measuring Machine (NOM) überprüft werden. Mit der derzeitigen Apparatur können alle Gitter sowie die Spiegel in meridionaler Richtung vermessen werden. Die Vermessung der Spiegel in sagittaler Richtung ist auf-

grund der starken Krümmungen noch nicht möglich. Ein gemeinsames Projekt zur Weiterentwicklung und Aufrüstung der Messapparatur wird angestrebt.

### Wissenschaftliche Arbeiten

Am UV-Raman-Spektrometer UT-3 des Instituts für Angewandte Physik finden bereits Experimente statt, die als Vorbereitung für entsprechende Experimente am VUV-Raman-Spektrometer dienen. Im Mittelpunkt stehen dabei zur Zeit die orbitale Ordnung, die Phaseninhomogenität sowie die konkurrierenden Wechselwirkungen zwischen Gitter, Ladung, Spin und orbitalen Freiheitsgraden in den Manganaten [1, 2, 3]. Ein wichtiges Beispiel ist die detaillierte Untersuchung der orbitalen Ordnung in $LaMnO_3$ mittels der resonanten Raman-Streuung [2]. Die Doktorandin Rilana Maeser (geb. Krüger) wird hierzu auf dem APS March Meeting 2005 einen eingeladenen Vortrag halten. Im Bereich der Kupratsupraleiter wurden der Proximity-Effekt an Supergittern aus $YBa_2Cu_3O_7/PrBa_2Cu_3O_7$ sowie die Resonanzeigenschaften des Paarbrechungspeaks bzw. der Energielücke der Kuprate untersucht [4, 5, 6, 7]. Wir konnten mit unseren Resonanz-Untersuchungen zeigen, dass es sich bei dem Paarbrechungspeak und der verringerten Intensität in der supraleitenden Energielücke in den Spektren nicht um eine einzige Anregung, sondern um die Überlagerung verschiedener Anregungen unterschiedlichen Ursprungs handelt [7]. Dieses sehr überraschende Ergebnis konnte nur mittels resonanter inelastischer Lichtstreuung erhalten werden. An Halbleiterverbindungen mit Stickstoff-Verunreinigungen wurden die Veränderungen der Zustandsdichte an verschiedenen Punkten der Brillouin-Zone und das dadurch verursachte Schieben der Energielücken zwischen den Valenz- und Leitungsbändern untersucht [8].

## Chronologie

| | |
|---|---|
| Februar 2003 | Bewilligung der Anschubfinanzierung von 20.000 € (Universität Hamburg) bzw. 15.000 € (HASYLAB/DESY) für das Helmholtz-Forschungszentrum "Nanostrukturforschung an funktionalen Materialien mit kurzen Kohärenzlängen am TTF-VUV-FEL". |
| April 2003 | Der Hauptantrag für das Helmholtz-Forschungszentrum wird eingereicht. |
| Juli 2003 | Der BMBF-Antrag "Raman-Streuung im VUV an der TESLA Test Facility" für das VUV-Raman-Spektrometer wird eingereicht. |
| September 2003 | Der Antrag für das Helmholtz-Forschungszentrum wird von den Gutachtern positiv bewertet. |
| Januar 2004 | Eingang des offiziellen Zuwendungsbescheids für das Helmholtz-Forschungszentrum. |
| | Der BMBF-Antrag für das VUV-Raman-Spektrometer wird von den Gutachtern positiv aufgenommen. Voraussetzung für eine endgültige Bewillligung ist aber ein Technical Design Report. |
| Januar 2004 – Juni 2004 | Erstellung eines Technical Design Report für das VUV-Raman-Spektrometer. |

| | |
|---|---|
| April 2004 | Technical Design Review Workshop "High-Resolution Double Monochromator at the VUV-FEL of the TESLA Test Facility 2". |
| Juni 2004 | Das BMBF bewilligt Mittel in Höhe von 2,95 Millionen Euro für das VUV-Raman-Spektrometer. |
| September 2004 – November 2004 | Internationale Ausschreibung des VUV-Raman-Spektrometers: Aufruf zur Interessensbekundung |
| November 2004 | Michael Rübhausen wird nach Bleibeverhandlungen zur Abwehr eines Rufes an die Iowa State University und das Ames National Laboratory (USA) zum C4-Professor der Universität Hamburg ernannt. |
| | Einrichtung von Internetseiten für das Helmholtz-Forschungszentrum: http://www.physnet.uni-hamburg.de/institute/IAP/Group_N/e/hrc/index.html. |
| Dezember 2004 | Beginn der Evaluation der eingegangenen Interessensbekundungen zum VUV-Raman-Spektrometer. |

## Mitarbeiter des Projekts "VUV-Raman-Spektrometer"

| | |
|---|---|
| Dr. Katrin Buth<br>Research Associate | Organisation der internationalen Ausschreibung, Kommunikation mit den Wissenschaftlern, Redaktion des Technical Design Reports, Betreuung der Internetseiten |
| Dr. Benjamin Schulz<br>Postdoktorand | Optisches und mechanisches Design des Spektrometers, UV-Spektroskopie an korrelierten Elektronensystemen mit dem UT-3 |
| Dipl.-Phys. Ralf Rauer<br>Doktorand/Postdoktorand | Spektralaufgelöste magneto-optische Ellipsometrie an korrelierten Elektronensystemen (Manganate und Kobaltate) |
| Dipl.-Min. Sonja Müller<br>Doktorandin | Untersuchungen an Hochtemperatursupraleitern |
| Dipl.-Phys. Marta Bastjan<br>Doktorandin | Untersuchungen an Heusler-Legierungen und Manganiten |
| Dipl.-Phys. Stefan Naler<br>Doktorand | Raman-Streuung an Manganaten am UT-3<br>Promotion Januar 2005 |
| Ilka Mahns<br>Diplomandin | Entwicklung einer Druckzelle für die inelastische Lichtstreuung |

## Veranstaltungen des Helmholtz-Forschungszentrums

**2. Workshop "Orbital Physics and Novel Phenomena in Transition Metal Oxides", 24. September – 25. September 2003, Hahn-Meitner-Institut, Berlin**
Organisatoren: Michael Rübhausen (IAP), Dimitri Argyriou (HMI)

**Technical Design Review Workshop "High-Resolution Double Monochromator at the VUV-FEL of the TESLA Test Facility 2", 19. April – 20. April 2004, HASYLAB/DESY, Hamburg**
Organisatoren: Katrin Buth (IAP), Michael Rübhausen (IAP), Josef Feldhaus (DESY)
Eingeladene Sprecher: Peter Abbamonte (Brookhaven National Laboratory, Upton, USA), Joseph Nordgren (Uppsala University, Sweden), Jan-Erik Rubensson (Uppsala University, Sweden), Ruben Reininger (SAS – Scientific Answers & Solutions, Madison, WI, USA)

**3. Workshop "Orbital Physics and Novel Phenomena in Transition Metal Oxides", 06. Oktober – 07. Oktober 2004, Hahn-Meitner-Institut, Berlin**
Organisatoren: Michael Rübhausen (IAP), Dimitri Argyriou (HMI)

Der 4. Workshop "Orbital Physics and Novel Phenomena in Transition Metal Oxides" wird voraussichtlich im Oktober 2005 am Institut für Angewandte Physik in Hamburg stattfinden.

## Gäste

Die wissenschaftlichen Arbeiten und der Aufbau des Spektrometers werden durch auswärtige Wissenschaftler unterstützt, die zu Forschungsaufenthalten oder Gastvorträgen an das Institut für Angewandte Physik kommen.

**2003**

| | |
|---|---|
| Miles V. Klein | University of Illinois at Urbana Champaign |
| Seokhyun Yoon | National Renewable Energy Laboratory, Colorado, 2 Besuche |
| John F. Mitchell | Argonne National Laboratory |
| Kee-Hoon Kim | Los Alamos National Laboratory |

**2004**

| | |
|---|---|
| Ruben Reininger | SAS – Scientific Answers & Solutions, Madison, WI, USA<br>mehrere Besuche |
| Lars Börjesson | Chalmers University of Technology, Göteborg, Schweden |
| Miles V. Klein | University of Illinois at Urbana Champaign, USA |
| Miroslav Abrashev | Universität Sofia, Bulgarien |
| Andrivo Rusydi | Brookhaven National Laboratory, Upton, NY, USA |
| Jacob Andreasson | Chalmers University of Technology, Göteborg, Schweden |
| Joakim Holmlund | Chalmers University of Technology, Göteborg, Schweden |

**2005**

| | |
|---|---|
| Ruben Reininger | SAS – Scientific Answers & Solutions, Madison, WI, USA |

## Konferenzbeiträge

**2. Workshop "Orbital Physics and Novel Phenomena in Transition Metal Oxides",
24. September – 25. September 2003, Hahn-Meitner-Institut, Berlin**

Rilana Krüger
"Orbital ordering in $LaMnO_3$ investigated by resonance Raman spectroscopy"
Eingeladener Vortrag

Ralf Rauer
"Magneto-optical response of $La_{0.7}Ca_{0.3}MnO_3$"
Vortrag

Jörg Kunze
"Optical study on thermal development of ordering in $La_{2-2x}Sr_{1+2x}Mn_2O_7$, $0.32 < x < 0.54$"
Poster

**3. Deutscher Workshop "Ellipsometrie",
23. Februar - 25. Februar 2004, Stuttgart**

Michael Rübhausen
"Generalisierte magneto-optische Ellipsometrie an ferromagnetischen Schichten"
Eingeladener Vortrag

**Technical Design Review Workshop "High-Resolution Double Monochromator at the VUV-FEL of the TESLA Test Facility 2",
19. April – 20. April 2004, HASYLAB/DESY, Hamburg**

Michael Rübhausen
"Strongly Correlated Materials and Resonant Raman Scattering"
Vortrag

Michael Rübhausen
"Detection Systems: Spectral and Time Resolution"
Vortrag

**3. Workshop "Orbital Physics and Novel Phenomena in Transition Metal Oxides",
06. Oktober – 07. Oktober 2004, Hahn-Meitner-Institut, Berlin**

Gerd Neuber
"Electronic Properties of thin $Ni_2MnIn$ Heusler films"
Poster

Rilana Krüger
"Temperature-dependent resonance Raman-scattering study at the heavy fermion compound $URu_2Si_2$"
Poster

Ralf Rauer
"Magneto-optical investigation of $La_{1-x}Sr_xCoO_3$ (x = 0.15, 0.2)"
Vortrag

**APS March Meeting 2004,**
**22. März – 26. März 2004, Montreal, Kanada**

D. Budelmann, J. Bäckström, R. Rauer, M. Rübhausen, H. Rodriguez, and H. Adrian
"$YBa_2Cu_3O_7/PrBa_2Ga_{0.1}Cu_{2.9}O_7$ superlattices studied by spectroscopic ellipsometry"
Vortrag

J. Kunze, S. Naler, R. Rauer, J. Bäckström, M. Rübhausen, and J. F. Mitchell
"Optical study on thermal development of ordering in $La_{2-2x}Sr_{1+2x}Mn_2O_7$"
Vortrag

B. Schulz, D. Chan, J. Bäckström, and M. Rübhausen
"Keratin-based materials: A deep-UV inelastic light scattering study"
Vortrag

D. Chan, B. Schulz, and M. Rübhausen
"In-vivo spectroscopic ellipsometry measurements on human skin"
Vortrag

R. Rauer, G. Neuber, J. Kunze, J. Bäckström, M. Rübhausen, T. Walter, and K. Dörr
"Magnetic phase transition of $La_{0.7}Ca_{0.3}MnO_3$ and $La_{0.7}Sr_{0.3}MnO_3$ - spin polarization studied by spectral generalized magneto-optical ellipsometry"
Vortrag

S. Naler, J. Bäckström, M. Rübhausen, Jakob Andreasson, J. Holmlund, L. Börjesson and B. Dabrowski
"Temperature dependent inelastic light scattering of doped $Sr_{1-x}Ca_xMnO_3$"
Vortrag

M. Rübhausen, D. Budelmann, B. Schulz, M. V. Klein, P. Guptasarma, D. Bonn, R. Liang, and W. Hardy
"Resonance phonon Raman scattering in high $T_c$ superconductors"
Vortrag

J. Bäckström, D. Budelmann, R. Rauer, M. Rübhausen, H. Rodriguez and H. Adrian
"High energy correlations and metallicity in $YBa_2Cu_3O_{7-\delta}$ and $PrBa_2Cu_3O_{7-\delta}$ films"
Vortrag

S. Yoon, M. Rübhausen, B. Schulz, and J. F. Geisz
"Nitrogen induced evolution of host electronic states in GaPN: Resonant Raman scattering study"
Vortrag

J. Andreasson, J. Holmlund, L. Börjesson, M. Käll, S. Naler, J. Bäckström, M. Rübhausen, A. K. Azad, and S.-G. Eriksson
"Inelastic light-scattering study of four double-perovskites"
Vortrag

M. Klein, M. Rübhausen, D. Budelmann, B. Schulz, P. Guptasarma, D. Bonn, R. Liang, and W. Hardy
"Probing the gap feature in high $T_c$ superconductors using resonance electronic Raman scattering"

**APS March Meeting 2005,**
**21. März – 25. März 2005, Los Angeles, USA**

Rilana Maeser
"Orbital excitations in $LaMnO_3$"
Eingeladener Vortrag

M. Rübhausen, S. Müller, R. Maeser, B. Schulz, I. Mahns, D. Budelmann, M.V. Klein, D. Bonn, W. Hardy, and R. Liang
"Resonance properties in optimally and overdoped Y-123 - investigation of phonons and the electronic background"
Vortrag

J. Andreasson, J. Holmlund, Mikael Käll, Lars Börjesson, Stefan Naler, Joakim Bäckström, Michael Rübhausen, Abul K. Azad and Sten Eriksson
"Resonant Higher Order Scattering in Double Perovskites"
Vortrag

Ralf Rauer, Michael Rübhausen, and J. F. Mitchell
"Magneto-Optical Investigation of $La_{1-x}Sr_xCoO_3$, (x = 0.15, 0.2)"
Vortrag

## Veröffentlichungen

[1] J. Kunze, S. Naler, J. Bäckström, M. Rübhausen, and J.F. Mitchell, "Optical Study of a Competition between Ordering and Metallicity in $La_{2-2x}Sr_{1+2x}MnO_7$", Phys. Rev. B **67**, 134417-1 (2003).

[2] R. Krüger, B. Schulz, S. Naler, R. Rauer, D. Budelmann, J. Bäckström, K.H. Kim, S-W. Cheong, V. Perebeinos, and M. Rübhausen, "Orbital ordering in $LaMnO_3$ investigated by resonance Raman spectroscopy", Phys. Rev. Lett. **92**, 097203-1 – 097203-4 (2004).

[3] R. Rauer, G. Neuber, J. Kunze, J. Bäckström, M. Rübhausen, T. Walter, and K. Dörr, "Magneto-optical investigation of spin polarisation of $La_{0.7}Ca_{0.3}MnO_3$ and $La_{0.7}Sr_{0.3}MnO_3$", Journal of Magnetism and Magnetic Materials, in press.

[4] D. Budelmann, J. Holmlund, J. Andreasson, H. Rodríguez, J. Bäckström, L. Börjesson, H. Adrian, U. Merkt, and M. Rübhausen, "The Antiferromagnetic and Superconducting Proximity Effects in $YBa_2Cu_3O_{7-y}$ / $PrBa_2Cu_3O_{7-y}$ Superlattices", Phys. Rev. B **67**, 140507-1 – 140507-4 (2003).

[5] J. Bäckström, D. Budelmann, R. Rauer, M. Rübhausen, H. Rodríguez, and H. Adrian, "Optical properties of $YBaCu_2O_7$ and $PrBaCu_2O_7$ films; High-energy correlations and metallicity", Phys. Rev. B **70**, 174502-1 – 174502-6 (2004).

[6] M. Rübhausen, M. V. Klein, D. Budelmann, B. Schulz, P. Guptasarma, M. S. Williamsen, Ruixing Liang, D. A. Bonn, and W. N. Hardy, "Resonance Raman study of the phonon spectra in supercondcuting Bi-2212 and Y-123", submitted, SNS Conference.

[7] M. Rübhausen, M. V. Klein, D. Budelmann, B. Schulz, P. Guptasarma, M. S. Williamsen, Ruixing Liang, D. A. Bonn, and W. N. Hardy, "Resonance Raman study af 2Δ gap-like features in superconducting Bi-2212 and Y-123", submitted, SNS Conference.

[8] S. Yoon, M. Rübhausen, B. Schulz, J. F. Geisz, Sung-Ho Han, and A. Mascarenhas, "Resonant Raman scattering spectroscopy studies of $GaP_{1-x}N_x$ and $GaAs_{1-x}N_x$ in the ultra-violet energy range", Phys. Rev. B, accepted.

[9] M. Rübhausen, M. V. Klein, D. Budelmann, B. Schulz, P. Guptasarma, M. S. Williamsen, Ruixing Liang, D. A. Bonn, and W. N. Hardy, "Resonance Raman study af 2Δ gap-like features in superconducting Bi-2212 and Y-123", submitted to Phys. Rev. Lett.

# Anlagen

- Technical Design Report, First Edition, June 2004 (79 Seiten)

- Programm des 2. Workshops "Orbital Physics and Novel Phenomena in Transition Metal Oxides" im September 2003 (3 Seiten)

- Programm des Technical Design Review Workshops "High-Resolution Double Monochromator at the VUV-FEL of the TESLA Test Facility 2" im April 2004 (4 Seiten)

- Programm des 3. Workshops "Orbital Physics and Novel Phenomena in Transition Metal Oxides" im September 2004 (4 Seiten)

- Ausschreibungstexte (Physik Journal, Physics Today) (2 Seiten)

**Technical Design Report**

# High-Resolution Double Monochromator at the VUV-FEL of the TESLA Test Facility 2

Michael Rübhausen,
Benjamin Schulz, Katrin Buth, Joakim Bäckström, Jörg Kunze,
Ruben Reininger, Joseph Nordgren, Johan Söderström, Jan-Erik Rubensson,
Lars Börjesson, Peter Abbamonte, S. Lance Cooper, Michael Martins,
Alexander Föhlisch, Wilfried Wurth, Josef Feldhaus, and Jochen Schneider

Editorial Coordination: Katrin Buth
katrin.buth@physnet.uni-hamburg.de

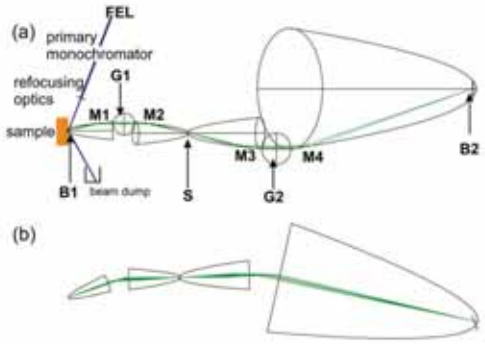


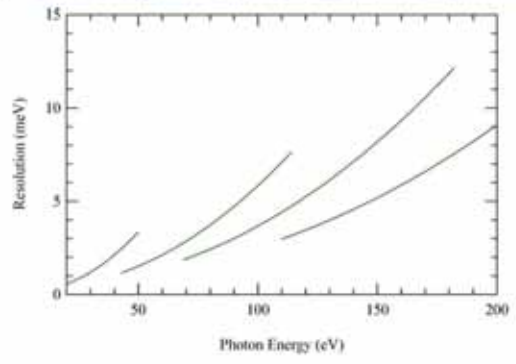



First Edition
Hamburg, June 2004

# List of Authors

Michael Rübhausen, Benjamin Schulz, Katrin Buth,
Joakim Bäckström, Jörg Kunze,

Institut für Angewandte Physik und Zentrum für Mikrostrukturforschung,
Universität Hamburg, Jungiusstraße 11, 20355 Hamburg, Germany

Ruben Reininger,

SAS - Scientific Answers and Solutions,
5708 Restal Street, Madison, WI 53711, USA

Joseph Nordgren, Johan Söderström, Jan-Erik Rubensson,

Physics Department, Uppsala University,
Box 530, 75121 Uppsala, Sweden

Lars Börjesson,

Department of Applied Physics, Chalmers University of Technology,
Kemigarden 1, Fysikgränd 3, 41296 Göteborg, Sweden

Peter Abbamonte,

SUNY Stony Brook, Brookhaven National Laboratory,
Upton, NY 11794-3800, USA

S. Lance Cooper,

Department of Physics and Materials Research Lab,
University of Illinois at Urbana-Champaign,
1110 West Green Street, Urbana, IL 61801-3080, USA

Michael Martins, Alexander Föhlisch, Wilfried Wurth,

Institut für Experimentalphysik, Universität Hamburg,
Luruper Chaussee 149, 22761 Hamburg, Germany

Josef Feldhaus, Jochen Schneider

HASYLAB/DESY,
Notkestraße 85, 22603 Hamburg, Germany

# Acknowledgements

We appreciate many discussions with

Ulrich Merkt,

Miles V. Klein,

David E. Moncton,

George A. Savatzky,

John Hill,

Young-June Kim,

Elke Plönjes,

Rolf Follath,

and Rolf Treusch.

We gratefully acknowledge financial support by

the Helmholtz-Gemeinschaft Deutscher Forschungszentren (HGF) through the Helmholtz Research Center 'Nanostructure Research on Functional Materials with Short Coherence Lengths at the TTF-VUV-FEL',

the Deutsche Forschungsgemeinschaft (DFG) via the Emmy-Noether program (Ru 773/2-1, Ru 773/2-2, Ru 773/2-3),

and the HASYLAB/DESY.

# Contents

# 1. Introduction

This technical design report describes the characteristics of a novel VUV-Raman spectrometer that is to be established at the VUV-FEL (vacuum-ultraviolet free electron laser) of the TESLA Test Facility 2 (TTF-2) at HASYLAB/DESY in Hamburg. Raman spectroscopy is a major optical method that has been commonly used for a long time in the visible spectral range and in the deep ultraviolet. The VUV-FEL of the TTF-2 and the future European X-Ray Laser XFEL at DESY enable Raman spectroscopy in the VUV and XUV range with unique spectral, spatial and temporal resolution. With an effective time resolution of 1 ps and an energy resolution of 2 meV the spectrometer will reach the Heisenberg limit $\Delta E \cdot \Delta t = \hbar$ and thus provide maximum information about the dynamical properties of solids and soft matter. Experiments related to physics, biology, chemistry, and medicine shall demonstrate the capability of the spectrometer and the VUV-FEL. Examples are given in chapter 2.

The VUV-FEL of the TTF-2, which is briefly presented in chapter 3, offers unparalleled possibilities for the investigation of condensed matter. Examples for the outstanding properties are high spectral intensity, high brilliance and high time resolution. At a wavelength of 30 nm photon pulses with a duration of 50 fs and a photon number of $6 \times 10^{13}$ can be generated in the femtosecond mode. One bunch train can contain up to 7200 pulses with a separation of 111 ns. Thus, with a repetition rate of 10 Hz up to 72000 pulses per second are possible. The energy range of the photon pulses reaches from 20 to 200 eV with a resolution of 0.5 eV before and 2 meV after the primary monochromator that is described in chapter 4.

The techniques for spectroscopy in the VUV spectral range differ from those in other spectral ranges. Conventional spectrometers from the visible to the upper VUV range use mirrors in normal incidence in order to limit aberrations. Spectroscopy in the VUV range requires grazing incidence optics. So far, only the use of single stage instruments with limited stray-light rejection and resolution has been possible. The high brilliance of the VUV-FEL permits the use of double monochromators. Therefore, the VUV-Raman spectrometer consists of a novel high-resolution double monochromator with parabolic mirror segments. This guarantees optimal stray-light rejection, ultimative resolution and high throughput. The specifications and the feasibility of the double monochromator are described in detail in chapter 5, which is the main part of this report.

# 2. Science

Raman spectroscopy analyzes inelastically scattered light that originates from atoms, molecules or quasi particles in solids such as optical phonons, magnons, plasmons or electronic excitations. Thus, it reveals valuable information on the properties of matter. It has been successfully employed for years in the visible spectral range and in the deep ultraviolet. With the VUV-FEL and the future XFEL Raman spectroscopy with unique spectral, spatial and temporal resolution will be possible in the VUV and XUV range.

The VUV-Raman spectrometer will make excellent use of the specific features provided by the VUV-FEL and there are various fields of physics, chemistry, biology and medicine that will benefit from it. For example, functional materials such as high-temperature superconductors, systems with colossal magnetoresistance, glasses, and bio-organic matter can be studied on shortest time and length scales. The resolutions of energy and time approach the Heisenberg limit $\Delta E \cdot \Delta t = \hbar$. High spatial resolution is achieved by combining reflective with diffractive optics (photon sieves). In the following sections we give a short overview of the research on strongly correlated materials and deliver an insight into the fields of atoms and molecules as well as biophysics.

## 2.1 Strongly Correlated Materials

Many-body problems in solids can be mastered by effective quasi-particle pictures that include interactions of particles by introducing an effective quantity. For instance, the difference between the effective mass and the free electron mass depicts the strength of the interaction with the solid. This yields new quasi-particle excitations such as polarons. In particular, classical semiconductors, insulators and metals are described successfully. But there are phenomena like the superconductivity, the colossal magnetoresistance and the fractional quantum Hall effect that indicate new states that have little relation to the properties of a single particle but are predominantly due to interactions [1].

Also metal-insulator-transitions in systems with strong electron-electron interaction cannot be described by a single-particle approximation [1]. Examples are cuprate-perovskites such as $YBa_2Cu_3O_{6+x}$ and manganate-perovskites such as $La_{1-x}Sr_xMnO_3$. The high-temperature superconductivity and the colossal magnetoresistance occur for nearly half-filled strongly correlated Hubbard bands [2, 3, 4]. Optical spectroscopy is well suited for the investigation of the various ordering states in these systems [5, 6].

In strongly correlated systems the mechanisms that develop a macroscopic order from short-range correlations can be probed on local and global length scales by a combination of different optical experiments. For example, this holds for magnetic

correlations in cuprates or for the development of the charge-ordered state in manganites [7, 8]. Recently the formation of the charge-ordered state in cuprates and manganites has been studied more extensively. In this case the optical methods revealed valuable information on the interplay of low- and high-energy properties as well as optical anisotropies. These anisotropies have been verified by optical microscopy of charge-ordered domains at low temperatures [7]. In general, direct methods like optical microscopy [7], electron microscopy [9] and scanning probe methods [10] facilitate the interpretation of the observed effects.

Spectroscopic techniques from the VUV to the deep UV spectral range allow to obtain information on ultra-short time and length scales. Therefore they are and will become even more decisive for the understanding of novel phenomena in materials such as colossal magnetoresistance in manganites, high-temperature superconductivity in cuprates or spin-orbit related instabilities in vanadates. As an example figure 2.1 shows resonant soft X-ray emission and inelastic light scattering in the UV in comparison. In both cases the spectra change drastically with the incident photon energy. The rich low-energy spectrum ($\leq$ 100 meV) excited in the UV - in this example due to the superconducting order parameter - is only revealed because of resonant excitation, high stray-light rejection and high resolution. The two black arrows in figure 2.2 depict multi-phonon excitations excited by soft X-ray radiation in hydrocarbons. It is evident, that these experiments again would benefit from higher resolution and better stray-light rejection.

With the free-electron laser also intrinsic time and length scales of modern semiconductor devices become accessible. Interactions of elementary excitations like phonons, magnons, and orbitons on these scales are of crucial importance in correlated materials. Understanding of the bulk as well as thin films is mandatory for the development of this field. New states of matter have been already reported that are not related to the bulk behavior alone, but also to its interactions with boundaries, pinning potentials, and strain [10, 14]. These effects influence the performance of possible devices like the spin transistor and non-volatile memories. In particular, this requires the control of the bulk properties and comparison with artificially patterned nanostructures. With the VUV-FEL it will be possible to study how imprinted nanostructures tune the bulk properties.

Photons from a broad spectral range, as they can be achieved by a combination of large and small scale facilities, have provided a wide variety of information about charge, spin, lattice, and orbital degrees of freedom that drive the physics of strongly correlated systems. Local and global ordering phenomena such as charge and orbital ordering as well as phase separation effects in manganites or cuprates determine the dynamic properties on time scales that range from seconds to femtoseconds and in an energy range from well below one milli-electron volt to several electron volts. We aim for inelastic photon scattering with a resolution of a few meV in the energy range from 20 to 200 eV for studies of excitations such as phonons, electron/hole pairs, and excitons.

X-ray emission and X-ray resonant Raman scattering provide a local probe of the electronic structure and all elementary excitations that modulate it. With these

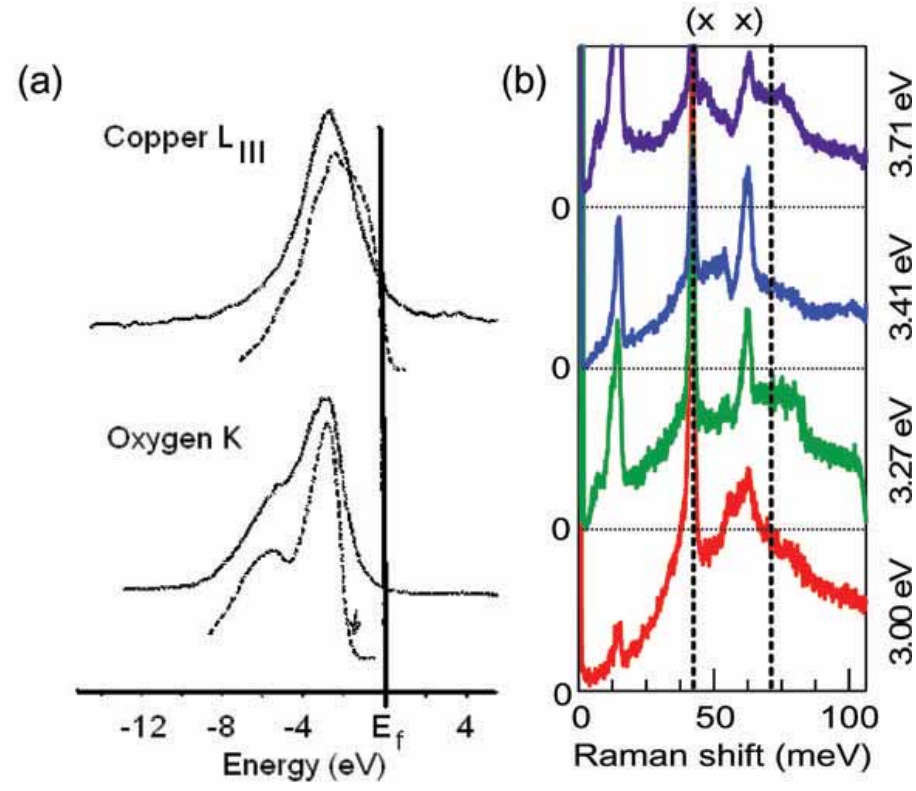


**Figure 2.1:** Soft X-ray emission data taken at an energy of 970 eV and UV-resonance Raman data from the high-temperature superconductor $YBa_2Cu_3O_7$. (a) The spectral features between 1 and 12 eV relate to excitonic states of the two elements of the copper-oxygen planes. (b) Low energy dynamics in the superconducting state between 1 and 100 meV. A number of $YBa_2Cu_3O_7$ specific phonon modes (sharp features) and the electronic background are shown. The broad features at 45 meV and at 65 meV are distinct contributions to the gap feature representing the superconducting order parameter. The energies on the right axis denote the incident photon energies used for the resonance experiment. Note, that the phonon as well as the electronic background change drastically when the incident photon energy is changed between 3 and 4 eV. The sharp intensity increase at 0 meV is the Rayleigh line that represents elastic scattering. From [11, 12].

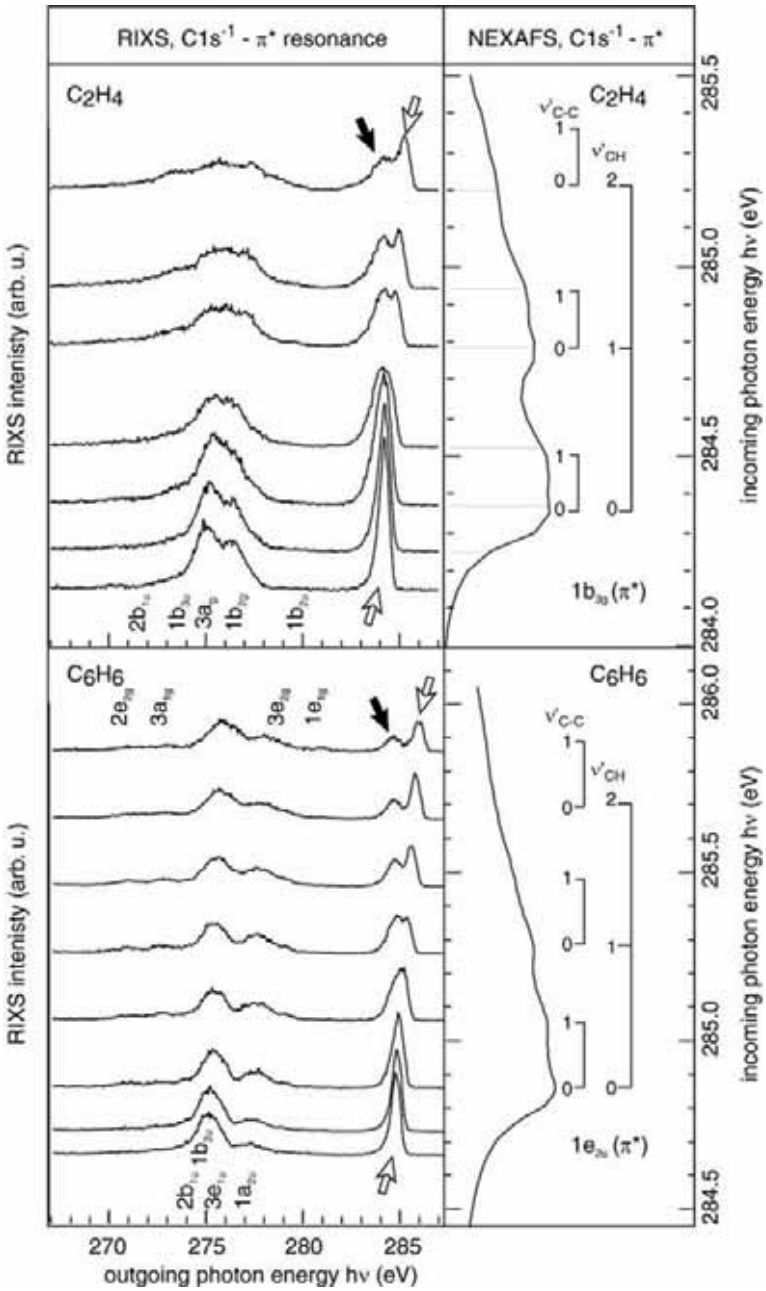


**Figure 2.2:** Resonant inelastic light scattering on $C_2H_4$- and $C_6H_6$-films as a function of the incident photon energy. Note that close to the incident photon peak one observes weakly dispersing features (black arrows) that represent multi-phonon excitations. The white arrows indicate the elastically scattered light. From [13].

methods it is possible to study extremely thin films that are only a few unit cells thick. As photon-in/photon-out techniques, X-ray emission and X-ray resonant Raman scattering are also able to probe to a distinct depth below the surface and thus enable the study of buried structures. The penetration depth is tuned by the incident photon energy. Thus, it is possible to separate the electronic structure of the surface from that of the bulk. For instance, this is important for strongly correlated oxides where the near-surface stoichiometry is difficult to control and where the surface behavior of order parameters is under debate. It is also advantageous for multilayer systems in semiconductor devices or magnetoelectronic applications.

Since soft X-ray emission has a low yield, it has to await bright sources for its broader exploitation. It is one of the few non-destructive experimental techniques that benefit directly from the increase of brightness of present and future synchrotron radiation sources. However, even at third generation synchrotron radiation sources, resolution has to be traded off for intensity. Accordingly, this area of science is expected to take a leap with a free-electron laser from the VUV to the soft X-ray range. With the free-electron laser and new improved optical systems it is technically feasible to achieve a spectral sharpness of a few meV for the photons behind the primary monochromator as well as for the resolution of the VUV-Raman spectrometer. This resolution is necessary to resolve spectroscopic features near the Fermi energy that determine the dynamic properties of the electron system in a solid.

The energy range and the high resolution of the new spectrometer provide a means to resonantly excite the Cu or Mn orbitals involved in the chemical bonding while studying low-energy excitations like phonons and superconducting gaps or high-energy excitations like orbitons and polarons. The high spatial resolution enables local studies, for example, of magnetic flux lattices in cuprate superconductors with high critical temperatures. The time structure of the photon pulses delivered by the free-electron laser provides an excellent tool for time-resolved probing of relaxation dynamics and couplings. This is of great importance for a better understanding of these materials.

## 2.2 Atoms and Molecules

Atomic and molecular physics provide the key for our understanding of the interaction between photons and matter. The experimental determination of fundamental parameters, such as transition energies and cross sections, allows to test advanced theories. Basic theories on electron correlations and dynamics can be verified by applying resonant inelastic soft X-ray scattering to simple atoms and molecules. Since different elements have different absorption edges, this method is element-specific. Thus, it is posssible to highlight specific atoms in complex compounds. The resonance energies for many atoms and ions lie within the photon energy range of the VUV-FEL at the TTF-2.

The interpretation of the spectra is often hampered by overlapping lines due to

satellite transitions or close lying core levels. One reason for these problems is the use of broadband photon sources. Up to now, soft X-ray and VUV scattering experiments on atoms and molecules have been very scarce, because even the most modern synchrotron radiation facilities cannot provide the brilliance necessary to achieve a sufficient spectral quality. Hence, these experiments will greatly benefit from the VUV-FEL which provides high brilliance and photon beams with considerably smaller bandwidths.

The few studies that have been performed in the VUV and soft X-ray range have addressed also fundamental questions in quantum mechanics. For example, it has been demonstrated that, contrary to the intuitive expectation, the localization of the core hole in a homonuclear diatomic molecule does not break the inversion symmetry [15]. The relaxation of the symmetry selection rules due to vibronic coupling in polyatomic molecules has been used to gain information on the dynamics in the range of femtoseconds [16, 17].

A classical experiment in order to test new synchrotron radiation sources is the study of double excitations in helium [18, 19, 20, 21]. These excitations lead to very intricate spectra. Since double excitations can proceed only by electron-electron correlation, the helium atom is commonly used as testing ground for correlation theories. For incident photon energies above 24.6 eV the helium atom can be singly ionized. The binding energy of the second electron is 54.4 eV. Double ionization of helium by a single photon becomes possible for photon energies higher than 79 eV. The energy is often not absorbed by one electron alone, but is shared by both electrons. At certain energies both electrons are excited to higher states. Such a doubly excited state is not stable. One electron can take over enough energy from the second one to become free, while the other drops to a lower level. This process is called autoionization. There is, however, also a non-negligible probability for radiative decay that often exceeds the one for autoionization [20]. In order to describe the experimental data, relativistic and radiative effects must be included [22]. Life times of doubly excited states lie in the range from some 10 fs to 200 ps. Some states may have even longer life times. Due to the variety of life-times, helium offers many possibilities for pump and probe experiments as well as time-resolved studies. For example, it would be easy to observe quantum beats. The VUV-Raman spectrometer enables measurements on helium atoms with enhanced resolution. Thus, previously unobservable states may be investigated.

With the high intensities that are provided by the VUV-FEL, it will become possible to study resonant inelastic soft X-ray scattering on dilute samples such as free atoms (not only rare gases, but also metals), ions, radicals and mass selected clusters. In particular, the physics of clusters is a rapidly growing field with influence on nanotechnology. Furthermore, non-linear optical effects like multi-photon excitations and dynamics of multiple excitations involving core levels can be studied for the first time. The high time resolution and the pulsed nature of the VUV radiation enable pump and probe experiments in order to study variations of the electronic structure on short time scales.

## 2.3 Biophysics

In recent years spectroscopic techniques for biophysical experiments have been advanced. An important new research area are functional biological systems on solid substrates such as nerve cells coupled to semiconductor chips [23] or biosensors. Lipid bilayers and biopolymers connect the biological system with the solid substrate. The functionality is determined by structure, elasticity and dynamic of these layers. These properties can be excellently studied by spectroscopic techniques. The high intensity and the high time resolution of the VUV-FEL at the TTF-2 and the XFEL will stimulate the further development of this field by introducing novel spectroscopic techniques. Existent synchrotron radiation sources provide time resolutions in the range of nanoseconds [24]. At the VUV-FEL the time resolution will lie in the order of 1 ps and thus enable the study of fast processes, for example, in proteins and biopolymers. By means of resonant Raman scattering single chemical elements can be traced in biological membranes.

Spectroscopy on biological tissues reveals valuable information that is particularly interesting for medical diagnostics. Up to now, however, the spectroscopic techniques face experimental limitations [25]. For example, the broad and strong autofluorescence in the spectral range from near infrared to the middle ultraviolet inhibits the observation of Raman scattering. In contrast, the VUV-FEL will enable element-specific excitations such as iron in haemoglobine or calcium and sodium in membranes. Another interesting research focus is the exploration of the human skin which is a very complex layer system. The optical properties are primarily determined by the keratin complex in the first 20 µm of the epidermis. Keratin is also a component of hair and fingernails [26]. Spectroscopy allows for the study of water contents [27], genetic expressions, chemical contamination and morphologic specifications such as filament structures. The results are not only valuable for biologists and chemists, but also for physicians [28] and the cosmetic industry [29]. The UV-Raman spectrometer UT-3 of the Institut für Angewandte Physik und Zentrum für Mikrostrukturforschung at the Universität Hamburg enables Raman measurements from the visible spectral range to the UV and upper VUV range. First experiments on human skin up to 5.2 eV have been performed [30]. The VUV-Raman spectrometer at the TTF-2 will make the whole VUV range accessible.

# 3. The VUV-FEL

The VUV-FEL at the TESLA Test Facility 2 (TTF-2) brings forth many promising experimental opportunities when compared to common photon sources such as synchrotron radiation sources or conventional lasers. The pulsed nature, the peak brilliance, and the phase coherence of the beam offer high spatial and spectral resolution enabling studies of non-linear optical effects and time-resolved experiments. When it comes to inelastic scattering, the VUV-FEL is expected to bridge the gap in energy-momentum space between the established techniques of light scattering (Raman and Brillouin scattering in the visible spectral range) on one end and inelastic thermal neutron scattering and inelastic X-ray scattering on the other (figure 3.1). This aims at the unification of inelastic light scattering techniques using photons from the near-infrared to the hard X-ray range. Thus, the inelastic light scattering techniques are extended from resonances with interband transitions to resonances of outer and deep core levels.

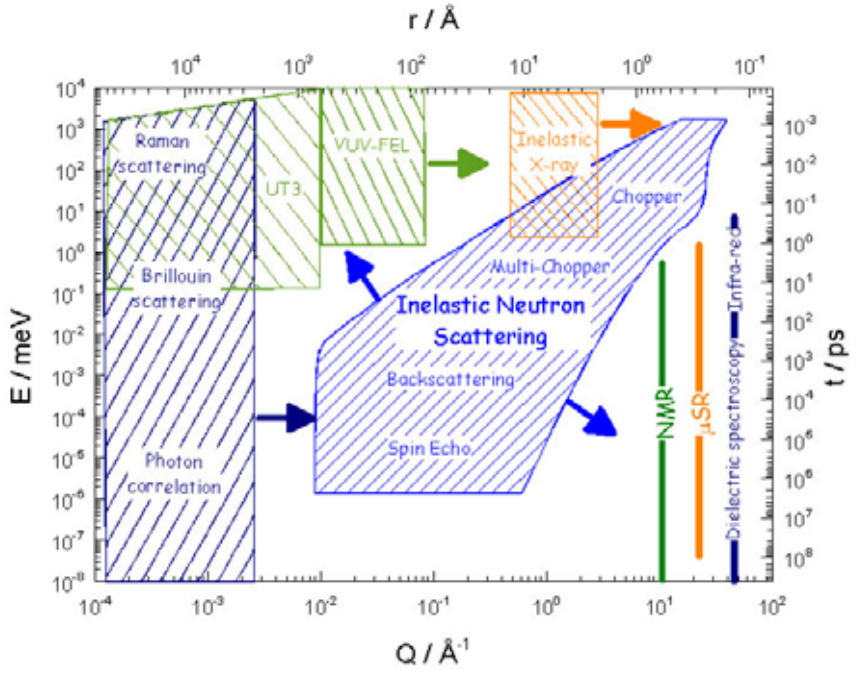


**Figure 3.1:** Energy-momentum space accessible with different techniques. The arrows mark the possible extensions to fill the 'missing areas'. For example the new high-resolution double monochromator at the VUV-FEL will bridge the gap between deep UV-Raman scattering and inelastic X-ray scattering. Already today the inelastic light scattering setup UT-3 in the group of Michael Rübhausen at the Institut für Angewandte Physik und Zentrum für Mikrostrukturforschung, Universität Hamburg connects the visible spectral range to the range covered with the VUV-FEL. From [31].

## 3.1 Design Parameters

The VUV-FEL at the TTF-2 is designed for covering continuously the wavelength range from 120 to 6 nm (10–200 eV). The high intensity of the radiation and the wavelength tunability is based on the SASE (Self-Amplified Spontaneous Emission) principle. Three modes of operation are envisaged: a short wavelength mode ($\lambda$ = 6–30 nm, pulse duration 200 fs), a long wavelength mode ($\lambda$ = 30–120 nm, pulse duration 1 ps), and a femtosecond mode ($\lambda$ = 30–120 nm, pulse duration 50–100 fs). Some design parameters are given in table 3.1. We concentrate on the energy range from 20 to 200 eV, but the VUV-Raman spectrometer will also work for energies down to 10 eV.

The VUV-FEL delivers the radiation in the form of bunches (pulses). One bunch train can contain up to 7200 pulses with a separation of 111 ns. Thus, with a repetition rate of 10 Hz, up to 72000 pulses per second are possible. The number of photons per pulse lies in the order of $10^{13}$–$10^{14}$. The peak brilliance is several orders of magnitude higher than that of third-generation synchrotron radiation sources.

## 3.2 Seeding Options

Due to shot noise, the photon beam of the VUV-FEL has typical bandwidths between 0.36 and 0.62 %. For example, at a photon energy of 95.4 eV a bandwidth of 0.46 % means that the photon beam has a width of 439 meV. This is several orders of magnitude too large in order to study inelastic light scattering with a high energy resolution of a few meV. To generate a high-resolution incident photon beam for such experiments, a high-resolution monochromator (see chapter 4) or seeding of the VUV-FEL is required.

A high-resolution monochromator behind the free-electron laser improves the energy resolution of the photon beam considerably, but it does not change the spiky structure of the photon pulse. This structure leads to strong fluctuations of the power densities on the sample and, accordingly, of the intensities of the inelastically scattered photons. Since the spiky structure differs from pulse to pulse, the characterization of every incident photon pulse is necessary. This causes severe limitations when integrating for longer time periods in case of weak signals. The time resolution of the photon beam depends crucially on the properties of the monochromator.

The ideal photon source would be a seeded VUV-FEL. A seeded free-electron laser provides extremely intense radiation that is coherent in space and time. Thus, it exhibits all the characteristics of classical lasers. In particular, high-resolution spectroscopy and all experiments that need full coherence would benefit from the improved beam properties. The seeding setup is an addition to a fully functioning SASE FEL. The description of the seeding project at the TTF-2 is based on the respective contribution [33] to the HASYLAB Annual Report 2001.

**Table 3.1:** Design parameters of the VUV-FEL at the TTF-2. Most of the values are taken from [32].

| | | **short wavelength mode of operation** | | | **long wavelength mode of operation** | |
|---|---|---|---|---|---|---|
| | Units | 6.4 nm | 13 nm | 30 nm | 60 nm | 120 nm |
| **Electron beam** | | | | | | |
| Energy | MeV | 1000 | 701.5 | 461.5 | 326.3 | 230.5 |
| Peak current | kA | 2.5 | 2.5 | 2.5 | 0.5 | 0.5 |
| Bunch length (FWHM) | µm | 120 | 120 | 120 | 590 | 590 |
| Bunch diameter (FWHM) | µm | 160 | 190 | 235 | 280 | 330 |
| Normalized emittance (RMS) | µm rad | $2\pi$ | $2\pi$ | $2\pi$ | $2\pi$ | $2\pi$ |
| Number of bunches per train | | 7200 | 7200 | 7200 | 7200 | 7200 |
| Bunch separation | ns | 111 | 111 | 111 | 111 | 111 |
| Repetition rate of bunch trains | Hz | 10 | 10 | 10 | 10 | 10 |
| **Undulator** | | | | | | |
| Period length | mm | 27.3 | 27.3 | 27.3 | 27.3 | 27.3 |
| Gap | mm | 12 | 12 | 12 | 12 | 12 |
| Peak magnetic field | T | 0.495 | 0.495 | 0.495 | 0.495 | 0.495 |
| Length of undulator module | m | 4.5 | 4.5 | 4.5 | 4.5 | 4.5 |
| Number of modules | | 6 | 6 | 6 | 6 | 6 |
| **FEL radiation** | | | | | | |
| Wavelength | nm | 6.4 | 13 | 30 | 60 | 120 |
| Photon energy | eV | 193.9 | 95.4 | 41.4 | 20.7 | 10.3 |
| Bandwidth (FWHM) | % | 0.36 | 0.46 | 0.62 | 0.45 | 0.57 |
| Spot size at undulator exit (FWHM) | µm | 140 | 170 | 210 | 240 | 350 |
| Angular divergence (FWHM) | µrad | 24 | 35 | 70 | 125 | 170 |
| Pulse duration (FWHM) | fs | 200 | 200 | 200 | 1000 | 1000 |
| Pulse energy | mJ | 0.56 | 0.49 | 0.38 | 0.32 | 0.28 |
| Number of photons per pulse | | $1.8 \times 10^{13}$ | $3.2 \times 10^{13}$ | $5.7 \times 10^{13}$ | $9.6 \times 10^{13}$ | $1.7 \times 10^{14}$ |
| Peak power | GW | 2.8 | 2.5 | 1.8 | 0.32 | 0.27 |
| Peak spectral brilliance | * | $2.4 \times 10^{30}$ | $8.1 \times 10^{29}$ | $2.0 \times 10^{29}$ | $2.4 \times 10^{28}$ | $8.0 \times 10^{27}$ |
| Average power | W | 40 | 35 | 27 | 23 | 20 |
| **Incoherent radiation** | | | | | | |
| Average power | W | 0.3 | 0.1 | 0.04 | 0.02 | 0.008 |

*in units of photons/sec/mrad$^2$/mm$^2$/(0.1 % bandwidth)

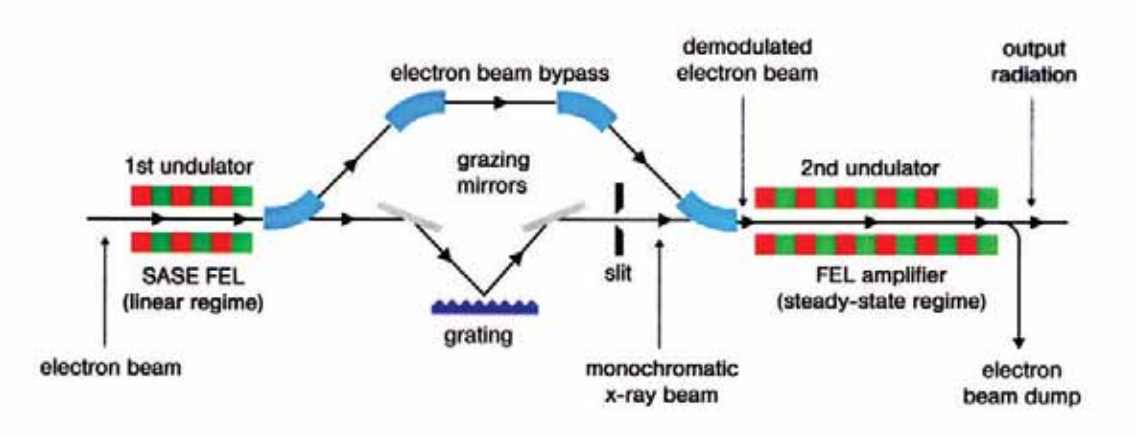


**Figure 3.2:** Scheme of the seeding setup at the TTF-2. From [33].

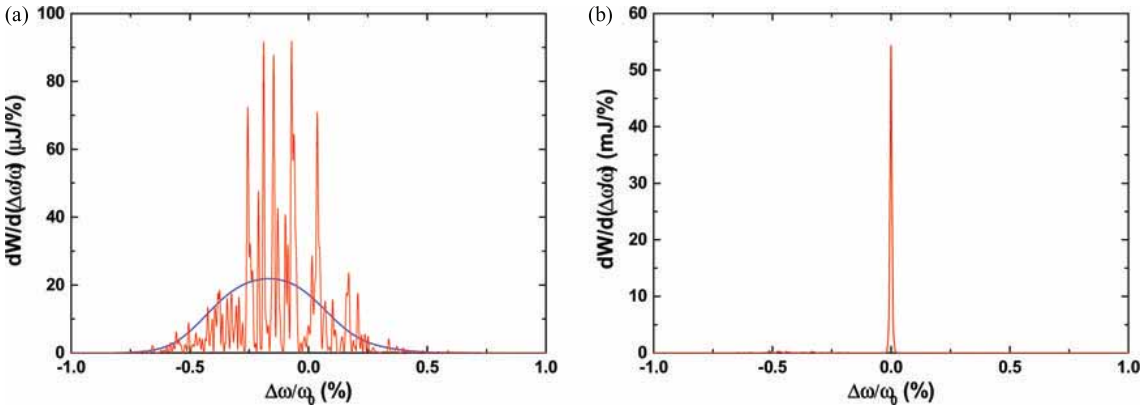


**Figure 3.3:** Simulation of the typical frequency spectrum of a single FEL pulse. (a) Spectrum behind the first undulator (SASE-FEL operating three orders of magnitude below saturation). (b) Spectrum at the exit of the second undulator (FEL amplifier). From [33].

The unseeded VUV-FEL consists of a single pass SASE-FEL that operates in the steady-state (saturation) regime. For seeding an FEL amplifier, the single pass SASE-FEL will be combined with a narrow-band monochromator. In this case, the SASE-FEL will operate in the linear (exponential gain) regime which is about three orders of magnitude below saturation. The general layout of the device is sketched in figure 3.2. In order to produce extremely intense and fully coherent radiation, the single pass FEL amplifier must be seeded by a coherent light beam resonant with the magnetic structure and collinear with the electron beam [34]. The coherent light beam must fulfill the following requirements: the photon wavelength has to be within the gain bandwidth of the FEL amplifier, the photon bandwidth has to be narrow enough to provide a coherence length as long as the electron bunch length, and the intensity has to be much larger than that of the shot noise originating from density fluctuations in the electron beam (spontaneous undulator emission along the first few gain lengths).

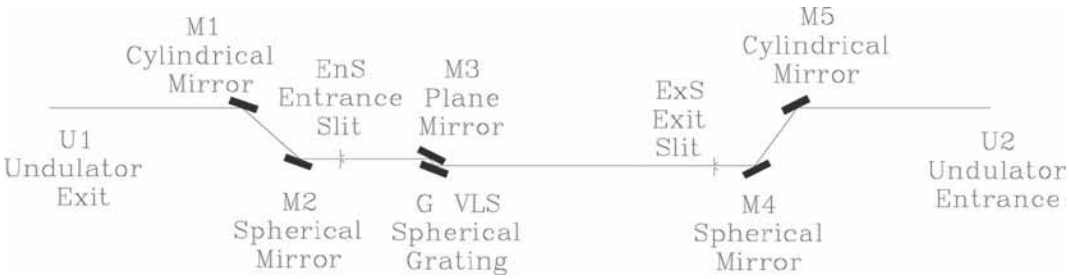


**Figure 3.4:** Photon beamline of the seeding setup at the TTF-2. It acts as a narrow-band filter that provides the coherent radiation seed which is amplified to saturation in the second undulator. From [33].

The first undulator in figure 3.2 is the SASE-FEL that produces intense but structured light pulses that are shown in figure 3.3(a). After the SASE-FEL the electrons and photons are separated. Due to the FEL process in the undulator the longitudinal density of the electron beam is modulated (microbunching). Therefore the electrons travel through a magnetic chicane that removes this microbunching. The photon beamline depicted in figure 3.4 consists of a varied line spacing (VLS) spherical grating monochromator with a pre-mirror and a pair of focusing mirrors on each side of the monochromator. The monochromator aims at a resolving power of $2 \times 10^4$. The optical system is designed to produce a 1:1 image of the complex conjugated wavefront at the entrance of the FEL amplifier, which is the second undulator. Thus, a longitudinal and transverse overlap between the seed pulse and the electron bunch is achieved. The optics were optimized for short wavelengths around 6.4 nm and will work satisfactorily up to about 60 nm. At 6.4 nm the overall efficiency of the beam line using carbon coated optics is around 10 %. This ensures that the monochromator delivers a coherent beam that dominates the shot noise in the second undulator. The second undulator amplifies the photon beam to saturation. The resulting spectral distribution is given in figure 3.3(b). Seeding increases the spectral brilliance by about a factor of 100. This means, that the output power of the seeded free-electron laser is concentrated in a single line which is about a hundred times narrower than the spectrum of the conventional SASE-FEL.

An exciting vision to further improve the beam properties of free-electron lasers is seeding with external lasers as proposed by the MIT/Bates X-ray laser concept [35]. According to this concept the electron beam is seeded with high harmonics generated by conventional optical lasers, for example a Ti:sapphire laser. Thus, spectral resolutions of about 1 meV or better can be achieved. It is possible to choose between seeding for an optimal energy resolution and seeding for an optimal time resolution. For example, once the frequency range for an excitation has been specified, the seeding for best time resolution and limited frequency resolution will enhance the possible time resolution in pump and probe experiments. For successful seeding the VUV pulses must be superimposed on the electron bunches with a temporal uncertainty of about 10 fs. This is one of the main challenges of the MIT project.

# 4. The Primary Monochromator

As described in the previous chapter, the bandwidth of the VUV-FEL is too large for inelastic light-scattering experiments that require a resolution of a few meV. For experiments that need such narrow bandwidths a high-resolution monochromator has been designed in a collaboration between the Universität Hamburg, BESSY, and HASYLAB. It is currently established at the TTF-2 by the group of Wilfried Wurth (Institut für Experimentalphysik, Universität Hamburg). Since this monochromator will provide the incident beam for the VUV-Raman spectrometer, we refer to it as primary monochromator.

The primary monochromator is a state-of-the-art plane-grating monochromator that uses collimated light [36]. It covers the energy range from 20 to 1000 eV. The basic layout is shown in figure 4.1. The plane mirror M1 deflects the beam of the VUV-FEL either into the monochromator beamline or into the non-monochromatized beamlines. The toroidal mirror M2 collimates the radiation in the vertical direction and focuses the light in the horizontal direction at the intermediate focus z. The mirror-grating unit, that consists of the pre-mirror M3 and the grating G, is placed

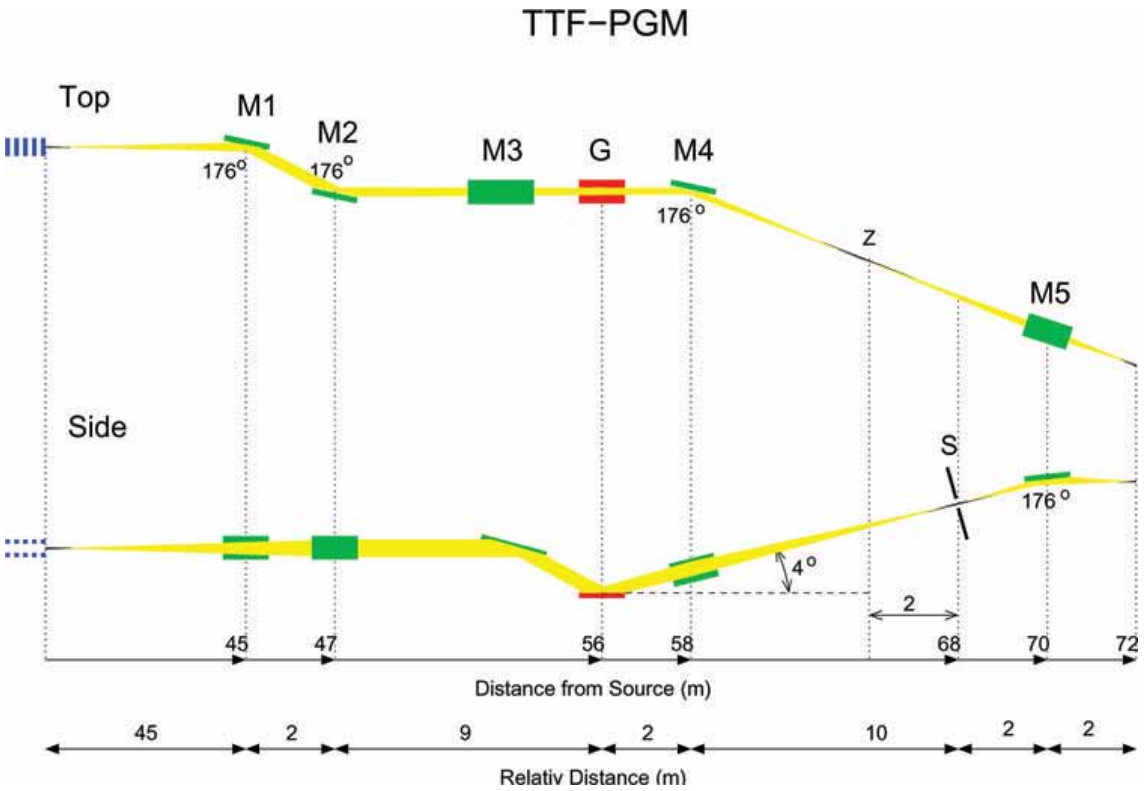


**Figure 4.1:** Basic layout of the high-resolution plane-grating monochromator. From [32].

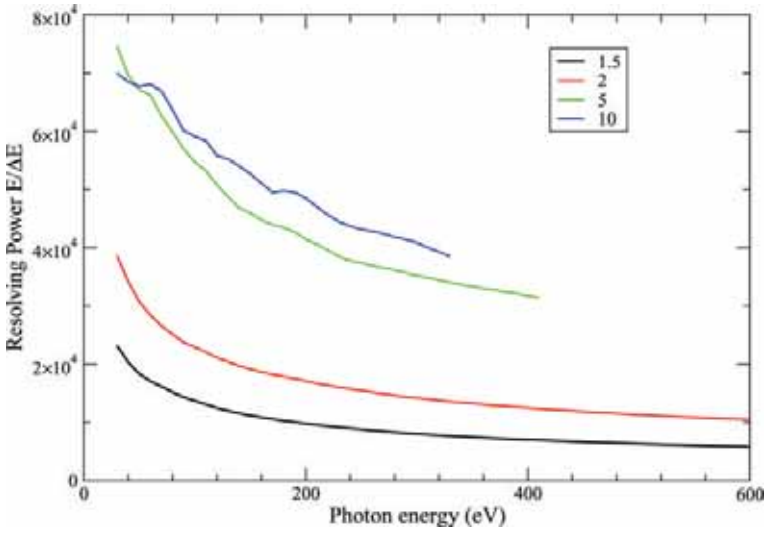


**Figure 4.2:** Resolving power of the monochromator beamline for four different values of the forgiveness factor $c_{\mathrm{ff}} = \cos\beta/\cos\alpha$ from 1.5 to 10 with the incident angle $\alpha$ and the diffraction angle $\beta$. For the calculations, a 1200 lines/mm grating, slope errors of 0.1 arcseconds for the spherical and plane optics as well as slope errors of 1 arcsecond for the cylindrical and toroidal mirrors have been assumed. The slit width has been varied.

in the usual SX700 mount [37]. In order to reduce the heat load on the pre-mirror, the dispersed beam behind the mirror-grating unit has an angle of 4° relative to the incoming beam. The switching mirror M4, located 2 m behind the grating, deflects the dispersed beam either to the experiment in the first branch or to the VUV-Raman spectrometer in the second branch. The beam exiting the primary monochromator exhibits astigmatism, this means that the horizontal and the vertical focus do not lie in the same point. This prevents the slit blades within the primary monochromator from overheating. The mirror M4 is a sagittal cylinder and focuses the radiation along the dispersion direction onto the exit slit for the selected branch. The focus point of the horizontal direction lies 2 m before the exit slit.

In the first branch, a refocusing mirror chamber equipped with a toroidal mirror M5 corrects the foci separation and focuses the monochromatized radiation onto the sample. The focus size is in the order of 100 µm$^2$. Figure 4.2 shows the resolving power $E/\Delta E$ that has been calculated by ray-tracing simulations. For the plane optics (mirrors M1 and M3, grating G) slope errors of 0.1 arcseconds and for the cylindrical and toroidal mirrors slope errors of 1 arcsecond have been assumed. The grating has 1200 lines/mm. At a photon energy of 100 eV and for a forgiveness factor $c_{\mathrm{ff}} = 10$, the maximum resolving power is $6 \times 10^4$ corresponding to a resolution of 1.7 meV. At a photon energy of 200 eV a similiar calculation yields a resolving power of $5 \times 10^4$ corresponding to a resolution of 4 meV. A similar resolution is expected for the second branch, that leads to the VUV-Raman spectrometer.

The VUV-Raman spectrometer requires a more complicated refocusing optics in order to achieve smaller spots on the sample. The refocusing optics that is proposed

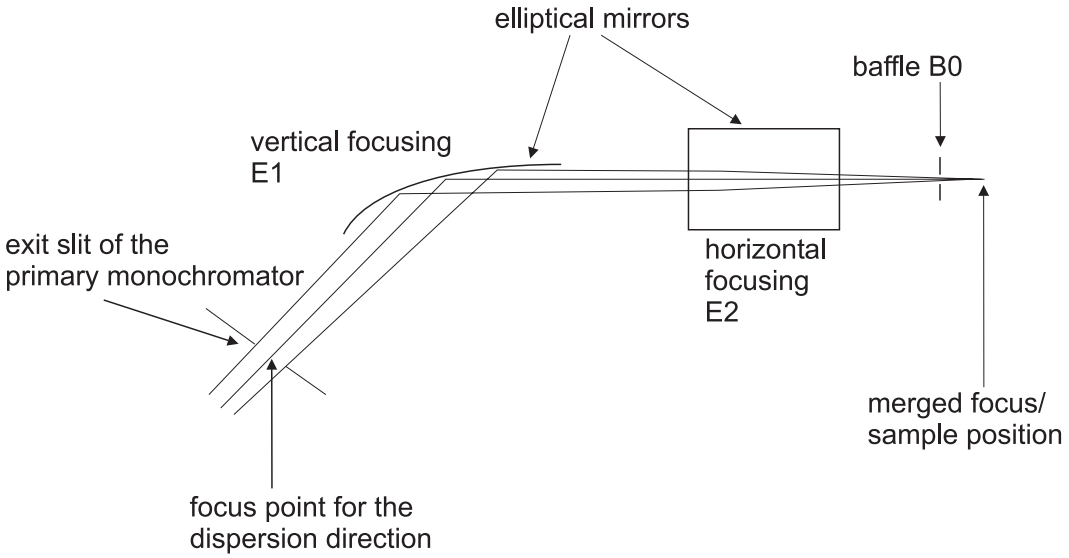


**Figure 4.3:** Sketch of the refocusing optics.

**Table 4.1:** Characteristic data of the elliptical mirrors of the refocusing optics.

| Name | Length × Width (mm × mm) | Magnification | Major Axis (mm) | Minor Axis (mm) | Incident Angle |
|---|---|---|---|---|---|
| E1 | 150 × 4 | 1/5.3 | 1250 | 79.9 | 85° |
| E2 | 33 × 16 | 1/14 | 2250 | 97.8 | 85° |

here aims at a spot size of 3 µm in the vertical (dispersion) and about 15 µm in the horizontal direction. At the focus position of the primary monochromator, the spot is fairly large in the dispersion direction. The exit slit in the focal plane of the primary monochromator confines the beam in the dispersion direction and thus generates the entrance image of the refocusing optics.

Figure 4.3 shows a sketch of the refocusing optics, that generates smaller spots and removes the astigmatism. It consists of a Kirkpatrick-Baez system [38] with two elliptical mirrors, one for the horizontal and one for the vertical (dispersion) direction. The first mirror E1 is located at a distance of 2.1 m from the exit slit of the primary monochromator. It images the exit slit and deflects the beam vertically by 10°. The second mirror E2 is located 0.1 m behind the mirror E1 and 0.3 m away from the sample. It images the intermediate focus z and deflects the beam horizontally by 10°. Some important parameters of the elliptical mirrors are given in table 4.1.

The vertical spot size on the sample is determined by the exit slit width and the slope errors of the refocusing optics. The horizontal spot size is mainly determined by the meridional slope errors of the mirrors M1, M2 and M4 and the slope errors

of the refocusing optics. Figure 4.4 shows the spot pattern at the sample position calculated by a ray-tracing simulation with the SHADOW code [39]. In the simulation 10000 rays with an energy of 100 eV have been sent through the primary monochromator with an exit slit width of 10 µm and a forgiveness factor $c_{\mathrm{ff}} = 5$. The value 170 µm for the spot size at the undulator exit and the value 35 µrad for the divergence have been taken from table 3.1.

Figure 4.4(a) shows the calculated spot pattern, when the optical elements have no slope errors. The expected spot size along the vertical (dispersion) direction is given by the ratio $10\ \mu\mathrm{m}/5.3 = 1.9\ \mu\mathrm{m}$ of the exit slit width and the demagnification of the mirror E1. Along the horizontal direction the expected spot size is determined by the product $170\ \mu\mathrm{m} \times (19/47) \times (1/14) = 4.9\ \mu\mathrm{m}$ of the spot size at the undulator exit and the magnifications of the mirrors M2 and E2. The values are in accordance with the ray-tracing simulation. This demonstrates that optical aberrations are negligible. The value of 8746 in the figure indicates that the transmission of the exit slit is 87 % at the given photon energy.

Figure 4.4(b) displays the spot pattern, when the slope errors of the monochromator elements are included in the simulation. Slope errors of 0.3 arcseconds for the meridian direction of the mirrors M2 and M4 and slope errors of 0.1 arcsecond for the grating G and the mirrors M1 and M3 have been assumed. The spot size in the vertical direction does not change, since only the slit is imaged. In the horizontal direction the spot is more than twice as large as in case of no slope errors. This is mainly due to the meridional slope error of the mirror M2. The slit setting and the slope errors yield an energy resolution of 2.2 meV. Since the focusing at the exit slit is impaired by the slope errors, the transmission decreases to 56 %.

For the simulation of the spot pattern displayed in figure 4.4(c), also the slope errors of the refocusing optics have been taken into account. The slope errors of the elliptical mirrors have been set to 0.3 arcseconds. The horizontal spot size stays almost the same, whereas the vertical spot size is more than twice as large as in the previous figure. Nevertheless, figure 4.4(c) demonstrates that a spot size of $3 \times 15\ \mu\mathrm{m}^2$ is achievable with the specified refocusing optics. A larger slope error of 1 arcsecond for the mirror E2 only increases the vertical beam size to 5.4 µm.

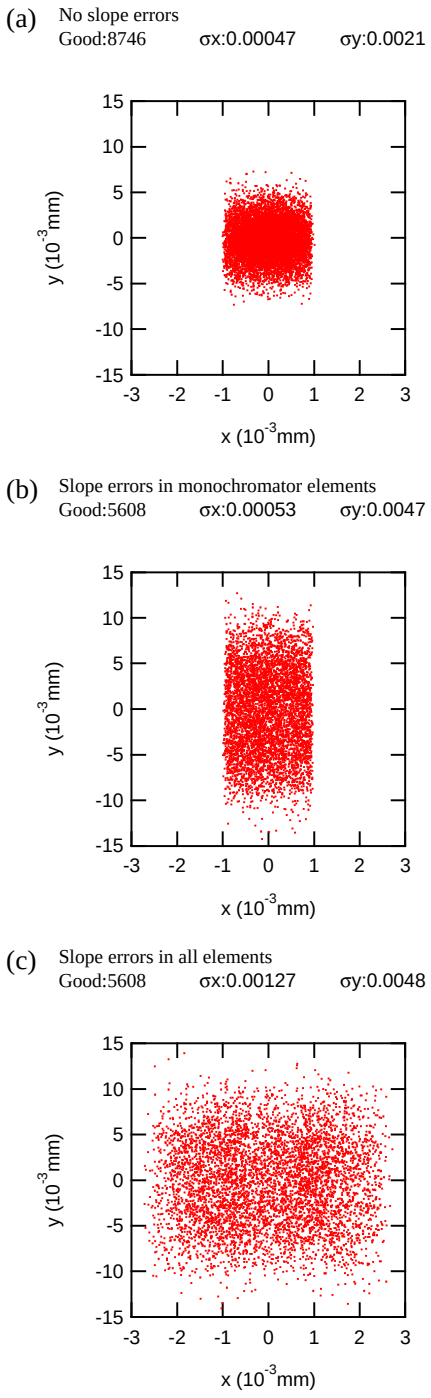


**Figure 4.4:** Spot patterns at the sample position for an incident photon energy of 100 eV and an exit slit width of 10 µm. The rms sizes of the spot $\sigma_x$ and $\sigma_y$ are given in mm. The dispersion direction is along the $x$-axis. (a) No slope errors are assumed for the optical elements. (b) The mirrors M2 and M4 have an rms slope error of 0.3 arcseconds along the meridian direction. The slope error of the grating G and the mirrors M1 and M3 is 0.1 arcseconds. (c) In addition to the slope errors of the monochromator elements, the slope error of 0.3 arcseconds along the meridian direction of the elliptical mirrors E1 and E2 is taken into account.

# 5. The VUV-Raman Spectrometer

Raman spectroscopy is well established from the visible to the upper vacuum ultraviolet spectral range. In this region the spectrometers use mirrors in normal incidence in order to limit aberrations. Table 5.1 shows technical data of several instruments for inelastic light scattering. By the use of double or triple monochromators a high energy resolution and a high suppression of stray light can be achieved. A good stray-light rejection enables measurements close to the Rayleigh line that represents the elastically scattered light. With the development of synchrotron radiation sources, inelastic light scattering has been extended from the VUV to the hard X-ray range. But compared to conventional lasers, even third-generation synchrotron radiation sources have much weaker brilliances. In order to achieve a sufficient photon flux, the bandwidth of the incident photons must be large. This limits the energy resolution. Moreover, spectroscopy in the VUV (below 165 nm) and XUV requires grazing incidence. Thus it has been only possible to use single stage instruments with limited stray-light rejection and resolution. These instruments are optimized for the study of Raman shifts larger than 100 meV of the scattered relative to the incident photon energy. The high brilliance of the free-electron laser makes experiments with an energy bandpass of only a few meV possible. The novel VUV-Raman spectrometer will be the first double-stage instrument for inelastic light scattering in the VUV and XUV range. In the following sections we describe in detail the characteristics, the design, and the feasibility of this instrument.

## 5.1 Characteristics of the VUV-Raman Spectrometer

The VUV-Raman spectrometer is intended to enable the study of various samples with different experimental requirements and to offer best possible resolution in combination with a high stray-light rejection. Spectroscopy in the energy range from 20 to 200 eV requires grazing incidence. Therefore, slope errors and surface roughness become more important. Due to lower reflection and grating efficiencies in this spectral range, the number of optical elements in a spectrometer is limited. The high brilliance of the VUV-FEL enables the use of a double monochromator that provides an enhanced stray-light rejection. Hence, the VUV-Raman spectrometer consists of a novel high-resolution double monochromator that is described in detail in section 5.2.

### 5.1.1 Stray Light Rejection

Many excitations are close to the energy of the incident photons, but their intensities are usually many orders of magnitude smaller than the intensity of the Rayleigh line.

**Table 5.1:** Instruments for inelastic light scattering in comparison with the new VUV-Raman spectrometer. Spectrometers in the low-energy range ($< 15\,\mathrm{eV}$) operate in normal incidence (NI). Spectroscopy in the high-energy range ($\geq 15\,\mathrm{eV}$) requires grazing incidence (GI). The values for the energy resolution $\Delta E/E_0$ and the collected solid angle are taken for certain incident photon energies $E_0$ given in the fourth column.

| Name/Location | Stages/ Type | Spectral Range | Energy Resolution $\Delta E/E_0$ | Smallest Entrance Slit Image | Solid Angle ($\mathrm{rad}^2/4\pi$) |
|---|---|---|---|---|---|
| UT-1<br>University of Illinois<br>at Urbana-Champaign,<br>Illinois, USA | 3/NI | 1.8–3 eV | $2 \times 10^{-4}$ at 2 eV | 50 µm | $1.2 \times 10^{-2}$ |
| UT-3<br>Universität Hamburg<br>Hamburg, Germany | 3/NI | 1.5–7.4 eV | $3 \times 10^{-5}$ at 4 eV | 25 µm | $6.5 \times 10^{-2}$ |
| IUVS<br>ELETTRA<br>Trieste, Italy | 1/NI | 5–11 eV | $3 \times 10^{-6}$ at 9 eV | 25 µm | – |
| Callcott<br>SURF/NBS<br>Gaithersburg,<br>Maryland, USA | 1/GI | 15–1000 eV | $1 \times 10^{-3}$ at 135 eV | 100 µm | $1.76 \times 10^{-4}$ |
| Nordgren<br>MAX-lab<br>Lund, Sweden | 1/GI | 50–1000 eV | $1 \times 10^{-4}$ at 135 eV | 10 µm | $2 \times 10^{-6}$ |
| VUV-Raman<br>HASYLAB/DESY<br>Hamburg, Germany | 2/GI | 20–200 eV | $1.5 \times 10^{-5}$ at 135 eV | 3 µm | $1.5 \times 10^{-4}$ |

Therefore, the elastically or quasi-elastically scattered light has to be suppressed sufficiently. Although the direct reflex is absorbed by a beam dump inside the recipient, a substantial quantity of elastically scattered light enters the spectrometer. This light originates from sample defects such as grain boundaries, tiny surface scratches or deposits on the sample surface. Particularly, polycrystalline materials create a lot of elastically scattered light that is nearly homogeneously spread over a large solid angle. With a double monochromator that offers a high stray-light rejection, also such imperfect samples can be studied. This is important since many samples are not available as single crystals or epitaxially grown films. The VUV-Raman spectrometer will also enable the investigation of small single crystallites that are embedded in a polycrystalline matrix.

### 5.1.2 Spectral Resolution

A high spectral or energy resolution is a main characteristic of the VUV-Raman spectrometer. Along with a high stray-light rejection, a high energy resolution makes measurements close to the Rayleigh line possible. Such low-energy excitations are interesting because they dominate the thermodynamic properties of solids. Moreover, quasi-elastic responses from incoherent scattering due to disorder can be investigated. With a resolution of 2 meV excitations that are only 20 meV away from the Rayleigh line can be measured with sufficient accuracy.

### 5.1.3 Time Resolution

The study of temporal changes in the spectra requires a sufficient time resolution. The time resolution is determined by the duration of the incident photon pulses. The VUV-FEL delivers pulses with lengths in the order of 100 fs. The primary monochromator broadens the pulses approximately by a factor of ten, when it operates with high energy resolution. With a pulse length of 1 ps and an energy resolution of 2 meV the VUV-Raman spectrometer will approach the Heisenberg limit $\Delta E \cdot \Delta t = \hbar$. The high time resolution enables pump and probe experiments.

### 5.1.4 Spatial Resolution

The spatial resolution depends on the spot size. Today, typical spot sizes lie in the order of $10 \times 30$ µm$^2$. With a refocusing optics after the primary monochromator, spot sizes of $3 \times 15$ µm$^2$ will be possible for the VUV-Raman spectrometer. It is expected that the seeded VUV-FEL with an improved microfocusing option will provide even smaller spot sizes. Higher spatial resolutions below 100 nm can be achieved by combining reflective with diffractive optics such as photon sieves.

### 5.1.5 Solid Angle

As a second-order process in terms of the vector potential of the electromagnetic field, inelastic light scattering is generally a weak probe. The signal strengths are proportional to the scattering volume that is determined by the optical properties of the sample. Since the scattering volumes are usually small and the signals weak, it is necessary to collect a significant solid angle in order to obtain sufficient photon count rates. With normal-incidence optics (incident angle $= 0°$) the photons can easily be focused onto small focal points. Hence, with a collection optics, it is possible to collect large solid angles up to $6.5 \times 10^{-2}\,\mathrm{rad}^2/4\pi$ (see table 5.1). Grazing-incidence spectrometers collect a solid angle that is typically two orders of magnitude lower than that of normal-incidence spectrometers. In order to achieve high energy resolution, present soft X-ray instruments collect the light by a slit that is several millimeters away from the sample. Thus, only a small fraction of the solid angle is collected. The VUV-Raman spectrometer aims at a solid angle of $1.5 \times 10^{-4}\,\mathrm{rad}^2/4\pi$. This value is comparable with the solid angle of, for example, the Callcott instrument

(table 5.1) that, however, offers an energy resolution two orders of magnitude lower than that of the VUV-Raman spectrometer.

### 5.1.6 Momentum Resolution

The momentum $k = E_0/(\hbar c)$ of the incident photons varies between $k_{\min} = 0.0101$ Å$^{-1}$ for $E_0 = 20\,\mathrm{eV}$ and $k_{\max} = 0.1014$ Å$^{-1}$ for $E_0 = 200\,\mathrm{eV}$. The momentum transfer $q \approx 2k \sin\frac{\theta}{2}$ depends on the scattering angle $\theta$ between the directions of the incident and the scattered photons. Accordingly, the momentum transfer varies between $q \approx 0$ in the near-forward scattering and $q \approx 2k$ in the near-backward scattering configuration. Since the energy resolution $\Delta E/E_0$ of about $1.5 \times 10^{-5}$ is high, the momentum resolution depends only on the collected solid angle. The larger the solid angle, the lower the resolution of the scattering angle. For the VUV-Raman spectrometer an angular resolution of $\Delta\theta = 2°$ is expected. The momentum resolution is given by $\Delta q = k\,\Delta\theta \cos\frac{\theta}{2}$. In the forward-scattering configuration one obtains $\Delta q = 0.0004$ Å$^{-1}$ for $E_0 = 20\,\mathrm{eV}$ and $\Delta q = 0.0037$ Å$^{-1}$ for $E_0 = 200\,\mathrm{eV}$. These values are extremely low and thus yield high momentum resolutions.

A high momentum resolution and a high momentum transfer allow to obtain the maximum information of elementary excitations. For a photon energy $E_0 = 20\,\mathrm{eV}$ the maximum field of view $L$ is defined by the inverse momentum transfer $2\pi/q = 31\,\mathrm{nm}$ and the inverse momentum resolution $2\pi/\Delta q = 1571\,\mathrm{nm}$. For $E_0 = 200\,\mathrm{eV}$ it is $3\,\mathrm{nm} < L < 170\,\mathrm{nm}$. Therefore, the instrument is well suited for the study of quasi-particles in artificially or naturally micro- and nanostructured systems. Examples are correlated compounds with charge-ordered stripes that have a typical width in the order of a few unit cells. Since typical unit cell dimensions in solids range from 0.5 to 2 nm, quasi-particles with a correlation length of only a few unit cells already leave a clear footprint in the inelastic measurements.

It is possible to study quasi-particles with phase velocities $v = L/\Delta t$. A Fourier transformation yields a time scale $\Delta t = h/\Delta E$. For $E_0 = 200\,\mathrm{eV}$ the energy resolution is $\Delta E = 9\,\mathrm{meV}$ and for $E_0 = 20\,\mathrm{eV}$ it is $\Delta E = 0.6\,\mathrm{meV}$ (see section 5.2.4). Thus, the time scale ranges from 0.46 ps to 6.89 ps. For $E_0 = 20\,\mathrm{eV}$ this yields a velocity range from $4.5 \times 10^3\,\mathrm{m/s}$ to $2.6 \times 10^5\,\mathrm{m/s}$ and for $E_0 = 200\,\mathrm{eV}$ from $6.5 \times 10^3\,\mathrm{m/s}$ to $3.7 \times 10^5\,\mathrm{m/s}$. By reducing the energy resolution, even higher velocities become accessible. Typical phase velocities of optical phonons are about $2 \times 10^3$ to $5 \times 10^3\,\mathrm{m/s}$. Also acoustic phonons with lower phase velocities including soft modes ($\omega \to 0$) indicative for phase transitions as well as surface plasmons at inner or real surfaces are within the available range of the instrument.

## 5.2 High-Resolution Double Monochromator

The main part of the VUV-Raman spectrometer is a high-resolution double monochromator whose stages are operated in an additive mode. The first stage acts as entrance objective that collects a relatively large solid angle and reduces the stray-light by several orders of magnitude. The second stage is the spectrograph stage that

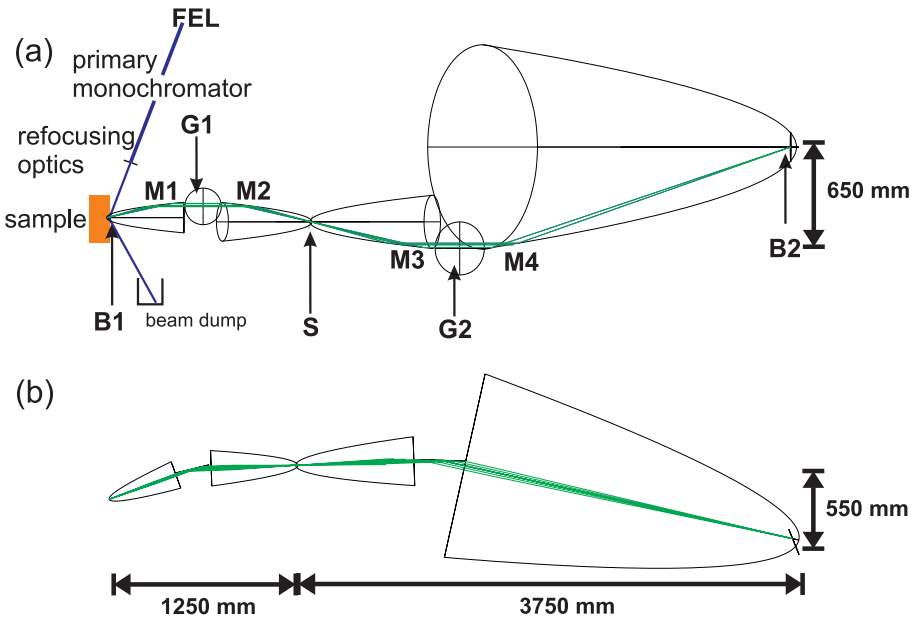


**Figure 5.1:** The high-resolution double monochromator in (a) the plane perpendicular to the dispersion direction of the gratings and (b) the plane in the dispersion direction. It consists of two gratings G1 and G2, four parabolic mirror segments M1–M4, a high-resolution slit S as well as two baffles B1 and B2.

disperses the light further onto the detector plane. The design of the double monochromator is depicted in figure 5.1. The length of first stage is 1250 mm, the length of the second stage 3750 mm. In both stages the parabolic mirrors deflect the beam perpendicular to the dispersion plane. Thus, the light is focused along the short axis of the parabola (sagittal focusing). This reduces the influence of slope errors (see section 5.2.4). The exit slit in the focal plane of the primary monochromator is re-imaged on the sample by the refocusing optics described in chapter 4. Hence, the exit slit simultaneously determines the spectral width of the incident photons and the vertical spot size on the sample. The illuminated spot on the sample can be virtually regarded as the entrance slit of the first stage.

The sample is located in the focal point of the first parabolic mirror M1. The aperture ratio of this parabola determines the maximum acceptance of the double monochromator. The maximum acceptance is $1.5 \times 10^{-4}\,\mathrm{rad}^2/4\pi$. The baffle B1 lets through only light within the solid angle that is collected by the first mirror. The light is collimated by the mirror M1 and directed to the grating G1. The dispersed light is refocused by the mirror M2 onto the intermediate slit S that is the entrance slit of the second stage. The magnification of the first stage along the horizontal axis is 1.67 corresponding to the ratio of the focal lengths of the mirrors M1 and M2. In order to obtain the magnification in the vertical direction, the ratio of the focal lengths must be multiplied by the ratio $\cos\alpha/\cos\beta$, with the incident angle $\alpha$ and the diffraction angle $\beta$. The magnification in the vertical direction varies between 0.76 and 1.2.

The double monochromator features two operation modes that are selected by adjusting the width of the intermediate slit. In the high-resolution mode a small slit width of about 3 µm creates a bandpass of about 20 meV and enables measurements with high energy resolution. The throughput is quite high, because the slit is located in the focal point of the second mirror, i. e. the beam waist. The slit opening is symmetric to the optical axis. In order to block the elastically scattered light the grating G1 is rotated, so that the mid-band frequency of the primary monochromator lies beside the optical axis. Since the desired frequencies lie near the optical axis, the images of the parabolic mirrors are almost free of aberrations. In the large-bandpass mode the slit width is several millimeters. Due to the large bandwidth of several eV, various excitations of quasi-particles can be detected simultaneously. Then, one can choose an interesting excitation and switch to the high-resolution mode, in which the excitation frequency is set on the optical axis. The large-bandpass mode offers high throughput and high time resolution but only limited energy resolution. The energy resolution depends on the spot size and the sample properties, because the image is not confined by the slit S. Hence, a high energy resolution requires an optimal interaction between the VUV-FEL, the primary monochromator, and in particular the refocusing optics. In order to achieve an optimal stray-light rejection the mid-band frequency of the primary monochromator is set on the optical axis, since in this mode the optical axis is obscured by the asymmetrically opened slit S.

The source point for the second stage lies in the slit plane S. The mirror M3 collimates the light and deflects it to the grating G2. Due to a higher groove density, the dispersion of the second grating is higher than that of the first grating. The mirror M4 images the beam onto the detector plane. The vertical magnification depends on the focal lengths of the mirrors M3 and M4 and on the ratio $\cos\alpha/\cos\beta$, with the incident angle $\alpha$ and the diffraction angle $\beta$. It varies between 0.4 and 1.8. The baffle B2 prevents unwanted beams from arriving at the detector.

In this design of the double monochromator imaging and dispersing are decoupled. The mirror positions are fixed, only the gratings have to be rotated in order to choose the wavelength. By using the gratings in zeroth order, any wavelength can be focused. This property will be used in the alignment process of the instrument.

### 5.2.1 Gratings

Each stage of the double monochromator comprises one planar reflection grating. The spectral resolution of a grating increases with the number of lines. The efficiency of a grating depends not only on its quality but also on the wavelength. For long wavelengths the grating acts like a mirror, i. e. most of the light is directed into the non-dispersed zeroth order. For short wavelengths the surface roughness becomes important and leads to lower efficiencies. The efficiency in a certain spectral range can be greatly improved by appropriate groove shaping (blazing) and an appropriate groove density. Blazed gratings direct much more light into some of the higher diffraction orders and, thus, make more efficient use of the light available. The gratings for the double monochromator are optimized for the first order. The blaze

**Table 5.2:** Characteristic data of the gratings.

| Name | Stage | Length × Width (mm × mm) | Coating | Spectral Range | Lines/mm | Blaze Angle | Efficiency |
|---|---|---|---|---|---|---|---|
| G1-1 | 1 | 200 × 50 | graphite | 20–50 eV | 300 | 2° | 30 – 53 % |
| G1-2 | 1 | 200 × 50 | molybdenum | 40–100 eV | 600 | 2° | 25 – 59 % |
| G1-3 | 1 | 200 × 50 | rhodium | 80–200 eV | 1200 | 2° | 22 – 52 % |
| G2-1 | 2 | 250 × 50 | graphite | 20–50 eV | 617 | 3.5° | 10 – 37 % |
| G2-2 | 2 | 250 × 50 | molybdenum | 43–114 eV | 1406 | 4° | 7 – 36 % |
| G2-3 | 2 | 250 × 50 | rhodium | 69–182 eV | 2250 | 4° | 7 – 30 % |
| G2-4 | 2 | 250 × 50 | rhodium | 110-200 eV | 3600 | 4° | 7 – 11 % |

angle is chosen to yield maximum efficiency in the middle of the desired energy range of the grating. In order to prevent scattering losses, the substrate rms roughness should be below 1 nm. The rms slope errors should be kept below 0.1 arcseconds in order to achieve the target energy resolution of 2 meV. Blazed gratings can be produced by mechanical ruling or holographic manufacturing followed by ion-beam etching. Holographic ion-milled master gratings usually offer the best quality. The gratings are coated with a material that is appropriate to the wavelength range.

To achieve both, high energy resolution and good efficiency, the energy region from 20 eV to 200 eV must be covered by several gratings. Three gratings for the first stage and four gratings for the second stage are needed. Their characteristics are given in table 5.2. Since the gratings have to operate under grazing incidence, they have to be quite large. The coating material has been chosen to guarantee an optimal reflectivity in the desired spectral range. Figure 5.2 shows the reflectivity of several coatings and figure 5.3 shows the efficiencies of the gratings. For energies from 20 to 185 eV the grating efficiency in the first stage lies clearly above 30 %. For energies from 185 to 200 eV it is still above 20 %. The grating efficiency in the second stage varies between 10 and 40 %. The gratings are used at a total included angle of 162°.

In addition the first stage should be equipped with a blank, that is a planar mirror. With a blank the first stage acts only as entrance objective, so that the double monochromator is operated as single-stage instrument. Assuming a graphite coating on the blank, the signal can be enhanced by a factor of 2–4. This option is intended for experiments for which high throughput is more important than optimal stray-light rejection.

The two grating mounts must be high-precision flexure mounts, that enable smooth rotations without slack. In order to achieve an energy resolution of 2 meV, the gratings must be positioned with an angular resolution that is of the same order of magnitude as the slope errors. An accuracy in the µm-range is required for translational displacements of the gratings. Mechanical stress that could cause damage or optical distortion at the submicron level should be minimized. Each grating mount

has to hold four gratings and should enable a fast and easy exchange as well as alignment of the gratings. Such grating mounts have to be designed especially for the high-resolution double monochromator.

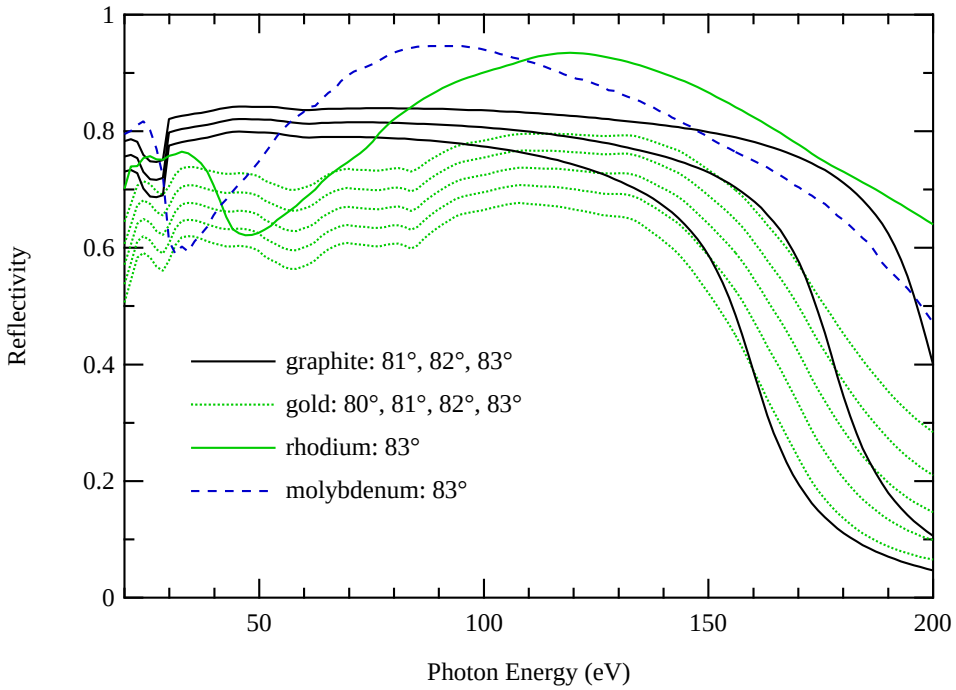


**Figure 5.2:** Reflectivity versus photon energy for different coating materials and incident angles. The larger the incident angle, the higher the reflectivity.

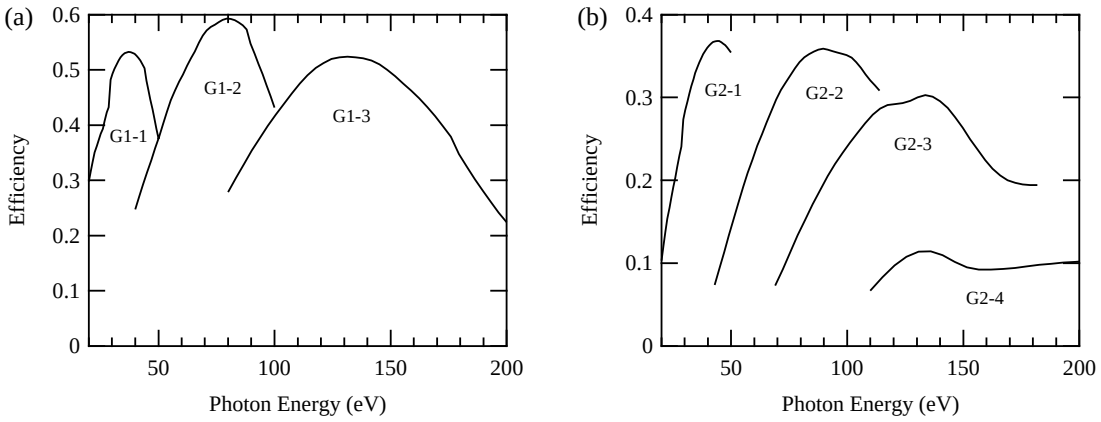


**Figure 5.3:** First-order efficiency of the gratings. (a) Gratings for the first stage. (b) Gratings for the second stage.

### 5.2.2 Mirrors

The four mirrors of the double monochromator will be off-axis parabolic mirror segments. The fabrication of parabolic mirrors is more difficult than that of spherical mirrors, but parabolic mirrors offer many advantages. For example, they are free of spherical aberration and thus focus a parallel beam to a point. 'Off-axis' means that the segments do not include the optical center of the mirror. Hence, the central part cannot obscure the beam path. Further advantages of off-axis parabolic mirror segments are the absence of coma, which normally occurs when the mirror operates under grazing incidence, as well as lower system sizes and weights, since only a part of the parabola has to be manufactured. The size of the mirrors must be fitted to the size of the gratings.

In order to prevent scattering losses, the surface may only have a roughness that is smaller than $\lambda/6 \approx 1\,\mathrm{nm}$. Since for grazing incidence even small slope errors lead to significant aberrations, the slope errors should be as small as possible. Targeted are slope errors below 0.5 arcseconds. The influence of slope errors on the energy resolution is discussed in more detail in section 5.2.4. Figure 5.2 shows the reflectivity of several coating materials, partly for different angles of incidence. The reflectivity increases with the incident angle. Larger angles, however, require longer mirrors in order to keep the acceptance constant. We chose an incident angle of 83° and graphite as coating material. Graphite provides a comparatively high and stable reflectivity over a large energy region. For energies up to 150 eV the reflectivity of graphite lies around 80–82 %. For higher energies it drops to 40 %. Thus, the total efficiency of all four mirrors lies between 41 % and 67 % for energies below 150 eV. For E = 200 eV it is about 2.5 %. The substrate material might be zerodur, which is a zero thermal-expansion ceramic. Some characteristics of the mirrors are summarized in table 5.3.

The mirrors are relatively large and heavy. The mirror mounts should enable a stress-free mounting, since mechanical stress caused by gravity sag and mechanical clamping forces can deform the optical surface. Such deformations would lead to a significant degrading of the wavefront quality. The lockings must assure a long-term stability of the mirrors's positions and orientations. Nevertheless the mirror mounts should facilitate a fast and easy alignment with an accuracy better than 0.5

**Table 5.3:** Characteristic data of the mirrors.

| Name | Stage | Length × Width (mm × mm) | Focal Length (mm) | Sagittal Radii (mm) beginning | center | end | Incident Angle |
|---|---|---|---|---|---|---|---|
| M1 | 1 | 208 × 10 | 300 | 63.1 | 73.1 | 87.1 | 83° |
| M2 | 1 | 200 × 10 | 500 | 108.0 | 121.9 | 131.9 | 83° |
| M3 | 2 | 280 × 15 | 700 | 151.1 | 170.6 | 184.7 | 83° |
| M4 | 2 | 288 × 45 | 2500 | 595.2 | 609.3 | 628.8 | 83° |

arcseconds for rotations and of a few µm for translational displacements. Therefore, the mirror mounts should be high-precision flexure mounts. Furthermore, the mirror mounts should minimize vibrational effects, withstand thermal variances and eliminate potential mirror drifts. The mounts must be purpose-built for the high-resolution double monochromator and should be matched to the mirrors already during fabrication.

### 5.2.3 Slits and Baffles

All slit blades must be adjustable with an accuracy better than 0.5 µm, since slit widths down to 1 µm are needed for the high-resolution mode. Translational displacements of the slits must be possible with a similar accuracy. Setting the slit width and the optical center line as well as displacing the entire assembly along and perpendicular to the optical axis should be easily accomplished. A safety mechanism is necessary in order to prevent slit blade collisions. The exit slit of the primary monochromator determines the vertical spot size. A confinement along the horizontal direction can be achieved by using a 4-jaw slit as exit slit or an additional horizontal slit. For the exit slit, water cooling might be necessary due to the high power densities of the VUV-FEL. This depends on the mirror M4 of the primary monochromator. If the horizontal and vertical focus of the mirror lie in the same point, the power density will be very high. In the current design the beam exiting the primary monochromator exhibits astigmatism. The slit S and the baffles of the high-resolution double monochromator do not require any cooling, because they are exposed only to the much weaker inelastically scattered light. All slits and baffles must be UHV compatible. Special locking mechanisms shall fix the settings and positions, so that they are stable. The baffles B0, B1 and B2 block unwanted beams. Since their apertures are several millimeters large, the accuracy of the blade positions must lie only around 100 µm.

The spectrometer is aligned in the near-forward scattering configuration. For that purpose, the slits and baffles can be provided with phosphor plates that make the beam directly visible or with gold nets. The directly reflected beam generates photo electrons in the gold and the photoemission current is proportional to the beam intensity. Furthermore, it should be possible to measure the photon flux on each of the electrically isolated jaws, in order to control the spot position relative to the optical axis.

### 5.2.4 Energy Resolution and Efficiency

The spectral or energy resolution of the high-resolution double monochromator depends on the spot size on the sample, on the width of the intermediate slit S, on the pixel size of the detector, and on the slope errors of the gratings and mirrors. In each stage, the first parabolic mirror generates a collimated beam incident on the grating. Accordingly, the spectral resolution limit due to the width $s_1$ of the

entrance slit is given by

$$\Delta\lambda_{s_1} = \frac{s_1 \cos\alpha}{gmr_1}, \tag{5.1}$$

with the incident angle $\alpha$, the groove density $g$, the diffraction order $m$, and the distance $r_1$ between the entrance slit and the first mirror of the stage. For the first stage the entrance slit width $s_1$ is given by the spot size on the sample. For the second stage it is given by the width of the intermediate slit S in the high-resolution mode or by the re-imaged spot size on the intermediate slit plane in the large-bandpass mode. Behind the grating the collimated beam is focused by the second paraboloid and the resolution due to the width $s_2$ of the stage exit slit is given by

$$\Delta\lambda_{s_2} = \frac{s_2 \cos\beta}{gmr_2}, \tag{5.2}$$

with the diffraction angle $\beta$ and the distance $r_2$ between the second paraboloid of the stage and the exit slit. The exit slit width $s_2$ of the first stage is equal to the entrance slit width of the second stage. For the second stage, the exit slit width is given by the pixel size of the detector. An rms slope error $\sigma_g$ of the grating leads to an rms spectral resolution of

$$\Delta\lambda_{g,rms} = \frac{2\sigma_g}{gm} \cos\left(\frac{\alpha+\beta}{2}\right) \cos\left(\frac{\alpha-\beta}{2}\right). \tag{5.3}$$

Slope errors in the order of 0.05 arcseconds are nowadays achieved for planar gratings.

Of crucial importance are the slope errors of the parabolic mirrors. If the mirror deflects the beam in the dispersion plane, the resolution term is proportional to the meridional slope error. If the mirror reflection plane is perpendicular to the dispersion plane, the resolution is proportional to the sagittal slope error multiplied by the 'forgiveness factor' $\cos\theta$. Here $\theta$ is the incident angle on the mirror. The optical design of the high-resolution double monochromator shown in figure 5.1 is based on sagittal focusing, because it reduces the influence of the slope error significantly. The beam is collimated before and behind the grating. Hence, the rms resolution limit due to a slope error $\sigma$ of the mirror is given by

$$\Delta\lambda_{m_1,rms} = \frac{2\sigma \cos\alpha}{gm} \cos\theta, \tag{5.4}$$

for the first mirror of each stage and by

$$\Delta\lambda_{m_2,rms} = \frac{2\sigma \cos\beta}{gm} \cos\theta, \tag{5.5}$$

for the second mirror of each stage.

Several manufacturers have been asked for the slope errors that can be achieved for parabolic mirrors with the specifications given in table 5.3. Erik Schoeffel from McPherson (USA) quoted that they could deliver paraboloids with an rms slope error

better than 1 arcsecond. Bernhard W. Bach from Bach Research (USA) stated that the slope errors of the mirrors could be measured down to 0.5 to 1 arcsecond. Hence, manufacturing with an rms slope error less than 1 arcsecond is possible. Andreas Seifert from Zeiss stated for the mirror M3 rms slope errors of 3 arcseconds in the sagittal direction and of 1 arcsecond in the meridian direction. The mirror M4 could be manufactured with rms slope errors of 1 arcsecond in the sagittal and 0.5 arcseconds in the meridian direction. For the other mirrors he gave no particulars, but declared that Zeiss was working on mirrors that are similar to the mirrors M1 and M2. The development of high-quality grazing-incidence mirrors for the VUV range is of general interest, since such mirrors are also needed for optical lithography. The mirrors of the second stage presumably can be verified by BESSY. The following calculations are based on the above information. The slope errors of all four mirrors are assumed as 1 arcsecond. As worst case, slope errors of 5 arcseconds are assumed for the mirrors M1 and M2, whereas the mirror M3 will have at worst a slope error of 3 arcseconds. The mirror M4 can be manufactured at worst with a slope error of 1 arcsecond.

Figure 5.4(a) displays the energy resolution limits that have been calculated according to the equations (5.1)-(5.3). The 'entrance slit width' has been set to 3 µm, which is the expected spot size in the dispersion direction on the sample. For the exit slit width 3.5 µm have been assumed. The rms slope error of the grating G1 has been set to 0.05 arcseconds. Three gratings cover the spectral range from 20 to 200 eV. The resolution due to the entrance slit is comparable with the one due to the exit slit. The limitations of the resolution due to the slope error of the grating G1 are significantly lower.

Figure 5.4(b) displays the resolution limits due to the slope errors of the mirrors M1 and M2 calculated by the equations (5.4) and (5.5). The resolution limits are proportional to the slope error. A comparison with figure 5.4(a) reveals that for slope errors of 5 arcseconds the limitations due to the mirrors are approximately twice as large as those due to the slits, whereas for slope errors of 1 arcsecond the limitations due to the slits are the most dominant factor. The total resolution of the first stage is obtained by the vector sum of the contributions due to the slits, the gratings, and the mirrors. It is depicted in figure 5.4(c) for two different slope errors of the mirrors. According to the vendors's statements we expect the resolution of the first stage to be close to the better estimate.

In the high-resolution mode the intermediate slit creates a new entrance image for the second stage. Hence, larger slope errors of the mirrors M1 and M2 or larger spot sizes on the sample do not influence the total resolution of the whole instrument, but decrease only the transmission. In the large-bandpass mode the intermediate slit is widely opened and cuts only the stray light. In this case the slope errors of the mirrors M1 and M2 increase the 'entrance slit' image of the second stage and thus decrease the total resolution.

Figure 5.5(a) shows the resolution limits due to an entrance slit width of 3.5 µm and an exit slit width of 5 µm, which is the intended pixel size of the detector. The rms slope error of the grating G2 has been set to 0.05 arcseconds. Four gratings cover

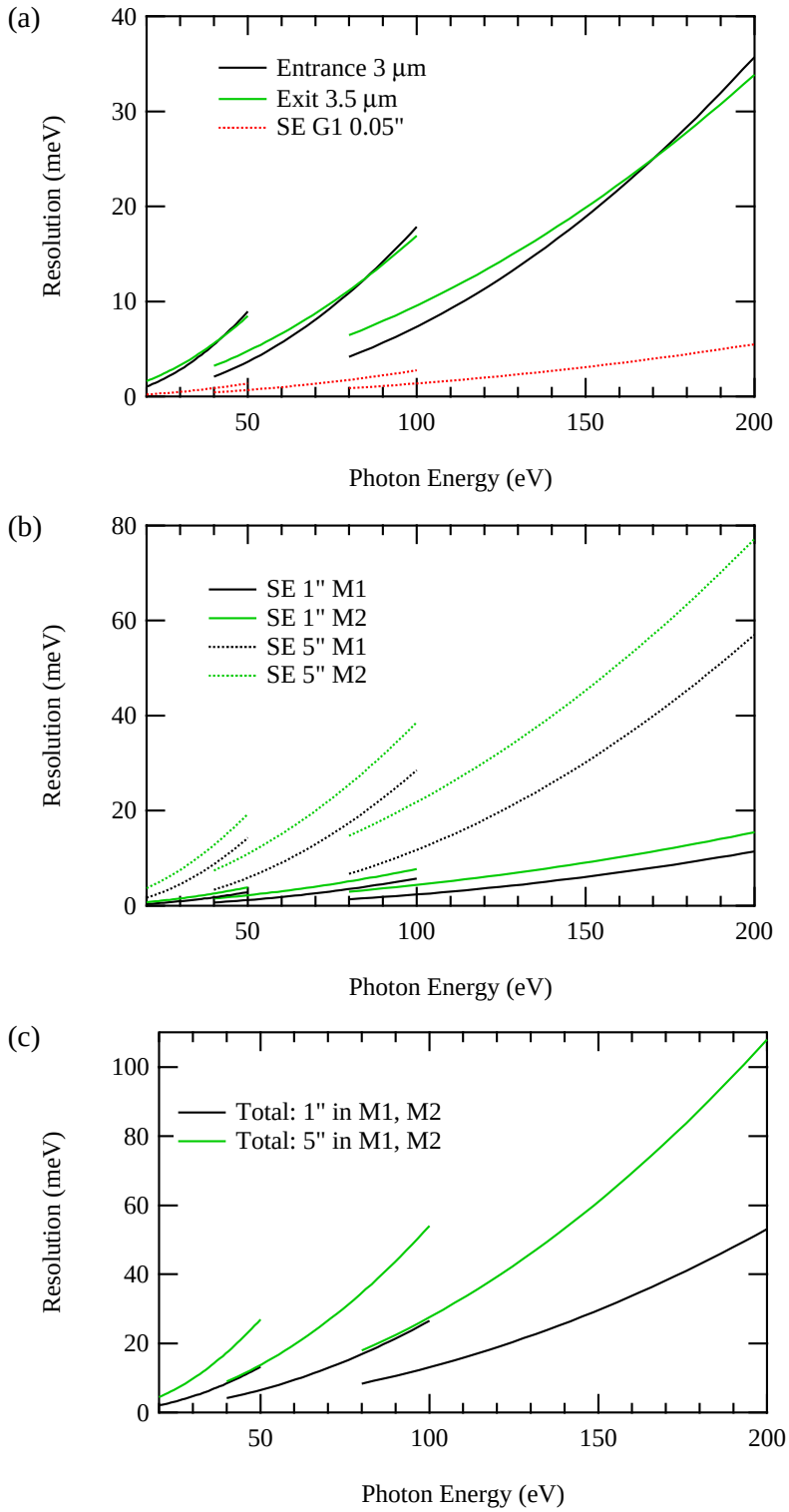


**Figure 5.4:** Energy resolution of the first stage. (a) Resolution limits due to the spot size on the sample (3 µm), the intermediate slit width (3.5 µm), and the slope error (SE) of the grating G1 (0.05 arcseconds). (b) Resolution limits due to the slope errors of the mirrors M1 and M2 (1 or 5 arcseconds). (c) Total resolution.

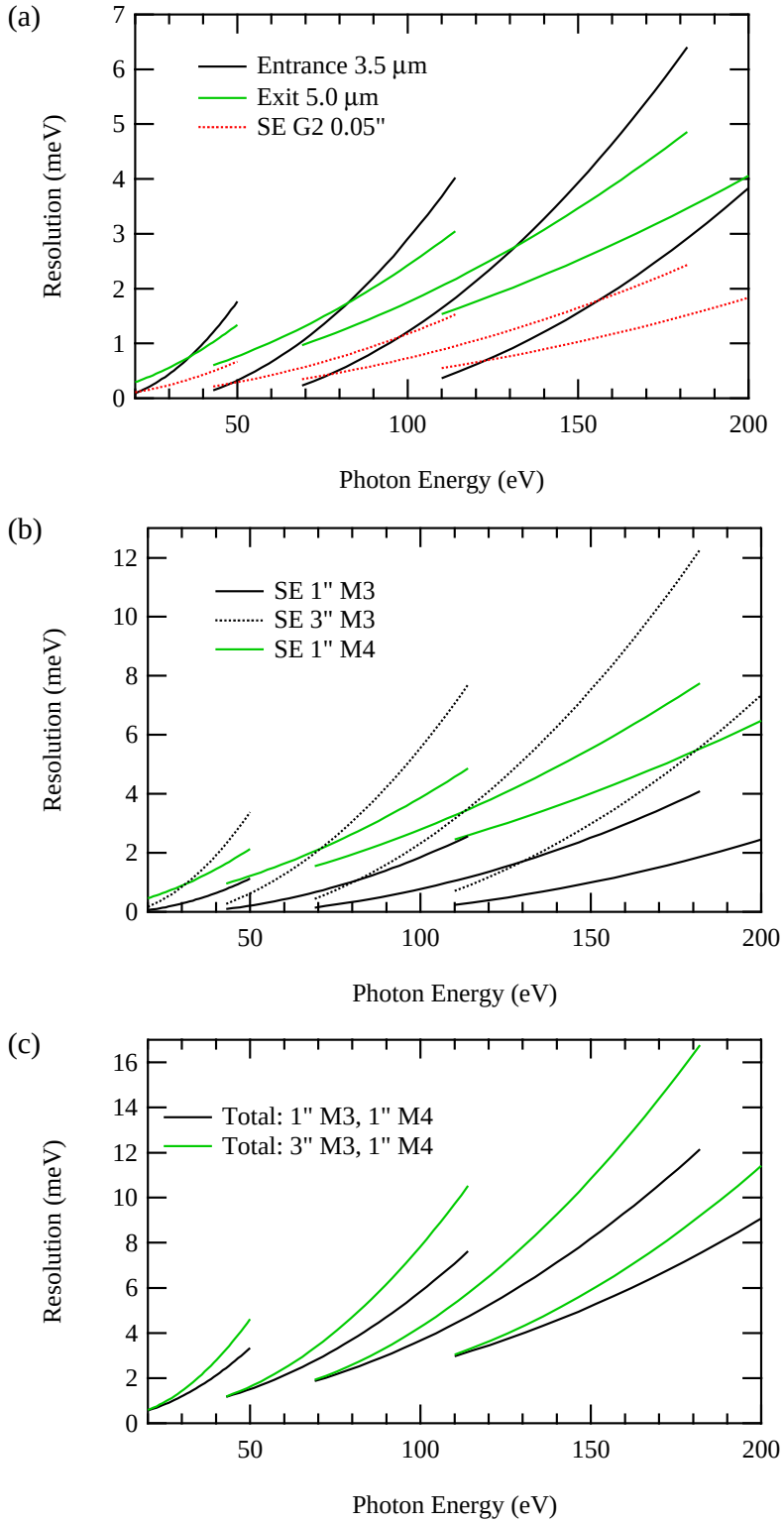


**Figure 5.5:** Energy resolution of the second stage. (a) Resolution limits due to the intermediate slit width (3.5 µm), the pixel size of the detector (5 µm), and the slope error of the grating G2 (0.05 arcseconds). (b) Resolution limits due to the slope errors of the mirrors M3 (1 or 3 arcseconds) and M4 (1 arcsecond). (c) Total resolution.

the spectral range from 20 to 200 eV. For each grating the limitation due to the exit slit dominates at low energies, whereas the limitation due to the entrance slit dominates at high energies. The contribution of the grating itself is less significant.

Figure 5.5(b) shows the resolution limits due to the slope errors of the mirrors M3 and M4. For slope errors of 1 arcsecond the resolution limits due to the mirrors are comparable to those due to the slits. The mirror M4 has more influence on the resolution than the mirror M3. The total resolution of the second stage is depicted in figure 5.5(c). Assuming a slope error of 1 arcsecond for both mirrors, the resolution is better than 3.8 meV for energies up to 100 eV and better than 5 meV for energies up to 150 eV. The energy resolution of the double monochromator depends crucially on the mirrors M3 and M4. Further improvements of the resolution can mainly be achieved by reducing the slope errors of these mirrors.

The resolution estimates depicted in the figures 5.4 and 5.5 have been checked by ray-tracing simulations with the SHADOW code [39]. The source has been assumed as a rectangle with a side length of 10 µm in the horizontal and 3 µm in the vertical (dispersion) direction. A number of 10000 rays is uniformly distributed over the solid angle 80 mrad (horizontal) × 24 mrad (vertical) that can be collected by the first mirror M1. Unless otherwise noted, the rms slope errors of the mirrors have been set to 1 arcsecond, the ones of the gratings to 0.05 arcseconds. We present results from a ray-tracing simulation with a photon energy of 100 eV. This means that the grating G1-3 (1200 lines/mm) and the grating G2-3 (2250 lines/mm) have been used for the first and the second stage, respectively. In the following figures the $x$-coordinate refers to the dispersion direction and the $y$-coordinate to the non-dispersion direction.

Figure 5.6(a) displays the spot pattern at the intermediate slit S, when the optical elements have no slope errors. The spot size in the non-dispersion direction is determined by the magnification, that is given by the ratio between the focal lengths of the mirrors M1 (300 mm) and M2 (500 mm). Since the source size is 10 µm, one expects a spot size of 16.66 µm in the non-dispersion direction. With a size of about 20 µm, the simulated spot is only slightly larger. The spot size along the dispersion direction corresponds to a resolution of 7 meV. This is in agreement with the results shown in figure 5.4(a) for the resolution limit due to the entrance slit. The effect of the slope errors is illustrated in figure 5.6(b). The spot size in the non-dispersion direction increases by almost 70 %, whereas the size in the dispersion direction increases only slightly. Thus, the resolution of the first stage is mainly determined by the slits. This has been also shown by the analytical results. Figure 5.7 shows that the total resolution of the first stage is indeed 13 meV, that is in accordance with the results presented in figure 5.4(c). The simulated resolution is actually better than the calculated one, because the contribution due to the intermediate slit is not included in the ray-tracing simulation.

Figure 5.8(a) displays the spot pattern at the detector plane, when the optical elements have no slope errors. The intermediate slit width has been set to 3.5 µm. The spot size in the non-dispersion direction can be calculated by the size at the intermediate slit plane (figure 5.6) times the magnification of the second stage (2500/700).

Again, the simulated spot size in the non-dispersion direction is slightly larger than the calculated value. The spot size in the dispersion direction corresponds to a resolution of 1.1 meV, that is in agreement with the results presented in figure 5.5(a) for the resolution limit due to the entrance slit of the second stage. The value of 8282 indicates that about 17 % of the rays are lost. Out of those, about 70 % are lost due to the over-illumination of the grating at this energy and the remaining 30 % are lost at the intermediate slit. The effect of the slope errors is depicted in figure 5.8(b). The resolution obtained from the spot size in the dispersion direction is better than 4 meV. Combined with a detector pixel size of 5 µm this yields a total resolution of 4.2 meV. This is in agreement with the results shown in figure 5.5(c). Not more than 26 % of the rays are lost. Out of those, about 35 % are lost at the intermediate slit.

Figure 5.9 displays the spot patterns at the intermediate slit plane and the detector plane in the large-bandpass mode. At the intermediate slit plane, the two lines that are shifted by 20 meV and 25 meV with respect to the Rayleigh line cannot be resolved. After the second stage the resolution is about 5 meV, so that the lines are clearly separated. This figure also demonstrates the excellent stray-light rejection of the high-resolution double monochromator: The Rayleigh line and the shifted lines do not overlap. All in all, the results of the ray-tracing simulations are in very good agreement with the analytical results shown in the figures 5.4 and 5.5. This holds also for ray-tracing simulations performed with other photon energies and higher slope errors.

Figure 5.10(a) shows the acceptance of the high-resolution double monochromator. The maximum acceptance is given by the solid angle that can be collected by the mirror M1. In their low-energy range the gratings are over-illuminated. This leads to lower acceptances. Since the energy ranges of the gratings overlap, it is possible to trade flux for resolution or vice versa by using the adjacent grating. The 'optical efficiency' in the high-resolution mode depicted in figure 5.10(b) results from the grating efficiencies, the mirror reflectivities, and the losses at the intermediate slit due to the source size and the slope errors of 1 arcsecond of the mirrors M1 and M2. The intermediate slit width has been assumed to be 3.5 µm. The total efficiency is the product of the acceptance and the optical efficiency. It is shown in figure 5.11 together with the energy resolution. For photon energies between 21 and 178 eV the total efficiency varies between $10^{-6}$ and $1.3 \times 10^{-5}$.

In conclusion, the VUV-Raman spectrometer will offer an energy resolution better than 10 meV. For photon energies up to 70 eV, the energy resolution will be even better than 2 meV.

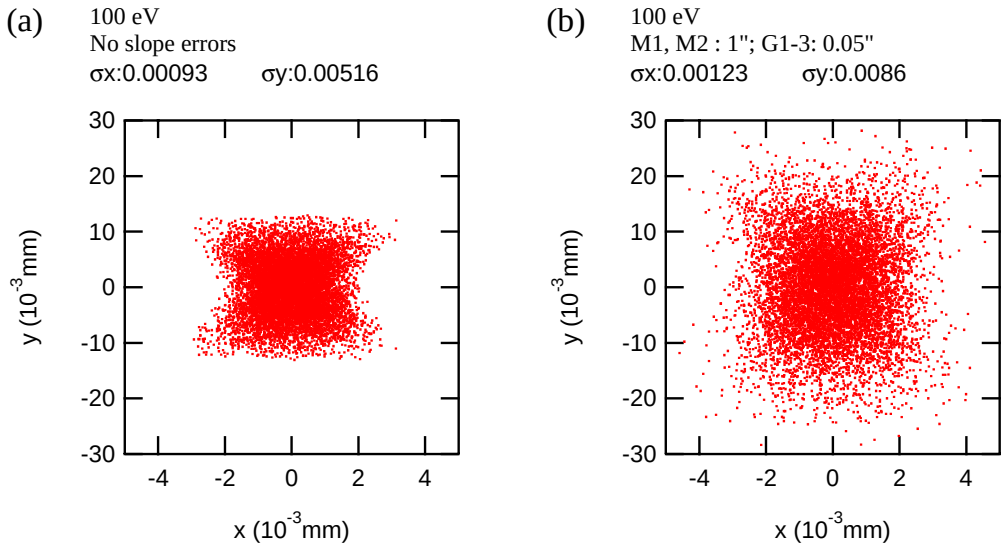


**Figure 5.6:** Spot pattern at the intermediate slit plane for an incident photon energy of 100 eV. The rms sizes of the spot $\sigma_x$ and $\sigma_y$ are given in mm. The dispersion direction is along the $x$-axis. (a) No slope errors are assumed for the optical elements. (b) The mirrors M1 and M2 have an rms slope error of 1 arcsecond, whereas the grating G1-3 has a slope error of 0.05 arcseconds.

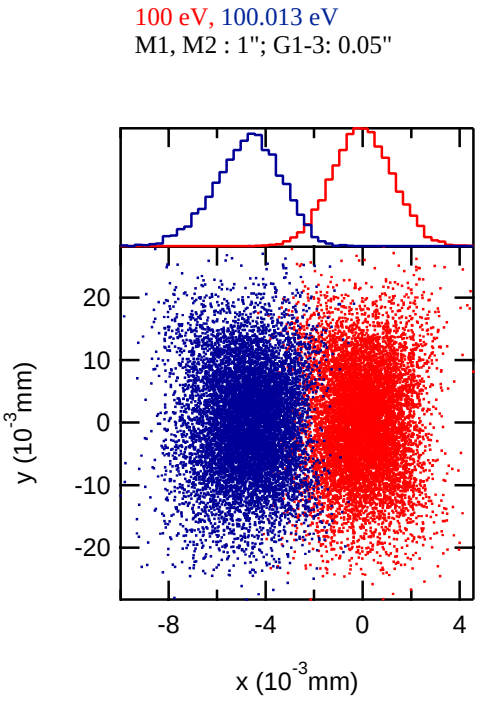


**Figure 5.7:** Spot patterns at the intermediate slit plane for an incident photon energy of 100 eV and an energy of 100.013 eV for the scattered photons. The source size ($3 \times 10$ µm$^2$) and the slope errors of the optical elements have been included in the ray-tracing simulation.

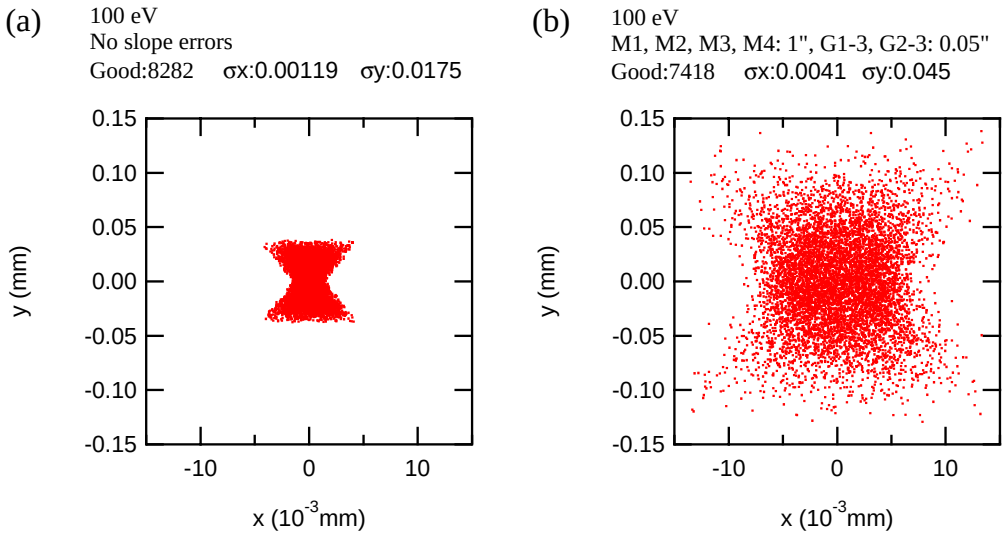


**Figure 5.8:** Spot pattern at the exit slit plane of the second stage for an incident photon energy of 100 eV. The rms sizes of the spot $\sigma_x$ and $\sigma_y$ are given in mm. (a) No slope errors are assumed for the optical elements. (b) The mirrors M1, M2, M3 and M4 have an rms slope error of 1 arcsecond, whereas the gratings G1-3 and G2-3 have a slope error of 0.05 arcseconds.

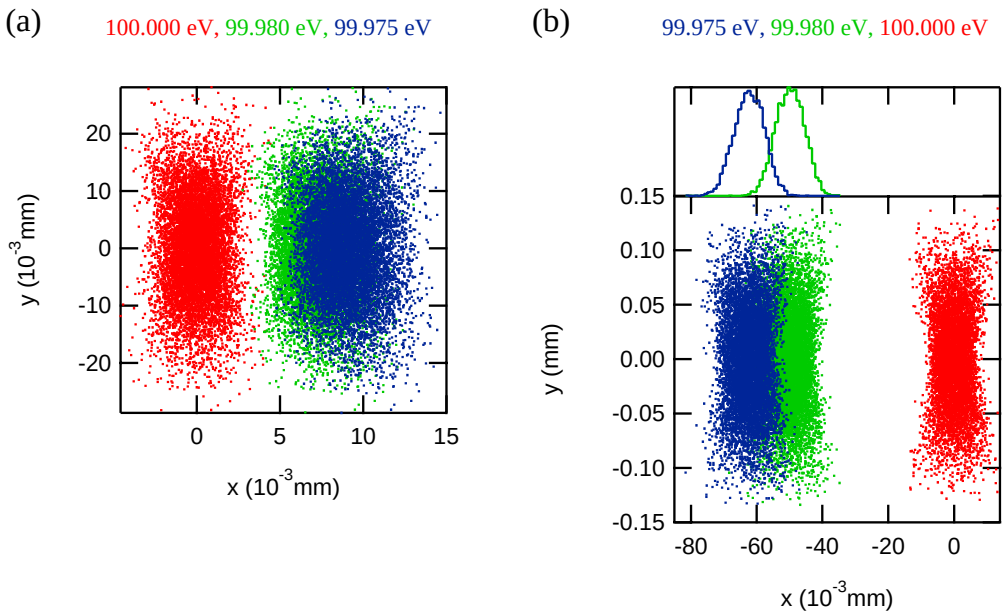


**Figure 5.9:** Spot patterns in the large-bandpass mode at (a) the intermediate slit plane and (b) the detector plane. The Rayleigh line lies at 100 eV.

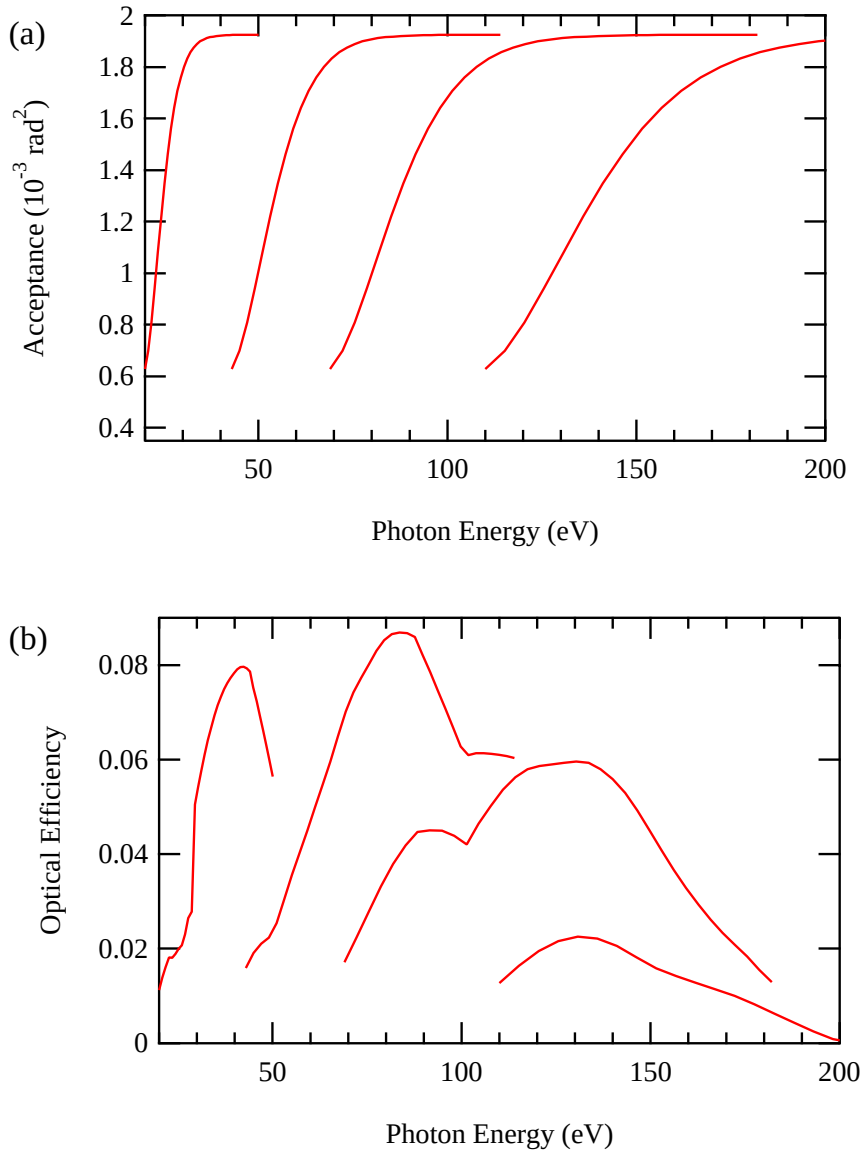


**Figure 5.10:** (a) Acceptance and (b) optical efficiency of the double monochromator in the high-resolution mode.

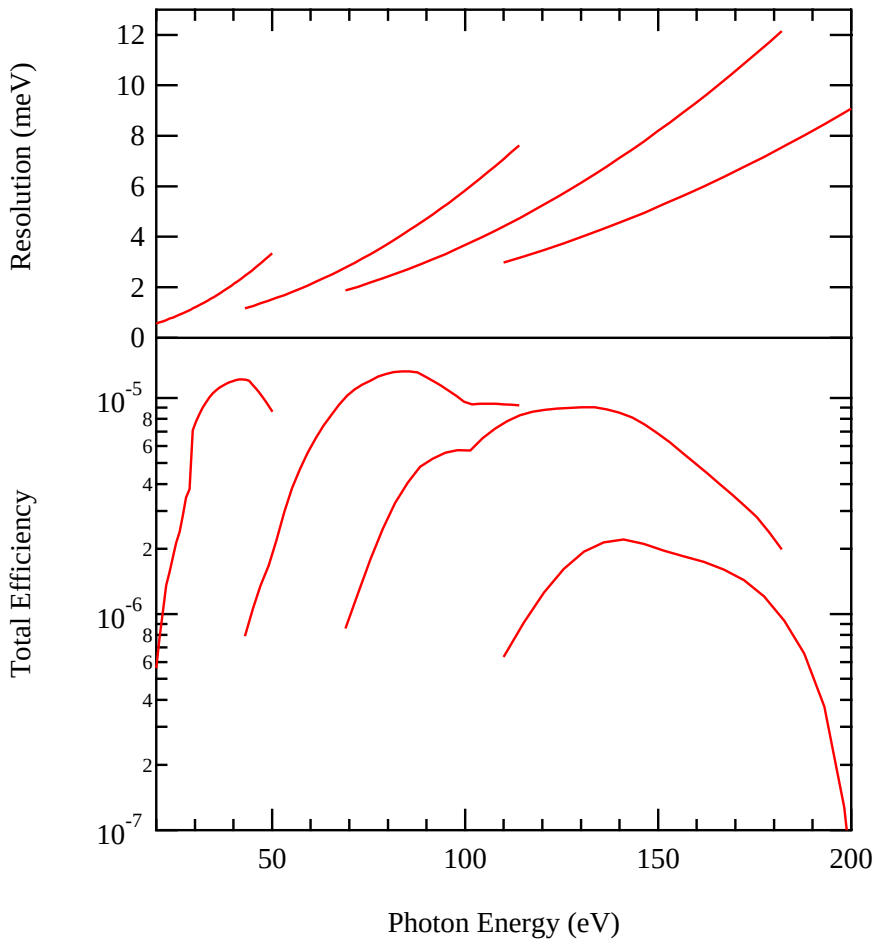


**Figure 5.11:** Energy resolution and total efficiency of the double monochromator in the high-resolution mode.

## 5.3 Essential Equipment

### 5.3.1 Housing and Mechanical Setup

The positions of the optical elements (mirrors and gratings) should be retained for a long time. Therefore, a stable housing that reduces the effects of vibrations is necessary. Each stage of the high-resolution double monochromator should be contained in a housing that is intended to be milled out of a monolithic aluminium block.

A plan and photos of the experimental hall at HASYLAB/DESY can be found in appendix B. The VUV-Raman spectrometer will be built up near the so-called laser hutch. It is imperative that the setup of the spectrometer is free of oscillation and ensures maximum stability. Figure 5.12 shows one idea of the mechanical setup. The high-resolution double monochromator will have a length of about 5 m. The photon beam exiting the primary monochromator is located about 2.6 m above the floor. For a vibration-free setup, a block of concrete or granite with a size of approximately 1.5 m × 5.5 m will be placed on the floor. It is intended to place one end of the double monochromator directly on this block. This ensures the stability and reduces the required amount of space on the floor. The steel pillars holding the instrument will be equipped with damping units to further reduce vibrations. The passageway near the wall will have a width of 1.13 m.

The exact details of the mechanical setup will be developed together with the staff from HASYLAB/DESY in order to consider their specific needs. For the development of the definite setup we require additional information such as measuring data on the vibrations of the building and the floor as well as a detailed plan of the predicted movements of persons and materials during the times of experiments and maintenance.

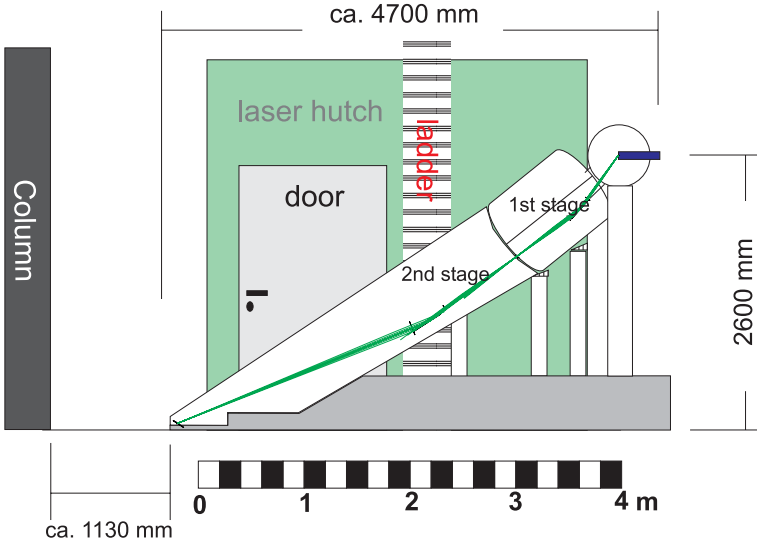


**Figure 5.12:** Possible setup of the VUV-Raman spectrometer.

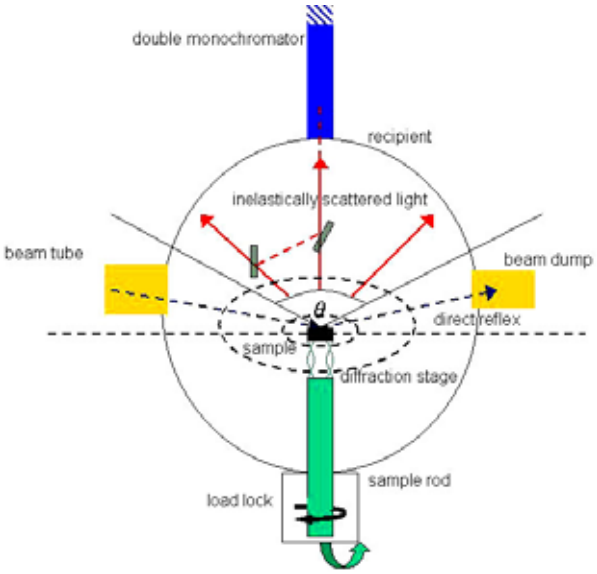


**Figure 5.13:** The VUV-Raman spectrometer and its multiple rotation options. The sample rod can be rotated along the longitudinal and the optical axis. A multilayer stage enables the variation of the scattering angle $\theta$.

### 5.3.2 Rotation Options and Multilayer Stage

Figure 5.13 depicts the setup of the VUV-Raman spectrometer and its multiple rotation options. The rotations enable, for example, measurements on different single crystal surfaces and with different polarizations. In particular, the variation of the scattering angle enables momentum-resolved measurements of quasi-particle excitations. The sample rod can be rotated along the longitudinal and the optical axis. The original idea to rotate the whole double monochromator had to be given up, because the amount of space in the experimental hall is limited. Thus, the double monochromator stays in a fixed position. The variation of the scattering angle will now be achieved by a multilayer stage that consists of two multilayer mirrors. The range of the scattering angle $\theta$ that is accessible by the multilayer stage is limited by the beam tube and the beam dump. We expect, that a rotation from $\theta_{\mathrm{min}} = 5°$ (near-forward scattering) to $\theta_{\mathrm{max}} = 175°$ (near-backward scattering) will be possible. This corresponds to a momentum transfer $q$ between $0.087\,k$ and $1.998\,k$. The angular resolution will be $\Delta\theta = 2°$.

In order to select the scattering angle, the two multilayer mirrors will be rotated simultaneously by the so-called two-theta stage depicted in figure 5.14(b). The first mirror collects the scattered light from the sample and directs it to the second mirror. The second mirror is located on the rotational axis and thus directs the light towards the mirror M1 of the high-resolution double monochromator. The size of the solid angle segment that is collected by the multilayer mirrors matches the numerical aperture of the mirror M1. Multilayer mirrors work only within a narrow spectral bandwidth of 1–2 nm. Thus, several multilayers are required. The spectrometer

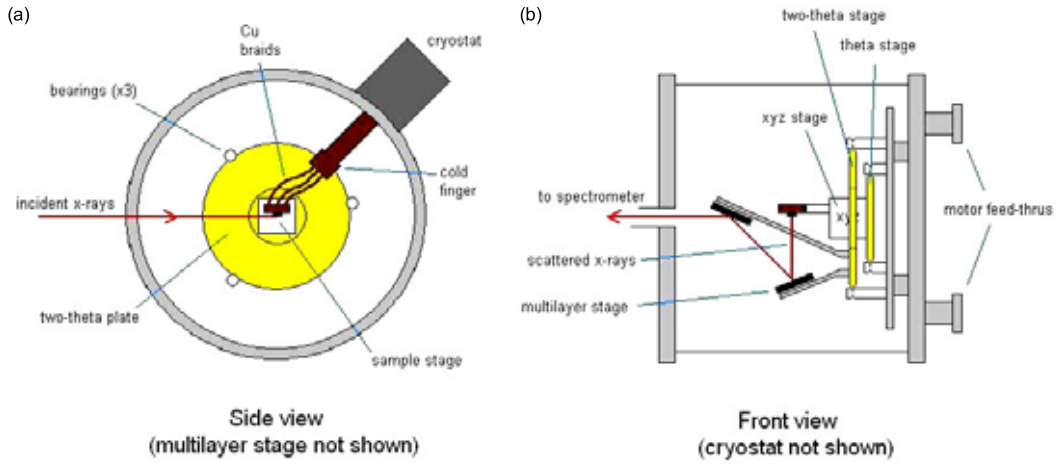


**Figure 5.14:** Multilayer stage and recipient for solid-state physics. (a) Side view. (b) Front view.

should be equipped with multilayers that work at important absorption edges, for example of Cu (75 eV, 77 eV, 122 eV), Mn (47 eV, 82 eV), Ni (67 eV, 111 eV) and Si (99 eV, 100 eV, 149 eV).

For measurements that do not require momentum resolution, the recipient for solid-state physics will be provided with an additional inset without multilayer stage. In this configuration the resonance energies can be determined in order to select the optimum multilayers for resonant measurements with momentum resolution.

### 5.3.3 Vacuum Vessel and Cryostat

The sample holder will be placed in a vacuum vessel with an UHV below $10^{-10}$ mbar. It will contain several samples that will be brought in position by a xyz-translation stage shown in figure 5.14(b). The translation stage is mounted on the so-called theta stage that enables rotations of the sample. Sample rotations perpendicular to the incidence plane of the incoming light enable the investigation of symmetry selection rules for a given set of polarizations of incident and scattered photons with respect to the crystal axes. The sample holder will be inserted into the recipient via an evacuated transfer stage. Thus, the recipient itself needs not to be aerated in order to change the samples. This enables fast changes of the samples during the limited beam time. A beam dump absorbs the directly reflected radiation.

To the vacuum vessel shown in figure 5.14(a) belongs a $^4$He cryostat that allows for measurements down to 4.2 K. The exact minimum temperature depends on the size of the temperature increase due to the photon flux after the primary monochromator and on the quality of the thermal contact of the Cu braids that connect the sample to the cryostat. With a heater mounted to the heat exchange part defined sample temperatures up to 800 K will be reached. For this purpose, a heat shield that is actively cooled by liquid nitrogen is required to prevent the rest of the system from

overheating. In the future, the system should be extended in order to provide still lower and higher temperatures as well as magnetic fields.

For gas-phase studies a specific recipient is required. Figure 5.15 shows a schematic setup. The sample gas beam will be inserted by a hypodermic needle that will be positioned close to the incident photon beam. The region where the sample gas beam crosses the incident photon beam generates the source for the VUV-Raman spectrometer. The crossing region must lie in the focal point of the mirror M1. The source size is defined in the vertical direction by the refocusing optics and in the horizontal direction by the opening diameter of the hypodermic needle.

The high intensity of the VUV-FEL makes possible experiments with gases at relatively low pressures. In order to separate the sample gas from the UHV of the refocusing mirror chamber, a pinhole wall that allows differential pumping will be used. The pinhole should be positioned close to the focus of the refocusing optics and match the cross section of the photon beam. The pinhole diameter will be about 100 µm. The thickness of the wall depends on the pressure difference. The pressure of the sample gas should lie in the order of at least $10^{-4}$ mbar, whereas the refocusing optics needs a pressure below $10^{-10}$ mbar.

It is unavoidable that a part of the incident photon beam hits the hypodermic needle and produces a large amount of secondary photons, electrons and ions. The radiation produced by the incident photons or secondary particles hitting the needle, the baffles or the chamber walls will cause signals that are much larger than those of the sample gas. Therefore, a suitable baffle arrangement is needed to block this radiation. The setup includes a detector for secondary ions and electrons as well as for the characterization of the incident photon beam behind the sample.

The simple setup in figure 5.15 will be sufficient for the first experiments. Later, a multilayer stage for the variation of the scattering angle and a laser for pump and probe experiments might be added. With an additional differential pumping stage, higher sample gas pressures will become possible. Further developments should enable studies of more dilute samples such as free atoms, ions, radicals, metal vapors and clusters.

### 5.3.4 Vacuum System

Spectroscopy in the VUV spectral range requires a vacuum system. The vacuum system must be compatible with the UHV of the VUV-FEL. This means, that for the vacuum vessel, which is in direct connection to the VUV-FEL, a pressure below $10^{-10}$ mbar is needed. The double monochromator itself requires only a pressure below $10^{-7}$ mbar that can be achieved by ion-getter and turbo-molecular pumps. For the double monochromator, there will be probably two vacuum chambers, one for each stage. In order to enable rotations of the samples, the sample recipient must be pumped differentially. The number of vacuum pumps depends on the effective surface of the spectrometer, which has a length of roughly 5 m. We estimate that 3 ion-getter pumps for the UHV and 10 ion-getter or turbo-molecular pumps with a sufficient number of roughing pumps are required. Each pump should be supplied

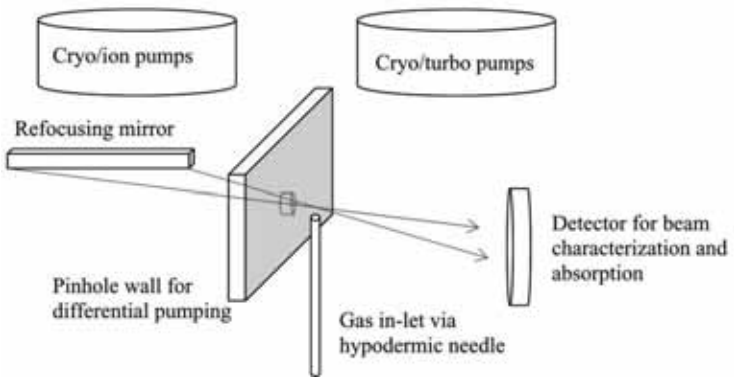


**Figure 5.15:** Schematic setup for gas-phase studies.

with an extra valve, so that a damaged pump can be easily exchanged when this valve is closed. By closing one of these valves, it is also possible to simulate a pump failure and to test the reliability of the vacuum system. The number of pumps should be high enough to compensate for the failure of one or two pumps. Between the vacuum vessel and the VUV-FEL a fast safety valve is needed to protect the UHV of the VUV-FEL in case of a major system failure.

### 5.3.5 Detectors

The two operation principles of the VUV-Raman spectrometer require different detection systems. In the high-resolution mode, which provides high energy resolution, the pixel size of the detector should be as small as possible. More precisely, the pixel size should be virtually equal to the slit width of the intermediate slit, in order to obtain the best possible resolution. Since slit widths of 1–3 µm are envisaged, a pixel size below $5 \times 5$ µm$^2$ is needed. At present, backthinned liquid-nitrogen cooled CCD detectors with pixel sizes in the order of $13 \times 13$ µm$^2$ and chip sizes up to $2048 \times 2048$ pixels are the best available detectors for the VUV and XUV spectral range. These detectors, which are produced by the Roper Scientific GmbH, have quantum efficiencies above 40 % for photon energies between 25 and 200 eV and of 60-80 % for energies between 200 and 1 keV. New detection systems are developed within the KOSAR (Optische Komponenten und Strahlungsquellen für zukünftige Anwendungen im Röntgenbereich) project, which is a cooperation of several Fraunhofer institutes and the AIXUV GmbH in Aachen. It is intended to use a scintillating crystal with a thickness of only 100 nm to transform the XUV radiation into visible light. The visible light can be magnified by a lens and then detected by a commercially available high-resolution CCD camera. The effective pixel size of the detection system depends on the magnification factor. For example, with a magnification factor of 5 and a CCD camera with a pixel size of $13 \times 13$ µm$^2$, the effective pixel size is $2.6 \times 2.6$ µm$^2$. The quantum efficiency of such a setup depends on the quality of the scintillating crystal and is expected to lie around a few %. This is sufficient, because the read-out noise is low.

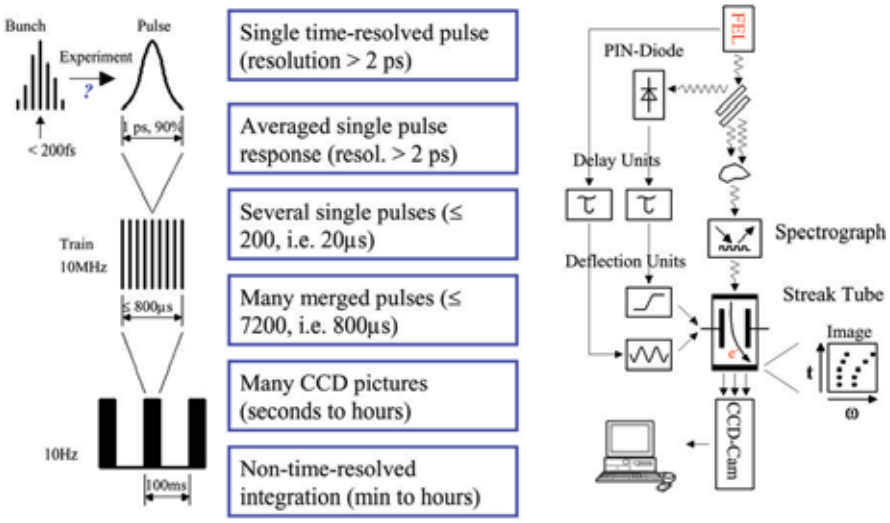


**Figure 5.16:** Scheme of the detection system for time-resolved experiments. The system combines a pump and probe setup for the photons with an X-ray streak camera.

For measurements in the large-bandpass mode without time resolution the above mentioned backthinned CCD detectors are sufficient. For time resolved experiments a detection system that combines a pump and probe setup for the photons with an X-ray streak camera is planned to be developed by the Helmholtz Research Center 'Nanostructure Research on Functional Materials with Short Coherence Lengths at the TTF-VUV-FEL'. Through the pulse width, the pulse separation and the repetition rate of 10 Hz of the VUV-FEL, different time domains from femtoseconds to seconds become accessible. The intended detection system outlined in figure 5.16 should cover the whole time range. We estimate a quantum efficiency of roughly 1 % for this system. An X-ray streak camera that allows to store the time information on a CCD chip in the direction perpendicular to the frequency axis will be developed by the Japanese firm Hamamatsu Photonics.

# 6. Finance Plan

The resources for the setup of the VUV-Raman spectrometer should mainly be provided by the Helmholtz Association (HGF) and the Federal Ministry of Education and Research (BMBF) in Germany. Table 6.1 summarizes the applied resources for the first three years of the project. In autumn 2003, the Helmholtz Association granted the application for the Helmholtz Research Center 'Nanostructure Research on Functional Materials with Short Coherence Lengths at the TTF-VUV-FEL'. This research center is a cooperation between HASYLAB at DESY and the Institut für Angewandte Physik und Zentrum für Mikrostrukturforschung, Universität Hamburg. It provides a research associate, a scientist and an engineer as well as financial resources for consumables, traveling and meetings. For the VUV-Raman spectrometer itself as well as for additional personnel and materials we have applied in July 2003 at the Federal Ministry of Education and Research (BMBF).

The VUV-Raman spectrometer is a novel instrument that requires a large development effort. Qualified personnel is needed for the design, setup and operation of the spectrometer, for the development of optical, electronic and mechanical components, for the development of detection systems, for the vacuum system, for the organization of research and the establishment of a user facility as well as for the experiments. Table 6.2 gives an overview of the required personnel for the first three years. The Universität Hamburg provides the position of the project leader Michael Rübhausen and will be asked for the secretary after the granting by the BMBF. In addition, the Universität Hamburg supports the project by providing the facilities of the Institut für Angewandte Physik und Zentrum für Mikrostrukturforschung such as the clean room, the mechanical and electronic workshops, the laboratories for the UV-Raman spectrometer UT-3 and for Raman spectroscopy in the visible spectral range as well as the planned laboratory for biophysics.

The refocusing optics between the primary monochromator and the VUV-Raman spectrometer was part of an application for upgrading the primary monochromator by the group of Wilfried Wurth at the Institut für Experimentalphysik, Universität Hamburg. The Federal Ministry of Education and Research granted 200.000 € for the refocusing optics that comprises a slit, two mirror chambers for horizontal and vertical focusing as well as other necessary equipment such as vacuum pumps. Further contributions to the experimental environments, for example a He cryostat with pressure cell and a delay line, are expected from the international cooperation partners. From Sweden 250.000 € shall be provided for the extension of the VUV-Raman spectrometer. In Sweden a long-term participation within the scope of the European X-ray Laser Project XFEL at DESY is planned, so that additional financial support is possible. For their specific experiments the cooperation partners will apply for doctorate and postdoctorate positions at their respective funding agencies such as the Vetenskapsrådet in Sweden or the National Science Foundation and the Department of Energy (DOE) in the USA. We hope for a financial contribution of

the Freie und Hansestadt Hamburg in the order of the Helmholtz grant for further developments of the experimental environment.

Table 6.3 gives an advanced estimate for the VUV-Raman spectrometer. It is based on a preliminary offer by the firm McPherson (USA) and discussions with several other manufacturers for optical components such as Zeiss (Germany) and Bach Research (USA). Most of the components have to be developed specifically for the VUV-Raman spectrometer. Therefore, improvements of available products or new designs are necessary. The development costs of the manufactureres are included in the design and engineering hours. The assembly hours comprise the costs for tests of the single components and for the sub-assembly at the manufacturer. The actual costs can be specified only after the call for tenders. Thus, slight shifts of the costs from one matter of expense to another are still possible.

**Table 6.1:** Overview of the resources that have been applied for the first three years of the project. The personnel costs have been estimated by the respective cost rates of the Helmholtz Association (HGF) and the Federal Ministry of Education and Research (BMBF). The Helmholtz Association already completely granted the applied resources.

| | HGF | BMBF | Σ |
|---|---|---|---|
| **Personnel Costs for 3 years (€)** | | | |
| Research Associate (BAT IIa) | 175.500 | - | 175.500 |
| Beamline Scientist (BAT Ib) | - | 189.762 | 189.762 |
| Scientist (BAT IIa) | 351.000 | 178.212 | 529.212 |
| Engineer (BAT IVa) | 146.300 | 154.524 | 300.824 |
| | **672.800** | **522.498** | **1.195.298** |
| **Investment Costs for 3 years (€)** | | | |
| VUV-Raman Spectrometer | - | 2.793.000 | 2.793.000 |
| | **-** | **2.793.000** | **2.793.000** |
| **Material Costs for 3 years (€)** | | | |
| Consumables, traveling, meetings | 47.200 | 78.900 | 126.100 |
| | **47.200** | **78.900** | **126.100** |
| **Total (€)** | **720.000** | **3.394.398** | **4.114.398** |

**Table 6.2:** Personnel for the first three years. HGF: These positions have been already granted by the Helmholtz Association. BMBF: For these positions we have applied at the Federal Ministry of Education and Research. UNI: The Universität Hamburg provides the position of the project leader and will be asked for the secretary.

| | | | | |
|---|---|---|---|---|
| 1 | Project Leader | | Michael Rübhausen | UNI |
| 1 | Research Associate | BAT IIa | Scientific organization of the research center and participation at the research program | HGF |
| 1 | Secretary | BAT Vc | Administration, correspondence predominantly in english, organization of events and appointments, guest care | UNI |
| 1 | Beamline Scientist | BAT Ib | Preparation of a user facility, technical advice for users, adaptation of the VUV-Raman spectrometer to the VUV-FEL and development of experimental environments | BMBF |
| 3 | Scientists | BAT IIa | Design of the VUV-Raman spectrometer and development of the optical components | HGF |
| | | BAT IIa | Development of electronic systems for measurements and time synchronisation, development of detection systems | HGF |
| | | BAT IIa | Key experiments on correlated nanostructured solids or soft matter such as biological tissues | BMBF |
| 2 | Engineers | BAT IVa | Mechanical system integration, vacuum system, development of electronic components | HGF |
| | | BAT IVa | Setup, operation, maintenance and further development of the VUV-Raman spectrometer | BMBF |

**Table 6.3:** New cost estimate for the VUV-Raman spectrometer that has been applied at the Federal Ministry of Education and Research (BMBF).

| | |
|---|---|
| **Coupling to the primary monochromator** | |
| Adaptation of the recipient to the beam tube | 150.000 € |
| Baffle B0 | 12.500 € |
| | **162.500 €** |
| **High-Resolution Double Monochromator** | |
| Gratings G1-1, G1-2, G1-3<br>(Small gratings for the first stage) | 150.000 € |
| Gratings G2-1, G2-2, G2-3, G2-4<br>(Large gratings for the second stage) | 300.000 € |
| Grating Mounts | 300.000 € |
| Grating Angles (Encoders or interferometers) | 150.000 € |
| Mirrors M1, M2, M3, M4<br>(Parent off-axis parabolas with a slope error of 0.5 arcseconds and an rms roughness below 1 nm) | 300.000 € |
| Mirror Mounts | 200.000 € |
| High-Resolution Slit S | 25.000 € |
| Baffles B1, B2 | 25.000 € |
| | **1.450.000 €** |
| **Essential Equipment** | |
| Monolithic Housings | 10.000 € |
| Multilayer stage | 70.000 € |
| Hydraulic Systems and Base Frames | 100.000 € |
| Vacuum Vessel and Cryostat | 150.000 € |
| Vacuum System | 150.000 € |
| Detector for the High-Resolution Mode<br>(scintillating crystal, <5 $\mu m^2$ effective pixel size, low quantum efficiency) | 50.000 € |
| Detector for the Low-Bandpass Mode<br>(backthinned CCD camera, 13 $\mu m^2$ pixel size, high quantum efficiency) | 64.000 € |
| | **594.000 €** |
| **External Labor** | |
| Design Hours | 100.000 € |
| Engineering Hours | 200.000 € |
| Assembly Hours | 200.000 € |
| | **500.000 €** |
| **Total** | **2.706.500 €** |

# 7. Summary and Outlook

In this technical design report, a novel VUV-Raman spectrometer for the VUV-FEL of the TESLA Test Facility 2 (TTF-2) is described. The report demonstrates the feasibility of the project. The basic concepts have been developed and discussed in an international collaboration of scientists with a strong background in synchrotron radiation experiments. The full details can be specified only in cooperation with the manufacturers.

The VUV-Raman spectrometer will offer unprecedented possibilities for research in physics, chemistry, biology and medicine. Key experiments on solids, atomic and molecular systems as well as biological tissues will demonstrate its capability. It will be available to international research groups from science and industry. In particular, also the economic area of Hamburg and Northern Germany may benefit. Existing cooperations between the universities in this region and DESY will be strengthened. In addition, new cooperations will be established. The user facility will attract scientists from all over the world. Diploma and doctoral theses as well as postdoc positions will acquaint young people with the new technologies and research possibilities.

In less than ten years the European X-ray Laser XFEL shall offer an extended wavelength range, still higher brilliance and still higher time resolution. Thus, for example, real-time studies of the dynamics in functional materials like lattice excitations in crystalline solids or conformation changes in proteins, will become possible. The technology of the VUV-Raman spectrometer, such as the optical components and detection systems, will provide the basis for an effective use of the future XFEL. The development of experimental techniques for the hard X-ray range will benefit from the experiences with brilliant pulsed radiation sources in the VUV and soft X-ray range.

It is impossible to foresee today the whole extent of the eminent progresses that will be achieved by the VUV-FEL of the TTF-2 and the XFEL. The fascinating possibilities should be exploited.

# A. Technical Design Review Workshop

## A.1 Program

**Technical Design Review Workshop**

**High-Resolution Double Monochromator at the VUV-FEL of the TESLA Test Facility 2**

**April 19-20, 2004**
**Hamburg**

**Aim**

The workshop focuses on the design and the physical prospects of a novel high-resolution double monochromator to be established at the VUV-FEL of the TESLA Test Facility 2. This spectrometer for inelastic light scattering will offer fascinating possibilities for research in physics, chemistry, biology, and medicine. For example, functional materials like high-temperature superconductors, systems with colossal magneto-resistance, glasses and bio-organic materials can be studied on shortest time and length scales. During this workshop the technical requirements and the design of the double monochromator will be discussed.

**Organization**

The workshop is supported by the Helmholtz Research Center "Nanostructure Research on Functional Materials with Short Coherence Lengths at the TTF-VUV-FEL". The organizers are Josef Feldhaus from HASYLAB/DESY as well as Katrin Buth and Michael Rübhausen from the Institut für Angewandte Physik und Zentrum für Mikrostrukturforschung, Universität Hamburg.

**Venue & Accomodation**

The workshop will be held at HASYLAB/DESY in Hamburg, Germany. A limited number of rooms will be available in the DESY guest houses. For further information visit the DESY homepage:

http://desyntwww.desy.de/vgs/international/international.html

**Contact & Registration**

For registration or further information send an e-mail to

katrin.buth@physnet.uni-hamburg.de

Please register until **April 5, 2004**.

## Program

**Monday, April 19, 2004 – Building 25b / Room 109**

09:30 – 09:45 *Registration*

09:55 – 10:00 **Welcome Note**
Jochen Schneider
HASYLAB/DESY, Hamburg, Germany

**Session I: Instrumentation and State of the Art for Optical Elements**
Chair: Jochen Schneider

10:00 – 10:45 **Soft X-ray Resonant Inelastic Scattering Spectroscopy - A New Look on Matter**
Joseph Nordgren
Uppsala University, Sweden

10:45 – 11:00 *Coffee Break*

11:00 – 11:30 **Design Criteria for FEL Beamlines**
Rolf Follath
BESSY, Berlin, Germany

11:45 – 13:45 *Lunch Break*

**Session II: High Resolution Double Monochromator/Spectrometer: Research and Technology**
Chair: Wilfried Wurth

13:45 – 14:15 **Strongly Correlated Materials and Resonant Raman Scattering**
Michael Rübhausen
Institut für Angewandte Physik und Zentrum für Mikrostrukturforschung, Universität Hamburg, Germany

14:15 – 14:45 **Resonant Inelastic Scattering of VUV/Soft X-ray FEL Radiation Applied to Atoms and Molecules**
Jan-Erik Rubensson
Uppsala University, Sweden

14:45 – 15:15 **Energy Resolution Requirements for Momentum-Resolved Inelastic X-ray Scattering in the VUV**
Peter Abbamonte
Brookhaven National Laboratory, Upton, USA

15:15 – 15:30 *Coffee Break*

15:30 – 16:00 **Properties of the FEL and the High Resolution Monochromator**
Michael Martins
Institut für Experimentalphysik, Universität Hamburg, Germany

16:00 – 16:45 **Optical Design Studies**
Ruben Reininger
SAS - Scientific Answers & Solutions, Madison, USA

16:45 – 17:15 **Detection Systems: Spectral and Time Resolution**
Michael Rübhausen
Institut für Angewandte Physik und Zentrum für Mikrostrukturforschung, Universität Hamburg, Germany

**Session III: Technological Aspects**
Chair: Michael Rübhausen

17:15 – 19:00 **Discussion** (*Coffee*)

19:30 *Dinner*

**Tuesday, April 20, 2004 – Building 25f / Room 456**

**Session IV: Work Plan**
Chair: Josef Feldhaus

09:30 – 11:30 **Discussion on Work Plan, Work Packages, and Outside Contributions**

11:30 – 11:45 **Closing Remarks**
Jochen Schneider
HASYLAB/DESY, Hamburg, Germany

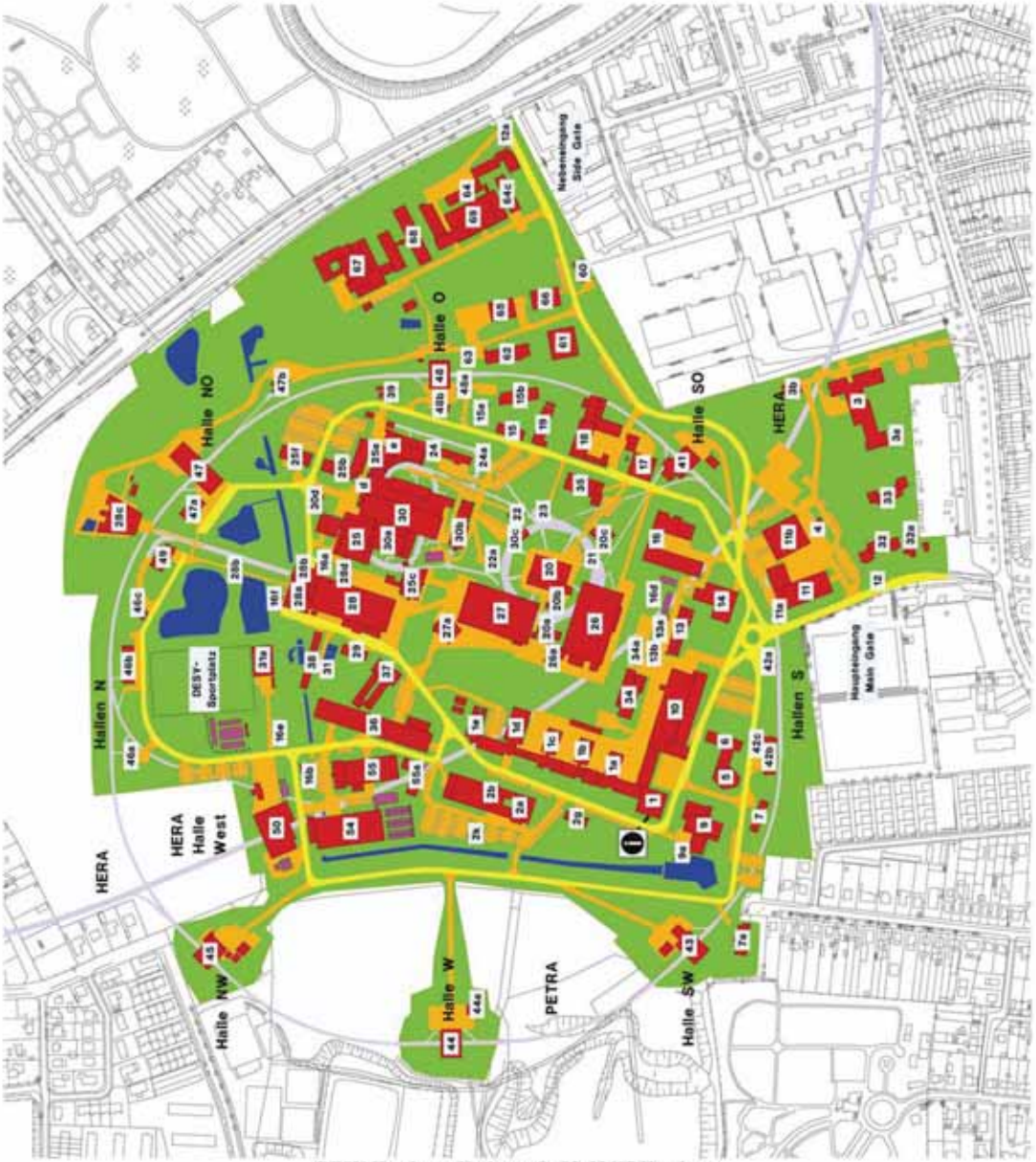


**DESY Hamburg, Notkestraße 85, 22607 Hamburg**

How to get to DESY:

http://desyntwww.desy.de/vgs/international/maps/maps.html

http://desyntwww.desy.de/vgs/international/external_links/external_links.html

## A.2 List of Participants

| | |
|---|---|
| **Organizers** | |
| Katrin Buth | Institut für Angewandte Physik und Zentrum für Mikrostrukturforschung, Universität Hamburg, Germany |
| Josef Feldhaus | HASYLAB/DESY, Hamburg, Germany |
| Michael Rübhausen | Institut für Angewandte Physik und Zentrum für Mikrostrukturforschung, Universität Hamburg, Germany |
| **Speakers** | |
| Peter Abbamonte | Brookhaven National Laboratory, Upton, USA |
| Rolf Follath | BESSY, Berlin, Germany |
| Michael Martins | Institut für Experimentalphysik, Universität Hamburg, Germany |
| Joseph Nordgren | Uppsala University, Sweden |
| Ruben Reininger | SAS - Scientific Answers & Solutions, Madison, USA |
| Jan-Erik Rubensson | Uppsala University, Sweden |
| Jochen Schneider | HASYLAB/DESY, Hamburg, Germany |
| **Participants** | |
| Joakim Bäckström | Institut für Angewandte Physik und Zentrum für Mikrostrukturforschung, Universität Hamburg, Germany |
| Lars Börjesson | Chalmers University of Technology, Göteborg, Sweden |
| Dirk Budelmann | Institut für Angewandte Physik und Zentrum für Mikrostrukturforschung, Universität Hamburg, Germany |
| Danny Chan | Institut für Angewandte Physik und Zentrum für Mikrostrukturforschung, Universität Hamburg, Germany |
| Alexander Föhlisch | Institut für Experimentalphysik, Universität Hamburg, Germany |
| Ulrich Hahn | HASYLAB/DESY, Hamburg, Germany |
| Lucia Incoccia-Hermes | DESY-HS, Projektträger des BMBF, Hamburg, Germany |
| Ulrich Merkt | Institut für Angewandte Physik und Zentrum für Mikrostrukturforschung, Universität Hamburg, Germany |
| Sonja Müller | Institut für Angewandte Physik und Zentrum für Mikrostrukturforschung, Universität Hamburg, Germany |
| Stefan Naler | Institut für Angewandte Physik und Zentrum für Mikrostrukturforschung, Universität Hamburg, Germany |
| Elke Plönjes | HASYLAB/DESY, Hamburg, Germany |
| Ralf Rauer | Institut für Angewandte Physik und Zentrum für Mikrostrukturforschung, Universität Hamburg, Germany |
| Benjamin Schulz | Institut für Angewandte Physik und Zentrum für Mikrostrukturforschung, Universität Hamburg, Germany |
| Kai Tiedtke | HASYLAB/DESY, Hamburg, Germany |
| Rolf Treusch | HASYLAB/DESY, Hamburg, Germany |
| Wilfried Wurth | Institut für Experimentalphysik, Universität Hamburg, Germany |

## A.3 Work Groups

The workshop resulted in the formation of the work groups given in table A.1. These work groups developed and worked out the basic concepts that are presented in this technical design report. They are most likely the basis for further cooperations during the whole project.

**Table A.1:** Work Groups. The coordinators of the groups are given in italics.

| **Work Group** | **Members** | **Task** |
|---|---|---|
| High-Resolution Double Monochromator | *Ruben Reininger*<br>Michael Rübhausen<br>Benjamin Schulz | The concept of the high-resolution double monochromator has been accepted at the workshop. Nevertheless, this group will further improve the design and study the tolerances. |
| Slope Errors | *Ruben Reininger*<br>Michael Rübhausen<br>Rolf Follath | This group examines concepts from BESSY to measure and improve slope errors. |
| Refocusing Optics | *Michael Martins*<br>Joakim Bäckström<br>Benjamin Schulz<br>Jan-Erik Rubensson | This group delivers a basic design for the refocusing optics that connects the primary monochromator with the VUV-Raman spectrometer. The refocusing optics creates a spot size of $3 \times 15$ µm$^2$. In a second step, spot sizes down to $3 \times 6$ µm$^2$ should be possible. The spot size and the laser power should be monitored. |
| Rotations | *Peter Abbamonte*<br>Michael Rübhausen<br>Alexander Föhlisch<br>Joseph Nordgren<br>Jan-Erik Rubensson | This group should develop a basic concept for the rotation stages that are necessary in order to study polarization effects and to achieve momentum resolution. A promising idea, that has been proposed at the workshop, is to use a multilayer diffractor. In addition, the main layout of the two sample chambers should be developed. The first one for solid state physics will be designed by Peter Abbamonte and Michael Rübhausen and the second one for gas phases by Jan-Erik Rubensson. |
| Mechanics and Mounts | *Michael Rübhausen*<br>Benjamin Schulz<br>Michael Martins<br>Elke Plönjes<br>Joseph Nordgren | This group examines mechanical problems that, for example, relate to mounts, translation possibilities, thermal stability or the Experimental Hall in general. |
| Detectors | *Michael Rübhausen*<br>Alexander Föhlisch<br>Joseph Nordgren | At present, CCD cameras from Roper Scientific offer the smallest pixel sizes with $13.5 \times 13.5$ µm$^2$. This group reviews new concepts in order to achieve pixel sizes of $5 \times 5$ µm$^2$ by conversion of photons. |

# B. Experimental Hall

The experiments for the VUV-FEL at HASYLAB/DESY will be built up in the experimental hall (building 28c), that was used for expositions during the EXPO 2000.

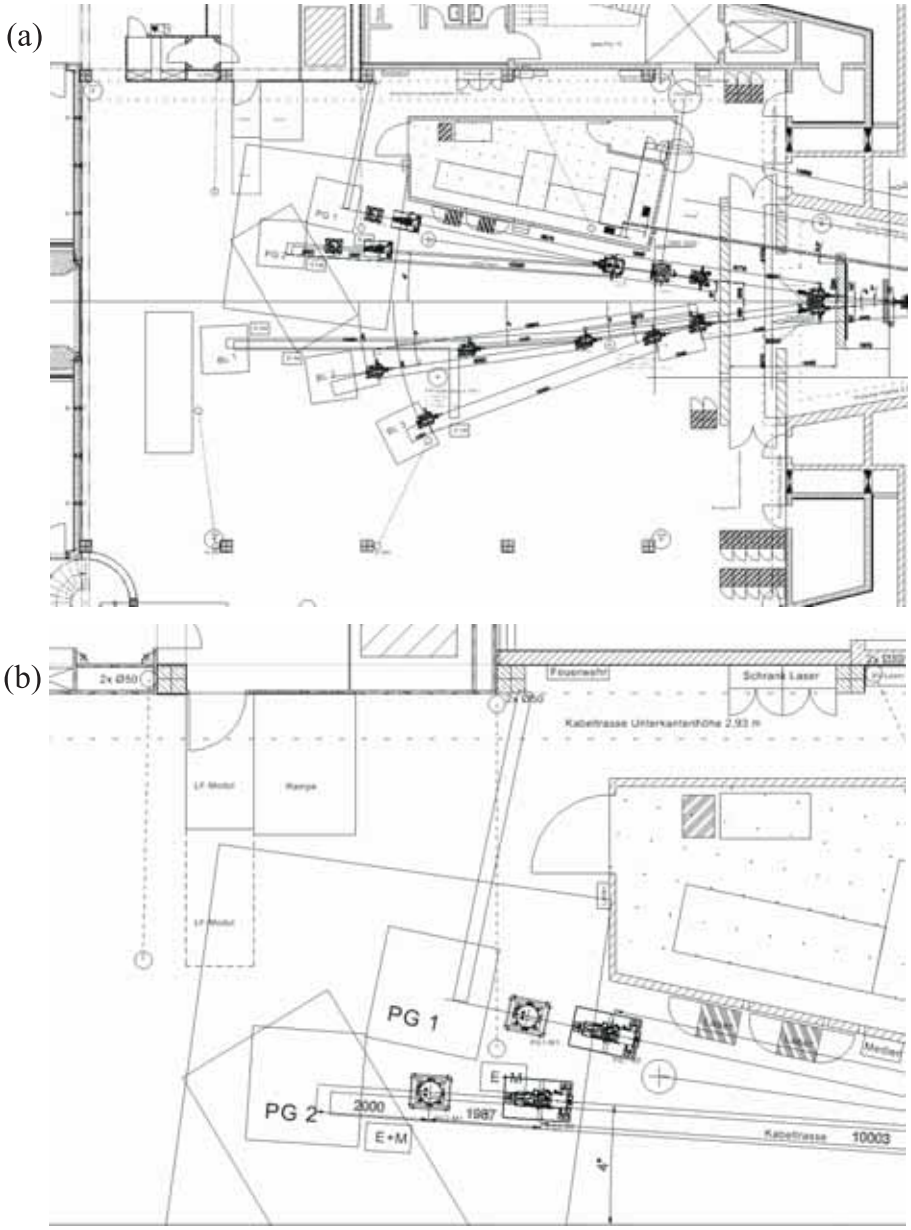


**Figure B.1:** (a) Drawing of the experimental hall. (b) The VUV-Raman spectrometer (PG 1) will be located near the so-called laser hutch. From [40].


**Figure B.2:** Photos of the experimental hall.


**Figure B.3:** Panorama photos of the experimental hall.

# C. Letters of Support

**David E. Moncton, Massachussetts Institute of Technology**

**Miles V. Klein, University of Illinois at Urbana-Champaign**

MASSACHUSETTS INSTITUTE OF TECHNOLOGY
Department of Physics
Cambridge, Massachusetts 02139

D.E. Moncton
Rm. 13-2038
Tel: 617/253-8333
Email: dem@mit.edu

April 8, 2004

Re: Letter of support for the High-Resolution Double Monochromator at the VUV-FEL of the TESLA Test Facility 2

Dear Ladies and Gentleman:

I am writing in strong support of the proposal and technical design report for a novel high-resolution double monochromator at the VUV-FEL of the TESLA Test Facility 2 at HASYLAB. The current developments in the field of synchrotron radiation provide opportunities for unprecedented brilliance levels at pulsed FEL sources. Exploiting these opportunities in spectral ranges covering the vacuum ultraviolet, soft x-ray, and hard x-ray ranges demands the development of novel time-resolved instrumentation with high energy resolution that will work at the Heisenberg limit. The unique instrument proposed by Rübhausen *et al.* would provide an excellent research tool for inelastic x-ray scattering experiments in this demanding range, leading to a significant increase in experimental capability, and therefore in science.

Sincerely yours,

David E Moncton
Director, MIT Nuclear Reactor Laboratory, and
Adjunct Professor of Physics

UNIVERSITY OF ILLINOIS
AT URBANA-CHAMPAIGN

Department of Physics
Loomis Laboratory of Physics
1110 West Green Street
Urbana, IL 61801-3080

14 April, 2004

To Whom it May Concern:

I write in support of the proposal and technical design report for a high resolution double monochromator at the vacuum ultraviolet free electron laser (FEL) at HASYLAB's TESLA Test Facility 2. The present trend to develop synchrotron radiation that will provide unprecedented brilliance at pulsed FEL sources over a wide spectral range requires the parallel development of novel instrumentation with high energy resolution in order to work at the transform limit with the new pulsed sources. The unique double monochromator instrument proposed by Rübhausen *et al.* would provide this capability together with the rejection of elastically scattered light needed for inelastic scattering experiments in the demanding range that covers the vacuum ultraviolet. This will enable new probing of excitations involving the valence electrons in atoms and in condensed matter systems.

Sincerely yours,

Miles V. Klein
Research Professor

Office: 1020 MRL • Phone: (217) 333-1744 • Fax: (217) 244-8544 • E-Mail: mvklein@uiuc.edu • MC-704

# Bibliography

[1] E. Fradkin, *Field Theories of Condensed Matter Systems*, volume 82 aus *Frontiers in Physics*, Addison Wesley, New York, 1991.

[2] P. W. Anderson, *The Theory of Superconductivity in High $T_c$-Cuprates*, Princton University Press, Princeton, 1997.

[3] W. Hanke, R. Eder, and E. Arrigoni, *SO(5)-Theorie der Hochtemperatur-Supraleitung: ein neues Symmetriekonzept in der Festkörperphysik*, Phys. Bl. **54**, 436–439 (1998).

[4] A. P. Ramirez, *Colossal magnetoresistance*, J. Phys.: Condens. Matter **9**, 8171–8199 (1997).

[5] G. Blumberg, P. Abbamonte, M. V. Klein, W. C. Lee, D. M. Ginsberg, L. L. Miller, and A. Zibold, *Resonant two-magnon Raman scattering in cuprate antiferromagnetic insulators*, Phys. Rev. B **53**, R11930–R11933 (1996).

[6] M. Rübhausen, *Electronic Correlations in Cuprate Superconductors - An Inelastic Light Scattering Study*, Ph.D. Thesis, Universität Hamburg, Shaker, Aachen, 1999.

[7] S. Yoon, M. Rübhausen, S. L. Cooper, K. H. Kim, and S.-W. Cheong, *Raman scattering study of anomalous spin, charge, and lattice dynamics in the charged-ordered phase of $Bi_{1-x}Ca_xMnO_3$ (x>0.5)*, Phys. Rev. Lett. **85**, 3297–3300 (2000).

[8] M. Rübhausen, S. Yoon, S.L. Cooper, K.H. Kim, and S-W. Cheong, *Anisotropic Optical Signatures of Orbital and Charge Ordering in $Bi_{1-x}Ca_xMnO_3$*, Phys. Rev. B **62**, R4782–R4785 (2000).

[9] K. Hiraga, D. Shindo, M. Hirabayashi, M. Kikuchi, K. Oh-Ishi, and Y. Syono, *Direct Observation of Atomic Arrangement of High-$T_c$ Superconductor $YBa_2Cu_3O_{6.74}$ by High-Resolution Electron Microscopy*, Jpn. J. Appl, Phys. **26**, L1071–L1073 (1987).

[10] I. Maggio-Aprile, Ch. Renner, A. Erb, E. Walker, and Ø. Fischer, *Critical currents approaching the depairing limit at a twin boundary in $YBa_2Cu_3O_{7-\delta}$*, Nature **390**, 487–490 (1997).

[11] J. Nordgren, G. Bray, S. Cramm, R. Nyholm, Rubensson J.-E, and N. Wassdahi, *Soft X-ray emission spectroscopy using monochromatized synchrotron radiation*, Rev. Sci. Instrum. **60**, 1690–1695 (1989).

[12] M. V. Klein, B. Schulz, D. Budelmann, D. Bonn, W. Hardy, and M. Rübhausen, *unpublished*.

[13] A. Föhlisch, M. Nagasono, F. Hennies, A. Pietzsch, W. Wurth, and M. N. Piancastelli, *unpublished*.

[14] R. Krüger, B. Schulz, S. Naler, R. Rauer, D. Budelmann, J. Bäckström, K. H. Kim, S-W. Cheong, V. Perebeinos, and M. Rübhausen, *Orbital ordering in $LaMnO_3$ Investigated by Resonance Raman Spectroscopy*, Phys. Rev. Lett. **92**, 097203–1 – 097203–4 (2004).

[15] P. Glans, K. Gunnelin, P. Skytt, J-H-Guo, N. Wassdahl, J. Nordgren, H. Ågren, F. Kh. Gel'mukhanov, T. Warwick, and E. Rotenberg, *Resonant X-Ray Emission Spectroscopy of Molecular Oxygen*, Phys. Rev. Lett. **76**, 2448–2451 (1996).

[16] K. Gunnelin, P. Glans, J.-E. Rubensson, C. Såthe, J. Nordgren, Y. Li, F. Kh. Gel'mukhov, and H. Ågren, *Bond-Length-Dependent Core Hole Localization Observed in Simple Hydrocarbons*, Phys. Rev. Lett. **83**, 1315–1318 (1999).

[17] P. Skytt, P. Glans, J.-H. Guo, K. Gunnelin, C. Såthe, H. Nordgren, F. Kh. Gel'mukhanov, A. Cesar, and H. Ågren, *Quenching of Symmetry Breaking in Resonant Inelastic X-Ray Scattering by Detuned Excitation*, Phys. Rev. Lett. **77**, 5035–5038 (1996).

[18] R. P. Madden and K. Codling, *New autoionizing atomic energy levels in He, Ne and Ar*, Phys. Rev. Lett. **10**, 516–518 (1963).

[19] K. Schulz, G. Kaindl, M. Domke, J. D. Bozek, P. A. Heimann, A. S. Schlachter, and J. M. Rost, *Observation of New Rydberg Series and Resonances in Doubly Excited Helium at Ultrahigh Resolution*, Phys. Rev. Lett. **77**, 3086–3089 (1996).

[20] J.-E. Rubensson, C. Såthe, S. Cramm, B. Kessler, S. Stranges, R. Richter, M. Alagia, and M. Coreno, *Influence of the Radiative Decay on the Cross Section for Double Excitations in Helium*, Phys. Rev. Lett. **83**, 947–950 (1999).

[21] R. Dörner, H. Schmidt-Böcking, Th. Weber, T. Jahnke, M. Schöffler, A. Knapp, M. Hattass, A. Czasch, L. Ph. H. Schmidt, and O. Jagutzki, *Double ionization by one and many photons*, Radiation Physics and Chemistry **70**, 191–206 (2004).

[22] T. W. Gorczyca, J.-E. Rubensson, C. Såthe, M. Ström, M. Agåker, D. Ding, S. Stranges, R. Richter, and M. Alagia, *Radiative and Relativistic Effects in the Decay of Highly Excited States in Helium*, Phys. Rev. Lett. **85**, 1202–1205 (2000).

[23] P. Fromherz, *Interfacing von Nervenzellen und Halbleiterchips*, Phys. Bl. **57**, 43–48 (February 2001).

[24] *TESLA*, Technical Design Report, Part I-VI, DESY, March 2001.

[25] V. V. Tuchin, *Light scattering study of tissues*, Phys. Usp. **40**, 495–515 (1997).

[26] B. Schulz, D. Chan, J. Bäckström, M. Rübhausen, K.P. Wittern, S. Wessel, R. Wepf, and S. Williams, *Hydration Dynamics of Human Fingernails – an Ellipsometric Study*, Phys. Rev. E **65**, 061913–1 061913–7 (2002).

[27] P. J. Caspers, G. W. Lucassen, E. A. Carter, H. A. Bruining, and G. J. Puppels, *In Vivo Confocal Raman Microscopy of the Skin: Noninvasive Determination of Molecular Concentration Profiles*, J. Invest. Dermatol. **116**, 434–442 (2001).

[28] A. Schwarz, S. Ständer, M. Berneburg, M. Böhm, D. Kulms, H. van Steeg, K. Grosse-Heitmeyer, J. Krutmann, and T. Schwarz, *Interleukin-12 suppresses ultraviolet radiation-induced apoptosis by inducing DNA repair*, Natural Cell Biology **4**, 26–31 (2002).

[29] K. Martin, *4. Infrared and Raman Studies of Skin and Hair: A review of cosmetic spectroscopy*, The Internet Journal of Vibrational Spectroscopy **3**, Edition 2 (1999).

[30] D. Chan, B. Schulz, and M. Rübhausen, *unpublished*.

[31] ESS Council, *The ESS Project*, Volume I-V, May 2002.

[32] The TESLA Test Facility FEL team, *SASE FEL at the TESLA Facility, Phase 2*, Technical Report, DESY, June 2002.

[33] R. Treusch, W. Brefeld, J. Feldhaus, and U. Hahn, *The Seeding Project for the FEL in TTF Phase II*, In: R. Gehrke, U. Krell, and J. R. Schneider, editors, *HASYLAB Annual Report 2001*, volume 1. HASYLAB/DESY, 2001.

[34] J. Feldhaus, E. L. Sadin, J. R. Schneider, E. A. Schneidmiller, and M. V. Yurkov, *Possible application of X-ray optical elements for reducing the spectral bandwidth of an X-ray SASE FEL*, Opt. Commun. **140**, 341–352 (1997).

[35] *X-ray Laser User Facility at Bates Laboratory*, Proposal to the National Science Foundation for a Conceptual Design Study, Massachusetts Institute of Technology, April 2003.

[36] R. Follath, *The versatility of collimated plane grating monochromators*, Nucl. Instr. Methods A **467-468**, 418–425 (2001).

[37] F. Riemer and R. Torge, *BESSY SX 700 UHV monochromator: design features and kinematic concept*, Nucl. Instr. Methods **208**, 313–314 (1983).

[38] P. Kirkpatrick and A. V. Baez, *Formation of optical images by X-rays*, J. Opt. Soc. Am. **38**, 766–774 (1948).

[39] C. Welnak, G. J. Chen, and F. Cerrina, *SHADOW: A synchrotron radiation and X-ray optics simulation tool*, Nucl. Instr. Methods A **347**, 344–347 (1994).

[40] N. von Bargen, HASYLAB/DESY, private communication, 2004.

Hahn-Meitner-Institut Berlin

Berlin Neutron Scattering Center

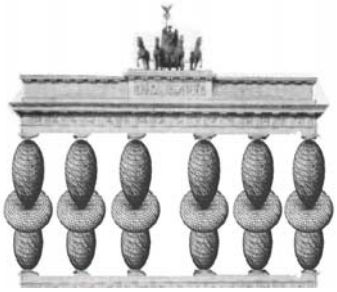

# 2nd Berlin Workshop on Orbital Physics and Novel Phenomena in Transition Metal Oxides

Hahn-Meitner-Institut Berlin
Auditorium
24-25 September 2003

## Wednesday, 24th of September

**8:45** Welcome by Prof. Michael Steiner (Scientific Director of HMI)

**Session 1: Orbital Ordering and Electronic Structure in Manganites**
Chair: M. Rübhausen

**9:00** R. Krüger (Univ. Hamburg)
*Orbital ordering in $LaMnO_3$ investigated by resonance Raman spectroscopy* (invited)

**9:35** B. Büchner (RWTH Aachen)
*Orbital degree of freedom in single layered manganites $LaSrMnO_4$*

**9:55** G. Allodi (Univ. Parma)
*Evidence for an orbital liquid state in low-doped insulating Manganites from $^{55}Mn$ NMR*

**10:15** J. Deisenhofer (Univ. Augsburg)
*The orbital order parameter in $La_{0.95}Sr_{0.05}MnO_3$ probed by ESR*

10:35-11:00 Coffee break

**Session 2: Magnetism and Lattice Structure in Manganites**
Chair: S. Hébert

**11:00** P. Reutler (Univ. Dresden)
*Magnetic Polarons: Magnetism in hole doped single layered manganites $La_{1-x}Sr_{1-x}MnO_4$*

**11:20** R. Rauer (Univ. Hamburg)
*Magneto-optical response of $La_{0.7}Ca_{0.3}MnO_3$*

**11:40** H. Nunes-Bordallo (HMI Berlin)
*Lattice Dynamics Simulation on the Layered Manganite, $La_{2-2x}Sr_{1-2x}Mn_2O_7$, $x=0.4$*

**12:00** J.-U. Hoffmann (HMI Berlin)
*Magnetic short range order in $La_{1-x}$ $Sr_xMnO_3$, x=0,0.1,0.15,0.2*

12:20-13:35 Lunch break

**Session 3: Transition Metal Oxides Part I**
Chair: B. Büchner

**13:35** S. Hébert (Laboratoire CRISMAT, Caen)
*Magnetic and transport properties of cobalt oxides with low dimensionality* (invited)

**14:10** C.A. Kuntscher (Univ. Stuttgart)
*Electronic and magnetic properties of the titanate $LaTiO_{3.41}$*

**14:30** T. Rudolf (Univ. Augsburg)
*Broadband dielectric and optical spectroscopy in $LaTiO_3$*

14:50-15:10 Coffee break

**Session 4: Theory**
Chair: V. Eyert

**15:10** D. Khomskii (Univ. Köln)
*Charge and orbital structure of manganites in the band approach* (invited)

**15:45** G. Khaliullin (MPI-FKF Stuttgart)
*Orbital Peierls state in cubic Vanadates*

**16:05** P. Horsch (MPI-FKF Stuttgart)
*Orbital polarons and temperature dependence of spin-orbital dynamics in Manganites*

**16:25** K. Held (MPI-FKF Stuttgart)
*The LDA+DMFT approach to correlated electron systems*

**Session 5: Poster Session and extended coffee break**
**16:45-18:15**

**P1:** H.-J. Grafe (Univ. Dresden)
*$^{17}O$ Nuclear Magnetic Resonance in $La_{1.8-x}$ $Eu_{0.2}$ $Sr_xCuO_4$ ($0.08 \leq x \leq 0.2$)*

**P2:** S. Schuppler (FZ Karlsruhe)
*Flourescence-yield x-ray absorption of (Ba,K) $BiO_3$ and Ba(Pb,Bi) $O_3$: Coexisting bipolaronic and charge-density wave states*

**P3:** J. Kunze (Univ. Hamburg)
*Optical study on thermal development of ordering in $La_{2-2x}Sr_{1+2x}Mn_2O_7$, $0.32<x<0.54$*

**P4:** R. Klingeler (Univ. Dresden)
*Interplay of spin and charge in quasi 1D cuprates*

**P5:** A. Vasiliev (Moscow State Univ.)
*The search for and study of new low dimensional ladder-like metaloxide compounds*

**P6:** J. Hemberger (Univ. Augsburg)
*Evidence for Jahn-Teller distortions at the antiferromagnetic transition in $LaTiO_3$*

**P7:** K.-D. Schotte (FU Berlin)
*Orbital ordering in the layered perovskite $K_2CuF_4$ at ambient and high pressure*

**P8:** A. Chemseddine (HMI Berlin)
*Growth and Self-Assembling Process of Quantized Titania Nanocrystals*

**18:15 Closing and summary of the first day by D.N. Argyriou**
**18:40 Departure by bus to restaurant**
**19:00 Conference Dinner at Krongut Bornstedt**

## Thursday, 25th of September

**Session 6: Magnetism, Superconductivity and Metal to Insulator Transition**
Chair: P.G. Radaelli

**9:00** B. Keimer (MPI-FKF Stuttgart)
*Spin and orbital correlations in transition metal oxides* (invited)

**9:35** J. Strempfer (MPI-FKF Stuttgart)
*Diffuse scattering from $YBa_2Cu_3O_{6+x}$ observed by high energy x-ray diffraction*

**9:55** Ch. Milne (HMI Berlin)
*Superconductivity and Structure in $NaCoO_2:H_2O$*

10:15-10:45 Coffee break

**Session 7: Transition Metal Oxides Part II**
Chair: B. Keimer

**10:45** L.H. Tjeng (Univ. Köln)
*Orbital occupation and phase transitions in strongly correlated transition metal oxides* (invited)

**11:20** P. Lemmens (MPI-FKF Stuttgart)
*Giant phonon anomalies in the pseudo-gap phase of TiOCl*

**11:40** C. Ulrich (MPI-FKF Stuttgart)
*Orbital Peierls state in the magnetic insulator $YVO_3$*

12:00-13:15 Lunch break

**Session 8: Complex Spin Structures**
Chair: P. Horsch

**13:15** P.G. Radaelli (ISIS)
*Self-organized dimerisation patterns on a frustrated lattice: "octamers" and "helices"* (invited)

**13:50** Y. Su (FZ Jülich)
*The nature of the orbital ordering in ferromagnetic insulating $La_{1-x}Sr_xMnO_3$ (x=1/8)*

**14:10** V. Eyert (Univ. Augsburg)
*Extended Moment Formation and Magnetic Ordering in Hexagonal Magnetic Chain Compounds*

14:30-14:50 Coffee break

**Session 9: Perspectives and Funding of Research Networks**
Chairs: D.N. Argyriou, C. Bernhard, B. Büchner, M. Rübhausen

**14:50** J. Kowol-Santen (DFG Bonn)
*Network funding of the DFG*

**15:10** Open discussions

**16:30 Closing of the Workshop**

# Technical Design Review Workshop

# High-Resolution Double Monochromator at the VUV-FEL of the TESLA Test Facility 2

## April 19-20, 2004
## Hamburg

### Aim

The workshop focuses on the design and the physical prospects of a novel high-resolution double monochromator to be established at the VUV-FEL of the TESLA Test Facility 2. This spectrometer for inelastic light scattering will offer fascinating possibilities for research in physics, chemistry, biology, and medicine. For example, functional materials like high-temperature superconductors, systems with colossal magneto-resistance, glasses and bio-organic materials can be studied on shortest time and length scales. During this workshop the technical requirements and the design of the double monochromator will be discussed.

### Organization

The workshop is supported by the Helmholtz Research Center "Nanostructure Research on Functional Materials with Short Coherence Lengths at the TTF-VUV-FEL". The organizers are Josef Feldhaus from HASYLAB/DESY as well as Katrin Buth and Michael Rübhausen from the Institut für Angewandte Physik und Zentrum für Mikrostrukturforschung, Universität Hamburg.

### Venue & Accomodation

The workshop will be held at HASYLAB/DESY in Hamburg, Germany. A limited number of rooms will be available in the DESY guest houses. For further information visit the DESY homepage:

http://desyntwww.desy.de/vgs/international/international.html

### Contact & Registration

For registration or further information send an e-mail to

katrin.buth@physnet.uni-hamburg.de

Please register until **April 5, 2004**.

## Program

### Monday, April 19, 2004 – Building 25b / Room 109

09:30 – 09:45 *Registration*

09:55 – 10:00 **Welcome Note**
Jochen Schneider
HASYLAB/DESY, Hamburg, Germany

### Session I: Instrumentation and State of the Art for Optical Elements
Chair: Jochen Schneider

10:00 – 10:45 **Soft X-ray Resonant Inelastic Scattering Spectroscopy - A New Look on Matter**
Joseph Nordgren
Uppsala University, Sweden

10:45 – 11:00 *Coffee Break*

11:00 – 11:30 **Design Criteria for FEL Beamlines**
Rolf Follath
BESSY, Berlin, Germany

11:45 – 13:45 *Lunch Break*

### Session II: High Resolution Double Monochromator/Spectrometer: Research and Technology
Chair: Wilfried Wurth

13:45 – 14:15 **Strongly Correlated Materials and Resonant Raman Scattering**
Michael Rübhausen
Institut für Angewandte Physik und Zentrum für Mikrostrukturforschung,
Universität Hamburg, Germany

14:15 – 14:45 **Resonant Inelastic Scattering of VUV/Soft X-ray FEL Radiation Applied to Atoms and Molecules**
Jan-Erik Rubensson
Uppsala University, Sweden

14:45 – 15:15 **Energy Resolution Requirements for Momentum-Resolved Inelastic X-ray Scattering in the VUV**
Peter Abbamonte
Brookhaven National Laboratory, Upton, USA

15:15 – 15:30 *Coffee Break*

15:30 – 16:00 **Properties of the FEL and the High Resolution Monochromator**
Michael Martins
Institut für Experimentalphysik, Universität Hamburg, Germany

16:00 – 16:45 **Optical Design Studies**
Ruben Reininger
SAS - Scientific Answers & Solutions, Madison, USA

16:45 – 17:15 **Detection Systems: Spectral and Time Resolution**
Michael Rübhausen
Institut für Angewandte Physik und Zentrum für Mikrostrukturforschung, Universität Hamburg, Germany

## Session III: Technological Aspects
Chair: Michael Rübhausen

17:15 – 19:00 **Discussion** (*Coffee*)

19:30 *Dinner*

**Tuesday, April 20, 2004 – Building 25f / Room 456**

## Session IV: Work Plan
Chair: Josef Feldhaus

09:30 – 11:30 **Discussion on Work Plan, Work Packages, and Outside Contributions**

11:30 – 11:45 **Closing Remarks**
Jochen Schneider
HASYLAB/DESY, Hamburg, Germany

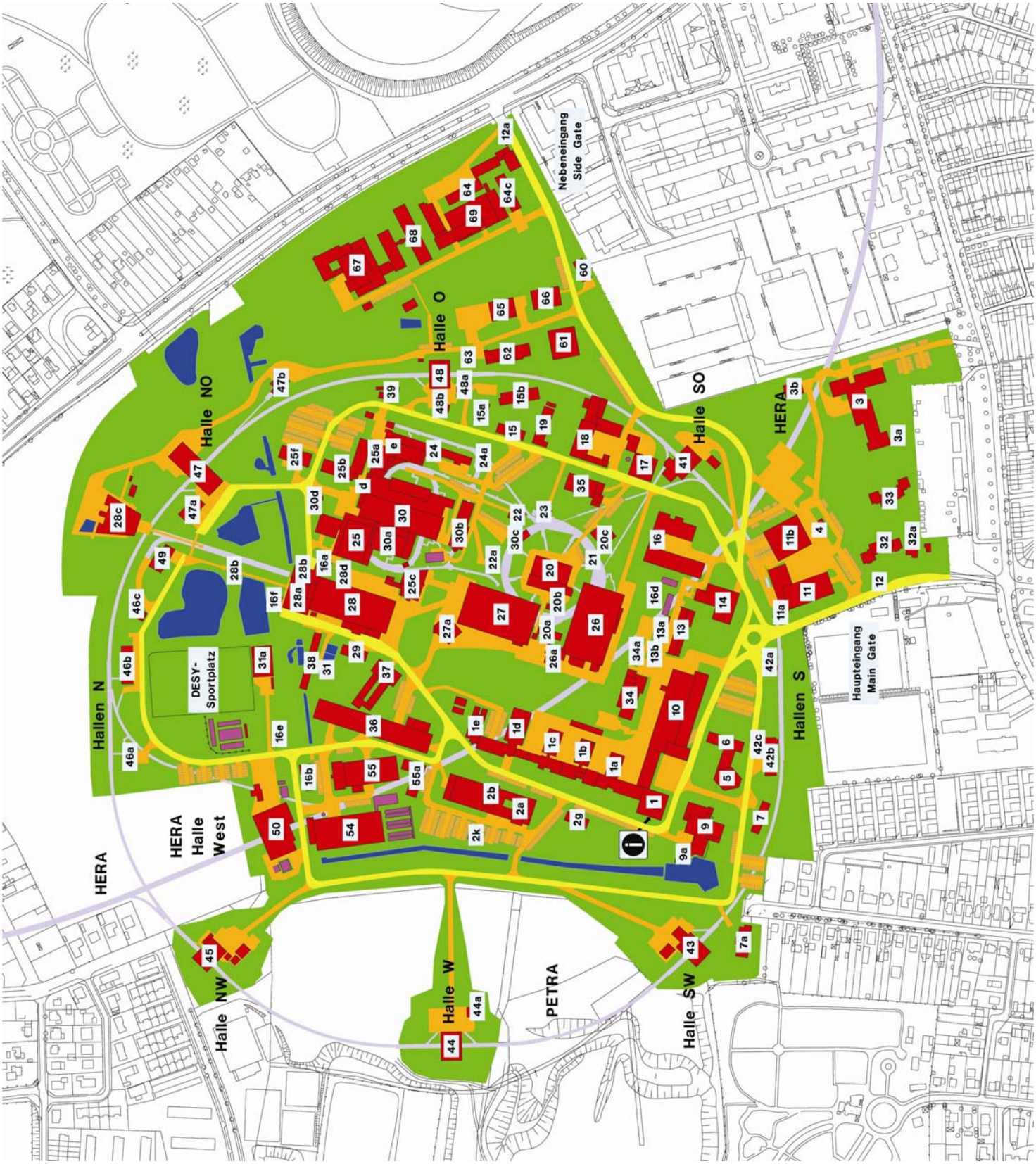


**DESY Hamburg, Notkestraße 85, 22607 Hamburg**

How to get to DESY:

http://desyntwww.desy.de/vgs/international/maps/maps.html

http://desyntwww.desy.de/vgs/international/external_links/external_links.html

Hahn-Meitner-Institut Berlin

Berlin Neutron Scattering Center

# 3rd Berlin Workshop on

# Orbital Physics and Novel Phenomena in Transition Metal Oxides

Hahn-Meitner-Institut Berlin, 6-7 October 2004
Auditorium

## Wednesday, 6th of October

**8:45** Welcome

**Session 1: Manganites 1: Ferroelectricity and Magnetism**
Chair: J.F. Mitchell

**9:00** T. Kimura (Los Alamos National Laboratory)
*Ferroelectricity, magnetocapacitance, and magnetoelectric effect in perovskite rare-earth manganites* (invited)

**9:35** J. van der Brink (Leiden University)
*Magnetism versus ferroelectricity; how orbitals combine both* (invited)

**10:10** L.C. Chapon (ISIS, Rutherford Lab)
*Structural anomalies and competing magnetic interactions in $TbMn_2O_5$*

**10:35** N. Aliouane (HMI Berlin)
*Complex magnetism in the ferroelectric manganite $TbMnO_3$*

**11:00** Coffee break

**Session 2: Manganites 2: Charge-Lattice-Spin Coupling**
Chair: C. Bernhard

**11:30** N.N. Kovaleva (MPI-FKF Stuttgart)
*Spin-controlled Mott-Hubbard bans in $LaMnO_3$ probed by optical ellipsometry*

**11:55** Neil Mathur (University of Cambridge)
*Weak charge-lattice coupling requires reinterpretation of stripes of charge order in $La_{1-x}Ca_xMnO_3$*

**12:20-13:20** Lunch buffet (1st floor of auditorium building)

**Session 3: Sodium Cobaltites**
Chair: A. Maignan

**13:20** A.T. Boothroyd (University of Oxford)
*Magnetic order and dynamics of $Na_xCoO_2$* (invited)

**13:55** P. Lemmens (MPI-FKF Stuttgart)
*Phase diagram and evidence for unconventional superconductivity in layered cobaltites with triangular lattice of $Co^{3+}/Co^{4+}$ sites* (invited)

**14:30** B. Büchner (IFW Dresden)
*Electronic and thermodynamic properties of $Na_xCoO_2$ with $0.3 < x < 0.9$*

**14:55** D.N. Argyriou (HMI Berlin)
*Phase diagram and structure in superconducting $Na_x(H_3O)_yCoO_2.zH_2O$*

**Session 4: Poster session and extended coffee break in room DV 108**
**15:20-17:20**

**P1:** Electronic properties of thin $Ni_2MnIn$ Heusler films
*G. Neuber (University of Hamburg)*

**P2:** Observation of a new triangular phase regime in paramagnetic $La_{1-x}Sr_xMnO_3$
*J. Deisenhofer (University of Augsburg)*

**P3:** Charge order, orbital order, and electron localization in the Magneli phase $Ti_4O_7$
*V. Eyert (University of Augsburg)*

**P4:** Frustrated orbital ground state in thiospinels
*J. Hemberger (University of Augsburg)*

**P5:** Observation of confined spin waves in quasi-metallic and ferromagnetic $La_{1-x}Ca_xMnO_3$ (x=0.17, 20): a unique tool for characterizing size and magnetic coupling of an assembly of intrinsic clusters
*M. Hennion (LLB Saclay)*

**P6:** Magnetic phase transition and short range order in $La_{0.125}Sr_{0.875}MnO_3$
*J.-U. Hoffmann (HMI)*

**P7:** Weak ferromagnetic spin and charge stripe order in $La_{5/3}Sr_{1/3}NiO_4$: Evidence for double exchange?
*R. Klingeler (IWF Dresden)*

**P8:** Temperature-dependent resonance Raman-scattering study at the heavy fermion compound $URu_2Si_2$
*R. Krüger (University of Hamburg)*

**P9:** Investigation of the orbital ordering in doped vanadates
*M.H. Sage (University of Groningen)*

**P10:** Intrinsic Josephson effects in the magnetic superconductor $RuSr_2GdCu_2O_8$
*T. Nachtrab (University of Tübingen)*

**P11:** Short-range antiferromagnetic fluctuations and polaron correlations as a function of temperature and applied magnetic field in the layered CMR manganites, $La_{2-2x}Sr_{1+2x}Mn_2O_7$, x=0.3, 0.35
*T. Perring (ISIS Facility)*

**P12:** Crystal and magnetic structure of $La_{1-x}Ca_xMnO_3$ compound $0.11 \leq x \leq 0.175$
*M. Pissas (National Center for Scientific Research, Demokritos)*

**P13:** Structural and magnetic phase transitions in mixed-valence cobalt oxides $ReBaCo_4O_7$ (Re = Lu, Yb, Tm)
*A.N. Sokolov (Moscow State University)*

**P14** Helical spin arrangement and spin dynamics in metallic $SrFeO_{3-\delta}$
*C. Ulrich (MPI Stuttgart)*

**P15:** Specific heat of $CdV_2O_4$, $ZnV_2O_4$ and $MgTi_2O_4$
*A.N. Vasiliev (Moscow State Univ.)*

**P16:** Spin liquid ground state in $BiCu_2PO_6$
*A.N. Vasiliev (Moscow State Univ.)*

**P17:** Resonant x-ray scattering from $Ca_2RuO_4$ at the Ru $L_{2,3}$- absorption edges
*I. Zegkinoglou (MPI-FKF Stuttgart)*

**P18:** Magnetoelectric phase transition in hexagonal $HoMnO_3$
*Th. Lonkai (University of Tübingen)*

**P19:** Charge order and magneto polarons in $Na_{0.82}CoO_2$
*Ch. Bernhard (MPI-FKF Stuttgart)*

**17:20** **Discussion: Physical Properties and Frustration**
Discussion leader: C. Bernhard

**18:20** End of first day

**18:40** **Departure by bus from HMI to restaurant**

**19:30** **Conference Dinner at the "12 Apostel" in Berlin-Mitte**

## Thursday, 7th of October

**Session 5:** **Cobaltite perovskites**
Chair: M. Rübhausen

**9:00** A. Maignan (Laboratoire CRISMAT, Caen)
*New phenomena in cobaltites: spin blockade and quantum tunnelling of the magnetization* (invited)

**9:35** J.F. Mitchell (Argonne National Laboratory)
*Spin states and magnetic order in a layered double perovskite* (invited)

**10:10** R. Rauer (University of Hamburg)
*Magneto-optical investigation of $La_{1-x}Sr_xCoO_3$ (x = 0.15, 0.2)*

**10:35** G. Khaliullin (MPI-FKF Stuttgart)
*Low energy electronic states in layered cobaltites*

**11:00** Coffee break

**Session 6:** **Manganites 3: Polaronic collerations**
Chair: T. Perring

**11:30** J. Geck (IWF Dresden)
*Orbital polarons in low doped perovskite manganites* (invited)

**12:05** P. Horsch (MPI-FKF Stuttgart)
*Colossal magnetoresistance in manganites: Role of orbital polarons*

**12:30** G. Papavassiliou (National Center for Scientific Research, Demokritos)
*NMR studies of intrinsically inhomogeneous phases in colossal magnetoresistive manganites*

**12:55-14:00** Lunch buffet (1st floor of auditorium building)

**Session 7: Cuprate and Ruthenate Superconductors**
Chair: B. Büchner

**14:00** P. Dai (University of Tennessee)
*Electronic competing phases and their magnetic field dependence in electron-doped superconducting* $Pr_{0.88}LaCe_{0.12}CuO_{4-\delta}$ (invited)

**14:35** M. Braden (University of Cologne)
*The phase-diagram of* $Ca_{2-x}Sr_xRuO_4$*: Relation between crystal structure and physical properties* (invited)

**15:10** D. Manske (MPI-FKF Stuttgart)
*Theory of Cooper-pairing in high-*$T_c$ *cuprates and* $Sr_2RuO_4$ *: Interplay between spin excitations and superconductivity*

**15:35** Coffee break

**16:05** **Discussion:** *To be announced*
Discussion leader: D.N. Argyriou, M. Rübhausen

**17:10** End of workshop

## Öffentlicher Teilnahmewettbewerb mit anschließendem Verhandlungsverfahren

Die Forschungsgruppe Nanostrukturphysik des Instituts für Angewandte Physik und Zentrum für Mikrostrukturforschung, Universität Hamburg, beabsichtigt im Rahmen eines BMBF-Projekts ein neuartiges

## VUV-Raman-Spektrometer

am VUV-FEL (Vakuum-Ultraviolett Freier Elektronen Laser) des HASYLAB/DESY in Hamburg aufzubauen.

Eine ausführliche Beschreibung des Spektrometers kann im Internet unter www.ausschreibungen.hamburg.de abgerufen werden. Darin sind insbesondere die optischen und mechanischen Komponenten wie Spiegel, Gitter, Halterungen, Manipulatoren sowie die Detektorsysteme, das UHV-System und der schwingungsgedämpfte Aufbau des Spektrometers beschrieben. Der Auftrag wird voraussichtlich an mehrere Unternehmen vergeben.

Die Teilnahmeanträge müssen Konzepte mit ersten Lösungsvorschlägen sowie Nachweise über die technische und wirtschaftliche Leistungsfähigkeit enthalten, aus denen unter anderem hervorgeht, dass die in der ausführlichen Beschreibung genannten technischen Spezifikationen erreicht werden. Die eingereichten Unterlagen werden von einem Gutachtergremium beurteilt. Ausgewählte Bewerber werden zu einem sich anschließenden Verhandlungsverfahren eingeladen.

Interessierte Unternehmen werden gebeten, ihre Unterlagen mit ersten Preisabschätzungen in deutscher oder englischer Sprache schriftlich in dreifacher Ausfertigung sowie zusätzlich eine elektronische Version auf CD bis zum 30.11.2004 an die Finanzbehörde Hamburg, Ausschreibungs- und Einkaufsdienste, Gänsemarkt 36, 20354 Hamburg zu schicken. Nähere Informationen zum Spektrometer erteilt Dr. Michael Rübhausen (ruebhausen@physnet.uni-hamburg.de; http://www.physnet.uni-hamburg.de/institute/IAP/Group_N/e/information/news/news.shtml), Auskünfte zum Verfahren die Finanzbehörde Hamburg (Uwe.Goedicke@fb.hamburg.de).

**Call for expressions of interest with subsequent negotiated procedure**

The research group "Nanostructure Physics" of the Institut für Angewandte Physik und Zentrum für Mikrostrukturforschung, Universität Hamburg, plans within a project, that is funded by the German Federal Ministry of Education and Research, to set up a novel

**VUV-Raman spectrometer**

at the VUV-FEL (vacuum-ultraviolet free-electron laser) of HASYLAB/DESY in Hamburg.

A detailed description of the spectrometer can be found in the internet under www.ausschreibungen.hamburg.de. In particular, the optical and mechanical components such as mirrors, gratings, mounts, manipulators as well as the UHV system and the vibration-free setup of the spectrometer are described. The contract will be awarded presumably to several undertakings.

Requests for participation must contain concepts with first suggestions for solutions as well as proofs of the technical capability and the economic standing, that demonstrate that the technical specifications stated in the detailed description can be achieved. The submitted documents will be evaluated by an advisory board. Selected candidates will be invited to a subsequent negotiated procedure.

Interested undertakings are requested to send three copies of their documents with first cost estimates in German or English in written form as well as an electronic version on CD until November 30, 2004 to the Finanzbehörde Hamburg, Ausschreibungs- und Einkaufsdienste, Gänsemarkt 36, 20354 Hamburg, Germany. Further information on the spectrometer gives Prof. Dr. Michael Rübhausen (ruebhausen@physnet.uni-hamburg.de; http://www.physnet.uni-hamburg.de/institute/IAP/Group_N/e/information/news/news.shtml), information on the procedure gives the Finanzbehörde Hamburg (Uwe.Goedicke@fb.hamburg.de).